2016

Synthesis of Well Dispersed Supported Metal Catalysts by Strong Electrostatic Adsorption and Electroless Deposition

John Meynard Macasero Tengco
University of South Carolina

Synthesis of Well Dispersed Supported Metal Catalysts by Strong Electrostatic Adsorption and Electroless Deposition

by

John Meynard Macasero Tengco

Bachelor of Science
University of the Philippines Los Baños, 2007

Submitted in Partial Fulfillment of the Requirements

For the Degree of Doctor of Philosophy in

Chemical Engineering

College of Engineering and Computing

University of South Carolina

2016

Accepted by:

John R. Regalbuto, Major Professor

John R. Monnier, Major Professor

John W. Weidner, Committee Member

Donna A. Chen, Committee Member

Lacy Ford, Senior Vice Provost and Dean of Graduate Studies

DEDICATION

To my parents, for making ends meet, together with my family for trusting, supporting, and understanding me in this endeavor.

ACKNOWLEDGEMENTS

Utmost appreciation is given to the following for their contributions in the completion of this work:

Prof. John R. “JR” Regalbuto, my adviser, for his efforts throughout the course of this doctoral study: from being my academic adviser back at the University of Illinois at Chicago and for offering me to work under his guidance at the University of South Carolina;

Prof. John R. Monnier, my co-adviser, for providing insight and wisdom into the projects I have undertaken;

Professors John W. Weidner and Donna A. Chen, my committee members, for their valuable scientific expertise;

Specific colleagues and researchers whom I’ve had the opportunity to work with for the studies presented in this dissertation: Dr. Weijian Diao, Dr. Yunya Zhang, Dr. Akkarat Wongkaew, Dr. Yuliana Lugo-Jose, Bahareh Tavakoli Mehrabadi, Ritubarna Banerjee and Taylor Garrick;

Research facilities and laboratories such as the Electron Microscopy Center at USC with Dr. Doug Blom, the Electron Microscopy Services at UIC with Dr. Alan Nicholls and Dr. Kebin Low, X-ray diffractometer at the USC SAGE Center; various analytical equipment with the help of Carol Stork.

Appreciation is also extended to members of the Regalbuto, Monnier, and Williams research groups for providing assistance and discussions for the research undertaken.

Portions of this work were funded by the following: Toyota Motor Company, USC ASPIRE Grants and the Center of Catalysis for Renewable Fuels (CReF).

In addition, grateful appreciation is given to friends and family for their support and encouragement.

ABSTRACT

Enhancing the catalytic performance of heterogeneous catalysts can be done by increasing active site count as well as modification of the physico-chemical characteristics of the catalyst material. For supported metal nanoparticles this can be achieved by decreasing particle size, thus increasing dispersion or metal utilization on the surface of the particles, while modification of metal properties can be attained by addition of a secondary metal that has a strong interaction to the primary metal, beneficial for a given reaction. In addition, the accessibility of the metal surface is necessary for reliable performance of catalysts. For carbon supported catalysts, Temperature Programmed Oxidation has been used to show the presence of decorating carbon on the metal surface, which can be cleaned by oxidative removal of the carbon overlayer.

In the preparation of supported metal catalysts, the methods of Strong Electrostatic Adsorption (SEA), and its incipient wetness analog, Charge Enhanced Dry Impregnation (CEDI), can yield supported metal nanoparticles with high dispersion and narrow size distribution. Catalysts prepared by SEA and CEDI therefore are desirable as seeds for addition of secondary metal using Electroless Deposition (ED), as the prepared bimetallic catalysts should be of similar dispersion as the base catalyst. These methods were used to demonstrate the preparation of two series of carbon supported bimetallic catalysts containing Pt which were then characterized and evaluated for oxygen reduction reactions. The first system used Pt as the base metal, prepared by SEA on XC72R carbon,

with Ru as the secondary metal added by ED. The second system used Co as base metal, prepared by a modified CEDI method on carbon black, with Pt added by ED.

With comprehensive characterization, the resulting Pt-Co/C catalysts had particles with irregular morphology that were larger than the seed Co particles. These were determined to have thin alloyed Pt-Co phases and domains of pure Pt. On the other hand the Ru-Pt/C catalysts did not have alloying of the component metals but do have real bimetallic surface composition. Electrochemical evaluation of these catalysts showed higher mass activities, with respect to platinum content, compared to commercially available monometallic and bimetallic catalysts. This enhancement in performance is associated with the electronic interaction between Pt and Ru on the catalyst surface and the lattice contraction for Pt-Co alloys.

TABLE OF CONTENTS

LIST OF TABLES

LIST OF FIGURES

CHAPTER 1

INTRODUCTION AND LITERATURE REVIEW

1.1 Introduction

Catalysts serve an important role in the chemical industry as it is estimated that 90 percent of processes employed are based on catalytic chemical synthesis. In metal catalyzed reactions, the use of metal dispersed as tiny particles on support material is considered cost efficient, as the catalyst is spread on high surface area thereby increasing accessible metal for reaction while decreasing the amount used. This is of particular significance when a valuable metal is used, such as Platinum or Gold. Availability of surface sites of metal nanoparticle catalysts is an important aspect of catalyst preparation, as overall activity of catalysts is largely dependent on the amount of active sites for molecular level reactions to occur on. When metals are anchored onto supports, it is often desired to have as much of it exposed on the particle surface. Metal atoms located inside nanoparticles are essentially unused. Thus, smaller particles are aimed for in catalyst preparation since these would have a high ratio of surface area to volume, therefore higher utilization of the metals on the nanoparticle surface. This generally translates to higher activity when normalized to the amount of metal. In modern catalyst research, particle sizes are often in the scale of a few nanometers with some cases having atomically dispersed metal.

The fraction of metal available on the surface is reported as dispersion and its measurement can be done with various techniques in catalyst characterization. Dispersion can be determined by selective adsorption and measurement of an analyte gas or by titration of a gas chemisorbed on the surface of the metal. From chemisorption, the amount of metal accessible on the surface of the catalyst nanoparticles can then be calculated from the measured gas based on a predetermined chemisorption stoichiometry.

Another way of determining dispersion is by measurement of particle size through conventional characterization methods such as x-ray diffraction (XRD) and electron microscopy (EM) and, by assumption of particle geometry, the amount of metal on the surface of nanoparticles can be calculated. In fact, the inverse can be done with chemisorption where the particle size can be estimated from the amount of surface atoms.

In the preparation of supported metal catalysts, there are a varied number of methods that have been developed, with some of these offering a better degree of control of the catalyst dispersion [1]. In particular, the method of Strong Electrostatic Adsorption has been used to prepare catalysts with very small particles, around a nanometer in size, with a narrow particle size distribution. While advancements have been made in impregnation of metal onto support and producing smaller particle sizes, further enhancement can be achieved by fine tuning treatment conditions, ensuring surface site accessibility as well as improvement of catalytic activity by doping with another metal.

Prior works have shown that catalyst surfaces can be blocked by layers of carbonaceous material. This overlayer can be hard to detect in conventional characterization techniques like XRD, electron microscopy and X-ray photoelectron spectroscopy. In this study, methods for the detection and treatment for removal of carbonaceous overlayer are developed using Temperature Programmed Oxidation (TPO).

Carbon supported noble metal catalysts are used in a variety of renewable energy applications such as fuel cells and chemical reforming processes. With the paradigm shift in energy production and policy, better performing catalysts are sought even more. Improving catalyst activity can be attained by modifying the metal composition of the catalyst, adding another metal, creating a bimetallic catalyst. There are evidences of

enhanced catalytic performance with particular combinations of metals. While commonly used methods involve simple concurrent or subsequent impregnation of two or more metals, these often lead to separate particles of inhomogeneous composition. Treatments that alloy the component metals may be suitable. However, as it is the particle surface that is involved in catalytic reactions, alloying in the bulk can be deemed unnecessary. There are also techniques that ensure mixing or close association of component metals but are not scalable for industrial use due to the complexity of these methods. The use of Electroless Deposition (ED) method can achieve targeted deposition of metals on the surface of catalyst nanoparticles. ED as an industrially scalable method of bimetallic catalyst preparation has been shown to produce catalysts that demonstrate superior catalytic performance due to better interaction between metal components at the surface [1]. Application of ED for preparation of well dispersed bimetallic fuel cell catalysts with high mass activity is explored in this study. Specifically, by deposition of Ruthenium on Platinum, and of Platinum on Cobalt, better performing fuel cell catalysts are created, in comparison to commercially available monometallic and bimetallic catalysts.

In general, this study involves the application of SEA and ED catalyst synthesis methods to prepare well dispersed supported metal catalysts. Specifically, carbon supported platinum based bimetallic catalysts for fuel cell applications are prepared and characterized with various techniques. In addition, surface site accessibility of carbon supported catalysts is probed with TPO.

1.2 Heterogeneous Catalysis

Catalysts are known to facilitate in reactions by lowering the activation energy for a specific reaction step. In a heterogeneous catalytic reaction, with the use of solid catalysts in fluid environments, the reactants are adsorbed on the surface of the catalyst with breaking or weakening of intramolecular bonds [2]. These adsorbed species then react in a series of steps, the mechanism of which is specific on the reactants as well as the catalyst employed, with resulting products desorbing from and recovering the catalyst surface. Changing conditions, particularly the catalyst, can alter the preferred pathway for the reaction mechanism.

The resultant rate of reaction in the presence of a catalyst will be dependent on the availability of sites where reaction occurs. Thus, increasing the amount of catalyst surface is necessary for commercial viability. High surface area catalysts, in the form of powders that may also be supported on a type of scaffolding for reactors are used widely in industry. These powders are often composed of metals dispersed as small particles supported on highly porous materials. The most common supports used are oxides such as titania, alumina, and silica, as well as carbon that have been treated for increased porosity. For such catalysts, metal particle sizes are often targeted in the sub-micron to nanometer range as this increases the fraction of metal available on the surface for catalytic reactions, enhancing the utilization of the metals and lowering the overall cost of the catalyst.

1.3. Supported Metal Catalyst Preparation

1.3.1 Overview

There are many different methods that have been developed for the preparation of supported metal nanoparticle catalysts. Not all are suitable for industrial scale usage as issues concerning material availability, complexity in production, and scalability have to be overcome. The most commonly used ones involve immersion of the support with a solution containing a precursor form of the metal. Depending on the chemistry involved, variations in the wet phase conditions and forms of the precursor create the capability to produce a range of particle sizes and morphology. Supports used can be oxides such as alumina, silica and titania or pure substances like carbon. Specific attributes of these substances such as stability, structure, conductivity, etc., coupled with the mass transfer characteristics and chemistry of the reactions intended for the catalysts, lend to the choice of support.

Methods of supported metal catalyst preparation can be grouped into two major classifications: metal synthesis (1) in solution and deposition onto a support and (2) from precursor adsorption at the solid-liquid interface. The most commonly used methods of impregnation, deposition-precipitation, and reduction-oxidation are grouped into the latter classification.

1.3.2 Metal synthesis in solution

One pathway for the synthesis of supported nanoparticle catalysts is by production of metal particles dispersed in a liquid environment and depositing them onto a desired support [1]. An illustration of this method of supported metal catalyst synthesis

is shown in Figure 1.1. The metal nanoparticles are formed either by precipitation or reduction from solution with a precipitating or reducing agent respectively. The particles dispersed in the liquid phase are prevented from agglomerating by encapsulation with a capping agent [3, 4], an organic molecule that binds to the surface of the particles. In the formation of the dispersed nanoparticles, there are many factors that can alter their size and morphology but it is largely affected by the rate of addition of precipitant or reductant [1, 3]. The type and amount of capping agent added in the system can also influence the rate of particle formation and the final particle size depending on its effectivity in controlling particle coalescence during nucleation and growth.

Anchoring of the particles on support can be achieved by simple physical mixing of the support with the dispersion. Adjusting the dispersion pH can enhance deposition of the particles on the support surface. By adjusting pH, the functional groups on the surface of the support can be protonated or deprotonated thereby creating a charged surface. Particles surrounded by capping agents that can become oppositely charged as the support surface at the same pH conditions can then be lodged to the support surface through electrostatic interaction, similar to SEA discussed in a latter section. Other means of anchoring particle on the surface such as chemical bonding of the capping agent with functional groups on the surface have also been successfully attempted.

Upon deposition of the particles on the support surface and subsequent removal of excess liquid, the capping agent is removed thermally. Thermal treatment is usually done in an oxidative environment which essentially burns off the organic residue. This however has to be carried out at a temperature where the sintering of metal particles is minimized.

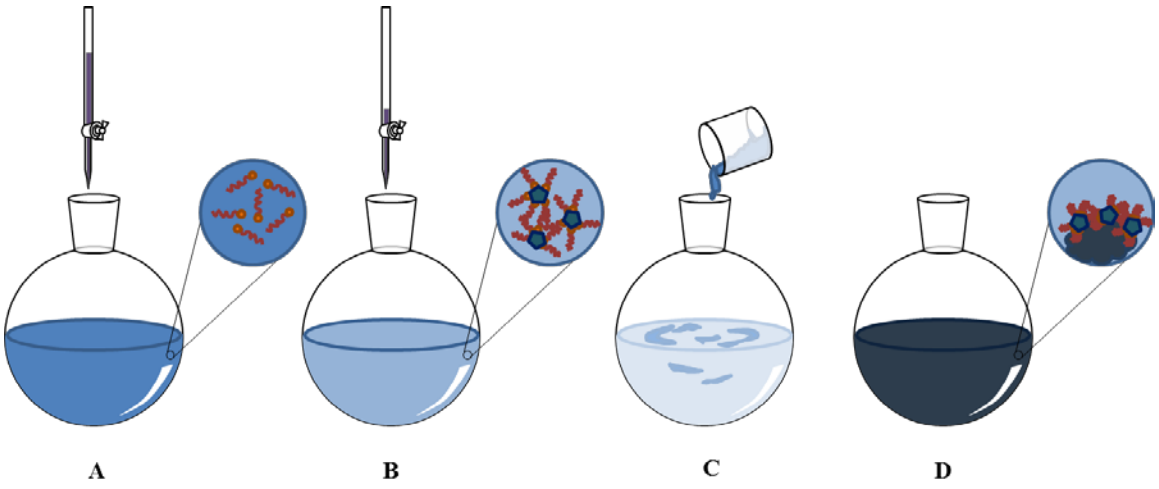

Figure 1.1 Illustration of metal synthesis in solution for catalyst preparation: (A) addition of reducing or precipitating agent to form nanoparticles; (B) attachment of capping agent for dispersing particles and controlling growth; (C) and (D) deposition and anchoring of particles on support.

1.3.3 Dry and Wet Impregnation

The simplest method of catalyst preparation is by dissolution of a precursor salt in a liquid solvent, often water, and permeating the solution into the support pores. Mixing an amount of the precursor solution in excess of the pore volume of the support, yielding a thin slurry, is called wet impregnation (WI). Limiting the solution amount to the pore volume is called dry or incipient wetness impregnation (DI). In WI, the impregnated support is filtered out, leaving excess liquid containing any precursor that was not retained by the support. This entails a need to recycle the excess liquid in order to minimize wastage of the precursor. The use of DI eliminates excess liquid and the need for a filtration step. However, the lack of filtration step during DI synthesis of catalyst means that any other component initially present in the solution will be retained in the

dried catalyst. If removal of these other substances is desired, further processing is necessary.

In order to obtain the final catalysts with the metal particles anchored onto the support, the impregnated powder is subjected to thermal treatment in a calcining or reducing environment. Precursor ligands are removed, either by decomposition or reacting with air/hydrogen producing gaseous molecules. Other components that do not form gaseous products, such as alkali metals or their salts, remain in the final catalyst.

Catalysts made by these impregnation methods do not usually produce particles with high dispersion due to the lack of induced interaction between the precursor and the support which allows mobility of the precursor. In DI, the pH of the resulting paste of support and impregnating solution is buffered around the point of zero charge (PZC) of the support, as the amount of hydroxyl groups on the support surface is orders of magnitude more than the acid or base in solution that can charge (protonate or deprotonate) the surface [5]. In the case of WI, even with excess liquid, upon filtration of the slurry the resulting filtered paste is still buffered around the PZC of the support. Without a strong interaction between the precursor and support, as drying ensues, loss of the solvent causes the moisture to migrate to the external surface of the support, causing the precursor to agglomerate together [1]. An illustration of this phenomenon is shown in Figure 1.2 Reduction of the dried precursor agglomerates will then result in larger particles.

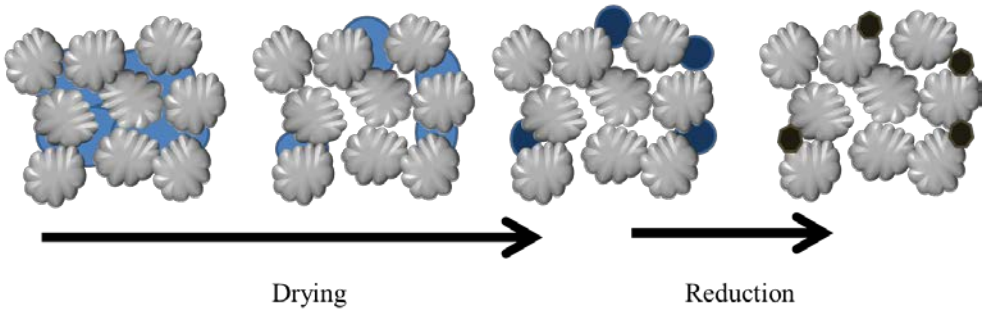

Figure 1.2 Illustration of precursor migration and agglomeration resulting in large particles.

1.3.4 Strong Electrostatic Adsorption and Charge Enhanced Dry Impregnation

In the synthesis of catalysts by DI and WI, the lack of strong interaction between the precursor and the support is the main reason for precursor migration and formation of large particles. This can be mitigated by using the method of Strong Electrostatic Adsorption (SEA) which is a special case of WI. In SEA, the pH of the impregnating solution is adjusted such that the amount of acid or base in solution is enough to charge the surface of the support and creating coulombic interaction between the support surface and the precursor[6]. Charge enhanced dry impregnation (CEDI) is a special case of SEA and DI where pore filling is done with the precursor solution containing an excess of acid or base such that the PZC buffering effect of the support is overcome [7]. A commonly used illustration of WI, DI, SEA, and CEDI comparing the volumes of impregnating solution to support and parameters of impregnation is shown in Figure 1.3.

In SEA and CEDI, the choice of pH used for the impregnation procedure depends on the support PZC and the precursor complex used. Referring to the illustration in Figure 1.4, the surface of the support can be protonated or deprotonated when in contact with a solution that is below or above the PZC, respectively [6]. The precursor chosen should be of the opposite charge as the support surface so that electrostatic interaction

will occur. A survey of precursor uptake is conducted at the desired surface loading of the support in the precursor solution and an optimal pH is determined where maximum uptake is observed. At extreme pH conditions, there is retardation of precursor adsorption due to high ionic strength [8]. Upon adsorption of the precursor on the support surface, it strongly retains hydration sheaths, that maintain the local adsorption conditions [9], which can be removed upon thermal treatment for reducing the precursor into well dispersed metal nanoparticles.

The use of SEA and CEDI methods in the preparation of bimetallic catalysts has been demonstrated [10, 11]. Compared to simple impregnation methods, the resulting catalysts from using SEA and CEDI were shown to have better mixing and interaction between the component metals as a result of the strong interaction of the precursor with the support.

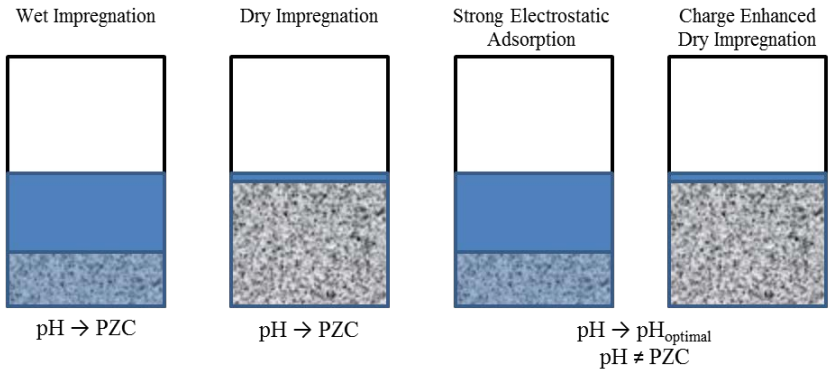

Figure 1.3 Illustration showing the differences between WI, DI, SEA, and CEDI.

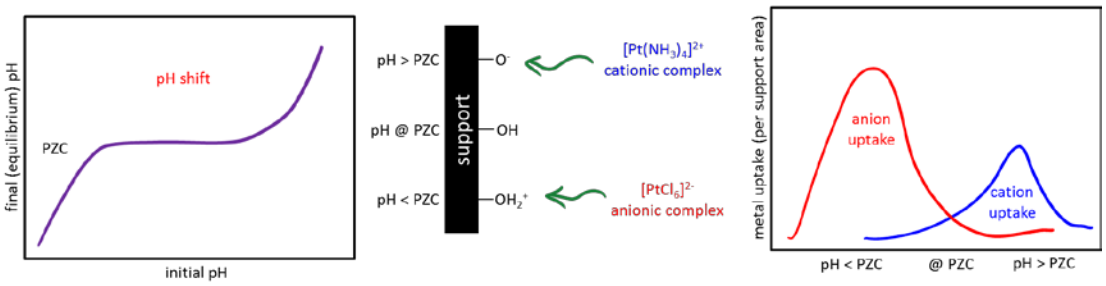

Figure 1.4 Illustration showing the method of strong electrostatic adsorption.

1.3.5 Deposition-Precipitation

The similar to the method of catalysts synthesis by metal formation in solution, the deposition-precipitation (DP) method uses a precipitating agent added to a suspension containing both the precursor salt and the support instead of the support being added later. Vigorous mixing of the suspension ensures homogeneous distribution of the precipitating agent. Nucleation of the particles on the surface of the support is desired over nucleation in solution. Metal salts are generally easy to precipitate in basic conditions such that sodium hydroxide and urea are commonly used as precipitating agents [12-14]. Addition of sodium hydroxide, being a strong base, can create high local concentrations of hydroxyl ions which is undesirable as this causes precipitation in solution. Urea has been shown to slowly decompose at elevated temperatures to yield hydroxyl ions which can then be distributed evenly in the suspension [15]. By ensuring homogenous distribution of the precipitating agent, DP can result in particles that are more evenly dispersed on the surface of the support compared to DI and WI [1].

1.3.6 Bimetallic Catalysts from Reduction-Oxidation on Support Surface

Bimetallic catalysts can be prepared by surface redox where reduction of a secondary metal on the surface of a primary or “seed” catalyst can achieve partial or full

coverage of the seed metal surface by the secondary metal. This method can be used to target the deposition of the secondary metal to the primary metal and not on the support surface [16, 17]. One way of doing this is by galvanic displacement (GD), where the secondary metal in precursor state can be easily reduced in the presence of the primary metal in reduced state due to thermodynamically favorable electrochemical potential difference in the half reactions of each metal [18-21]. If this is not possible, addition of a reducing agent can be done, which can either be in solution and activated on the surface of the base metal [16, 17, 22-26] or pre-adsorbed on the seed metal surface [18, 27, 28]. This latter method is called electroless deposition (ED).

In galvanic displacement, a net positive potential for the exchange of the two metals is necessary for GD to occur (Figure 1.5). However, the rate of displacement of the primary metal by the secondary metal can diminish through time as the exposed seed metal required for GD to proceed is replaced and the surface of the particles are covered up with the secondary metal. The blocking of the primary metal means that GD is limited to only up to monolayer loadings [19, 29]. Other factors may come into play in the GD mechanism such as diffusion of the primary metal or etching of the deposited secondary metal which may expose more surface for displacement [20].

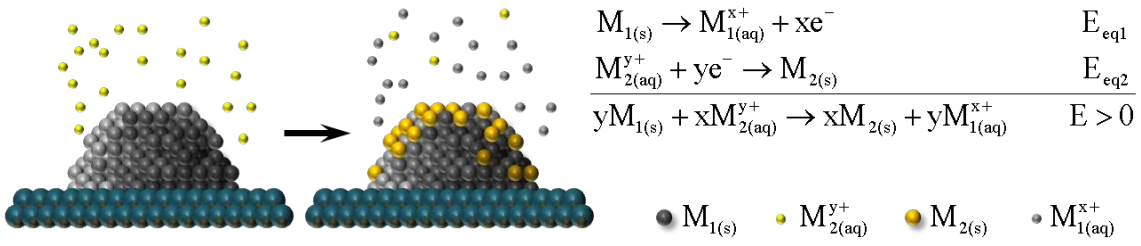

Figure 1.5 Illustration of the galvanic displacement synthesis method [1].

The mechanism for electroless deposition has been used in industry as an alternative to electrochemical plating [22, 26, 30]. In ED, the activated reducing agent on the surface of the seed metal reduces the secondary metal from precursor in close proximity [23]. Similar to GD, there should be thermodynamically favorable net potential of the partial reactions for the oxidation of the reducing agent (anodic) and the reduction of the secondary metal from precursor (cathodic).

The deposition of secondary metal can proceed either by further deposition on the seed metal surface, referred to as catalytic deposition, or by accumulating on initially deposited secondary metal, which is called auto-catalytic deposition [17]. Auto-catalytic deposition can occur if the secondary metal can activate the reducing agent thus acting as an active surface for the redox reaction to occur on. An illustration of the ED process is shown in Figure 1.6.

In the preparation of an electroless developer bath, solution stability is first evaluated where the secondary metal should only reduce in the presence of the seed metal and that it does not precipitate or spontaneously reduce in solution [16, 22]. Chelating agents can be added to the ED bath in order to stabilize the precursor [22, 23, 26]. For the choice of reducing agent, most commonly used are $NaBH_4$, dimethylamine-borane, NaH_2PO_2 and hydrazine which typically have high activity in basic conditions [22, 26, 30-38]. However, should the process require acidic conditions, other reducing agents such as formic acid and ascorbic acid have been shown to be active at low pH [24, 25, 39]. The pH of the ED bath will depend on the choice of precursor used and the catalyst support PZC. Bath conditions should be favorable for deposition of the secondary metal

on the seed metal and not adsorption of the precursor on the support which results in SEA.

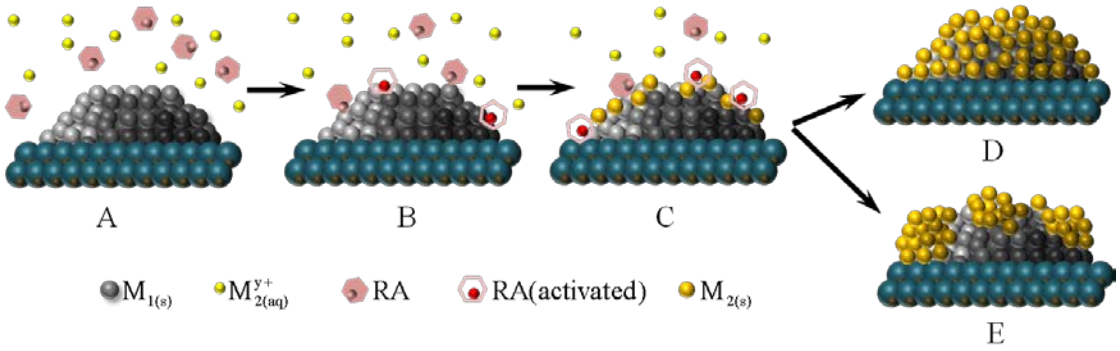

Figure 1.6 Synthesis of bimetallic catalyst by electroless deposition: (A) immersion of seed catalyst into the ED bath, (B) adsorption and activation of reducing agent, (C) reduction and deposition of secondary metal, (D) catalytic deposition, (E) Auto-catalytic deposition [1].

1.4 Carbon Decoration of Supported Metal Catalysts

A survey of literature and prior work with carbon supported catalysts has shown a discrepancy in the dispersion measurements from different characterization techniques, particularly XRD and chemisorption [40-44]. Discrepancies in catalysts wherein size estimates for chemisorption are larger than that of XRD and STEM are often attributed to loss of metal surface area by an occluding layer. In theory, estimates of particle size and dispersion through different characterization techniques should agree closely for well dispersed nanoparticles. One significant assumption in the back calculation of particle size from dispersion or vice-versa is that entire surfaces of particles are exposed and are measurable with chemisorption. Loss of surface by a covering material would result in underestimation of surface sites. This lower count of surface sites giving lower surface to bulk metal ratio will result in estimates with apparently larger particle sizes. This has

been observed for Pd/TiO_2 where, due to strong metal support interaction the support creeps up the surface of the metal nanoparticles [45] when subjected to high temperature [46]. A similar discrepancy has also been noticed for carbon supported catalysts while it is very rarely encountered with oxide (e.g. silica and alumina) supported ones.

In the discrepancy between chemisorption and XRD (or STEM) size estimates for carbon supported catalysts, sizes estimated from chemisorption are larger than that of the bulk characterization methods. This is commonly attributed to the formation of a carbon overlayer, or carbon decoration, over the metal nanoparticle surface [47]. Studies have reported carbon decoration on carbon supported palladium [48, 49] while carbon deposition on the surface and dissolution into Pd nanoparticles have been determined possible in a study of first principles simulation of carbon migration on palladium [50]. Such carbon cannot be easily discerned due to presence of adventitious carbon as well as bulk carbon support interference in conditions of common surface characterization techniques.

1.5 Fuel Cell Application of Bimetallic Catalysts

For decades, thorough researches on fuel cells have been done and a large amount of studies have been conducted on electrocatalyst development. While other types of catalysts have been developed, platinum based electrocatalysts are still widely used due to kinetic and stability issues [51-53]. Doping of the platinum metal with other transition metals have been shown to enhance catalytic performance in fuel cells [54-56]. For the alloyed form of these catalysts, the high activities are attributed to the contraction of Pt-Pt interatomic distance [57, 58]. Doping of the platinum surface by a transition metal has

also been demonstrated to enhance fuel cell catalytic activity [59]. For doped platinum catalysts, it has been shown that electronic effects, where changes in the electronic properties of the platinum particle brought about by the dopant metal, play a role in enhancing catalytic performance [60, 61].

In studies that have evaluated formulations of Pt-Ru and Pt-Co electrocatalysts, results have shown very high activity compared to Pt only. It is hypothesized that the addition of Ru on Pt helps in alleviating CO poisoning, a major problem with fuel cells that employ alcohol fuels [62]. For cobalt alloying with platinum, the decreased lattice parameter for Pt-Co alloy is cited as the main reason for enhanced mass activity of the electrocatalysts [58, 61, 63].

CHAPTER 2

EXPERIMENTAL PROCEDURES

2.1 Preparation of Pd/C Catalysts

Carbon support was obtained from BASF, identified as CP-97 with a surface area of 615 m^2/g and a PZC of 8.5. Palladium metal source used sodium tetrachloropalladate (Na_2PdCl_4, 98%) as precursor, sourced from Sigma-Aldrich.

The palladium precursor salt was dissolved in deionized water at a nominal concentration of 150 ppm and adsorption experiments were done by contact of the CP-97 support with this solution. The solution initial pH values were adjusted using different HCl and NaOH solutions. After adjustment of pH, aliquots for initial Pd concentration measurement were withdrawn and CP-97 was added at a surface loading of $500m^2/L$. Vigorous shaking of the resulting slurry was carried out at about 120 rpm for an hour. After the contact time of the support with the solution, the equilibrium pH of the slurries were recorded. Sample aliquots were withdrawn from each and subsequently filtered by syringe. The amount of initial Pd as well as Pd remaining in solution was measured by inductively coupled plasma (ICP) optical emission spectroscopy (Perkin Elmer Optima DV 2000). The difference in concentration was taken as Pd uptake. The final batches of catalysts were prepared at the optimal pH where maximum uptake by the CP-97 support of the tetrachloropalladate precursor was observed. After which, the slurries were filtered and dried. The initial and final Pd concentrations were also determined by ICP analysis and used for calculating the weight loading of Pd since slight changes in equilibrium pH can change the uptake of Pd [64]. Three Pd/C catalysts were prepared, each subjected to different initial thermal treatments before reduction at 350 °C for two hours to obtain the final catalyst. The first, Pd/CP97, was directly reduced at 150 °C for an hour; another was

annealed in helium first at 300 °C, labeled as Pd/CP97-A; and the final, Pd/CP97-C was calcined in air at 300 °C for an hour.

2.2 Temperature Programmed Analyses of Pd/C Catalysts

Temperature programmed oxidation was done using a custom TPx System fitted with an Inficon Transpector 2 Mass Spectrometer. Samples were loaded in a tubular TPx cell (6 mm, Pyrex) with an expanded bulb space fitted with a fritted glass disc for holding powder samples. Pretreatment by heating at 200 °C in flowing He was done to remove adsorbed moisture with monitoring of water signal until it is diminished. After cooling down, the experiment proceeded with TPO, with 10% O_2 - balance He flowed at 20 sccm and heating ramp rate of 5 °C/min. While the spectrum from 1 to 50 amu was recorded, the signals for oxygen and carbon dioxide were primarily monitored.

2.3 Preparation of Pt-Co/C Catalysts

For the base carbon supported cobalt catalyst, cobalt(II) nitrate hexahydrate ($Co(NO_3)_2 \cdot 6H_2O$) was used as the cobalt source. Citric acid was used as a metal complexing/wetting agent and acidifier. Both cobalt precursor salt and citric acid and were supplied by Sigma-Aldrich. The support, Acethylene Carbon Black (CB1, specific surface area: 320 m2/g) was obtained from Toyota Motor Engineering & Manufacturing North America, Inc., and has a PZC of 3.4.

For the electroless deposition experiments, Chloroplatinic acid (H_2PtCl_6) was used as the metal precursor for the ED bath. Dimethylamine borane (DMAB, 97% purity) was used as reducing agent. Ethylenediammene (EN) was added for thermal stability of

the precursor in the ED bath. The precursor, reducing agent, and stabilizer were all sourced from Sigma-Aldrich. The ED bath pH adjustment used water diluted solutions of sodium hydroxide (NaOH, 10N solution) and hydrochloric acid (HCl, 37%) both from Alfa Aesar. De-ionized water was used for preparation of all solution employed in experiments.

The pore volume of the CB1 powder was determined by careful impregnation of de-ionized water to incipient wetness and was calculated to be 3.5mL/g. Nominal loadings of 2.5 wt% and 5.0 wt% Co in the catalysts were used. Based on the weighed amount of carbon to be used, the corresponding amount of the cobalt (II) nitrate precursor needed for a specific loading was calculated and weighed. Citric acid in a 1:1 molar ratio to cobalt was also prepared. Both cobalt salt and citric acid were dissolved with water to a volume required for pore filling of the corresponding amount of CB1. The solution was then dropwise added to the carbon with vigorous mixing and the resulting paste was then dried at room temperature. The dried paste was annealed in helium for 4 h at a temperature determined from temperature programmed decomposition using a Micromeritics Autochem II 2920 analyzer. After annealing, the samples were reduced in 10% H_2/balance Ar at a temperature determined from temperature programmed reduction (using the Autochem II analyzer) to form metallic Co.

After characterization and determination of Co/C surface sites, the catalysts were then immersed in an electroless developer bath containing H2PtCl62- as Pt source, DMAB as reducing agent, and EN as stabilizer at a molar ratio of Pt : DMAB : EN = 1 : 5 : 4. Preliminary experiments were done to check the stability of the bath, taking care not to exceed the concentration (120 ppm Pt) and temperature (50 °C) where Pt will

spontaneously reduce in solution and not on the Co surface. All electroless deposition experiments were conducted for 1 h with an additional dose of DMAB, with the same amount as what was initially in solution, added 30 min into the experiment. Aliquots were withdrawn at the start (prior to adding DMAB) and at the end of the ED experiments for measurement of initial and final concentrations of Pt in solution as well as determination of Co leaching during immersion of the catalyst in the ED bath. The concentrations were determined by Atomic Absorption Spectrometry (Perkin Elmer AAnalyst 400). The final loadings of the prepared catalysts were then calculated from these concentration changes in solution through material balance.

2.4 Preparation of Pt-Ru/C Catalysts

For the base catalyst prepared by SEA used for this experiment, chloroplatinic acid (CPA, H_2PtCl_6) from Sigma-Aldrich was dissolved in de-ionized water (18.2 MΩ-cm) with a Pt concentration of 200ppm. Vulcan XC72-R carbon with a surface area of 250m^2/g and PZC of 8.5 was used as the support. Hexaammineruthenium(III) chloride ($Ru(NH_3)_6Cl_3$) obtained from Sigma-Aldrich was used as Ru precursor. Formic acid (HCOOH, 99%, FA) from Fluka was used as reducing agent for the ED bath. All solution pH adjustments were done either using dilute HCl or NaOH solutions.

Preparation of Pt/VXC72-R catalyst was done using SEA method [65]. The CPA solution was adjusted to pH 3, the initial pH needed for obtaining equilibrium pH of maximum uptake. This solution was then aged for 2 days and then readjusted back to the same initial pH. This aging cycle was done twice after which the pH of the solution is fairly stable. An aliquot of this solution was set aside for Pt concentration analysis with

ICP. A weighed amount of the XC72-R carbon was added into the solution, corresponding to 500m^2/L surface loading. The slurry was then shaken vigorously (~120rpm) for an hour. After the 1h contact time, the slurry pH was measured and was subsequently filtered. A sample of the filtered liquid was taken and also analyzed for Pt concentration with ICP. Using analysis of the initial and final concentrations of the Pt in solution, the loading of the catalyst prepared was determined. The filtered powder was then dried in an oven at 120°C overnight. After drying, the powder was then reduced at 200°C for 1 h with heating ramp of 2.5°C/min under 25% H_2 - balance He flow (200sccm total) in a horizontal tubular furnace. The resulting catalyst was cooled to room temperature prior to being stored.

The electroless deposition bath formulation used was based on prior work done with depositing Ru on commercial 20 wt% Pt/C [66]. The ED experiments on the SEA prepared base catalyst were done in entirely the same fashion as the ones done on commercial Pt/C. The Pt/C catalyst, 0.5g, was added to a bath volume of 100 mL with pH 3.0. The Ru : FA initial molar ratio is 1 : 6 and aliquots of FA, with the same amount as initially in solution, added every 30min. A series of ED experiments with varying theoretical monodisperse Ru coverages on the Pt surface was prepared at 90 °C water immersion bath temperature except at coverages higher than 0.82 ML which used oil immersion bath at 120 °C and a round bottom flask with a reflux condenser attached.

2.5 Characterization Techniques

Powder X-ray diffraction (XRD) of the catalyst samples were done at specific points of the studies conducted in this work. Samples were pressed on an amorphous glass backed, low background holder which were then loaded in a Rigaku Miniflex II benchtop diffractometer was used with a CuKα radiation source (λ=1.5406 Å) operated at 30 kV and 15 mA. The diffractometer is equipped with a Rigaku D/tex Ultra silicon strip detector capable of detecting sub-nanometer particles at low loadings [67].

A JEOL JEM-ARM200CF, cold field emission, probe aberration-corrected 200kV Scanning transmission electron microscope (STEM) was used to obtain high angle, annular dark field (HAADF) micrographs of the catalysts using either of the two detectors (JEOL and Gatan) fitted on the JEM-ARM200CF. The imaging resolution of the JEM-ARM200CF can go down to 0.078nm with an energy resolution of 0.35eV. X-ray energy dispersive spectroscopy (XEDS) microanalysis can also be done on the same instrument in order to generate elemental maps of bimetallic catalyst particles, acquires using an Oxford Instruments X-Max100TLE SDD detector.

Chemisorption analyses of the catalysts were done in a Micromeritics Autochem II 2920 analyzer which uses pulse chemisorption protocol. A tritration method was used for determining active surface of the Pd/C and Pt/C catalysts, where diluted hydrogen was pulsed on oxygen pre-covered metal surface. Catalysts were subjected to reduction pretreatment at the appropriate temperature and cooled down to 40 °C before being contacted with 10% O_2 balance He for 30 min after which Ar is flowed to purge physisorbed O_2. At the same temperature, 10% H_2 balance Ar is pulsed which reacts with the chemisorbed oxygen to form water and chemisorbed H. The stoichiometry of the

chemisorption is 0.667 Surface Metal : 1 H_2. Particle dispersion was then obtained from the hydrogen consumption and catalyst loading while size estimates were calculated assuming hemispherical geometry.

2.6 Electrochemical Evaluation

In testing the electrochemical performance of the bimetallic catalysts, cyclic voltammetry (CV) and rotating disk electrode (RDE) tests were done. An ink was prepared from the powders by weighing 10 mg and sonicating in a solution containing 5 mL each of de-ionized water and isopropyl alcohol. 18.5 µL of this ink was placed on a disk electrode, made of Pt for the Ru-Pt bimetallic catalysts and glassy carbon for the Pt-Co series. After drying, 5 µL of 5 wt% nafion in isopropyl alcohol was used to bind the powder on the disk electrode surface.

The electrolyte, counter electrode and reference electrodes used for the Pt-Co system was a 0.1 M $HClO_4$ soltion, Pt wire, and Ag/AgCl respectively. While for Ru-Pt system, a solution of 0.5 M H_2SO_4 with 1 M methanol was used as electrolyte, and luggin capillary Hg/HgSO4 and Pt wire were used as reference and counter electrode, respectively.

Conditioning scans for CV were done at 50 mV/s. and measurement scans were done at 5 mV/s. Scan windows for the Ru-Pt and Pt-Co systems were -0.1 to 1.3 V and 0.0 to 1.2 V versus SHE.

For the Pt-Co system, CV tests were done with nitrogen gas purging for the electrolyte. Upon completion of the CV scans, the gas was switched to oxygen, purging the electrolyte for at least 20 min before oxygen reduction reaction (ORR) experiments

were conducted. The 5 mV/s scan rate was also used for ORR measurements with rotating disk electrode configuration at rotation speeds from 350 to 1600 RPM.

CHAPTER 3

CHEMISORPTION – XRD PARTICLE SIZE DISCREPANCY OF CARBON SUPPORTED PALLADIUM: CARBON DECORATION OF PD?[1]

[1] Tengco, J.M.M., Lugo-Jose, Y.K., Monnier J.R., and Regalbuto, J.R.. 2015. *Catalysis Today*. 246: 9-14
Reprinted here with permission of publisher

3.1 Abstract

A systematic discrepancy is often observed between chemisorption versus X-ray diffraction and/or electron microscopy-determined nanoparticle size estimates for metals supported on carbon. It is hypothesized that lower than expected chemisorption capacity is due to decoration of the metal surface by the carbon support. To test this, a series of carbon supported Pd nanoparticles with different pretreatments was prepared and analyzed using Temperature Programmed Oxidation. Carbon oxidation peaks distinct from high temperature bulk carbon burn off were observed for all samples at around 250 °C and 300 °C. A short oxidation at the latter temperature appears to remove the decorating layer as the TPO peaks disappear and the reduced metal surface chemisorbs at close to the expected capacity.

3.2. Introduction

In the preparation of supported metal nanoparticle catalysts, activity is largely dependent on availability of surface sites to participate in a desired reaction. The degree of metal utilization is often reported as dispersion – the fraction of metal atoms at the surface of the particle. Smaller particles, having higher surface to volume ratio, have higher dispersion and more metal surface sites, which generally translates to higher activity per mass of metal.

Measurement of metal dispersion and nanoparticle size can be estimated with a variety of techniques. Chemisorption is commonly used by determining the amount of gas selectively adsorbing or reacting onto the surface of the metal and relating this to the number of surface metal sites using a predetermined chemisorption stoichiometry.

Assuming a particular geometry, dispersion can be simply converted to particle size. The common methods of powder X-ray diffraction (XRD) and electron microscopy (EM), determine the size of metal nanoparticles directly; XRD through application of the Scherrer equation, and EM, through image analysis. In theory, particle size and dispersion estimates of all three methods should agree.

In the case of carbon supported metal catalysts, we have noticed a systematic discrepancy between size/dispersion values obtained from chemisorption and XRD (and/or EM) in our lab and in the literature. This very rarely is the case with oxide catalyst supports (e.g. silica and alumina). A literature sampling of carbon supported catalysts exhibiting this discrepancy is shown in Table 3.1. In the studies that employed both XRD and EM it is noted that the size estimates of these two methods were in agreement. On the other hand, larger particle sizes are always reported from chemisorption, at differences as far apart as 500%.

We hypothesize that the endemic chemisorption – XRD (/EM) discrepancy is due to the formation of a carbon overlayer on the surface of the metal nanoparticles during preparation of these catalysts. This overlayer blocks access to the metal surface causing lesser gas chemisorbed than an unblocked surface, in turn giving a lower dispersion measurement than expected when compared to XRD. In the case of carbon supported palladium (Pd/C), it has been reported that there can be carbon decoration on Pd surface sites [48, 49]. Also, first-principles simulations of carbon dissolution have shown the possibility of carbon on the Pd surface or subsurface depending on the exposed facet [50].

Determination of surface contamination by carbon cannot be done in conventional characterization techniques (i.e. XPS, EM) due to the interference of adventitious carbon. In this study, we have employed Temperature Programmed Oxidation (TPO) as a diagnostic, with the idea that carbon directly on the surface of a good oxidation catalyst will burn away more quickly than the support carbon. From the TPO results, a method of recovering the metal surface was then developed.

Table 3.1 Carbon supported catalysts exhibiting a discrepancy between bulk sizing methods (XRD and/or EM) and Chemisorption estimated particle size.

Catalyst System[a]	**Metal Loading (%)**	**Chemisorption Size (nm)**	**XRD Size (nm)**	**EM Size (nm)**	
Pd/AC	7.8	131	20	49[b]	[40]
Pd/Graphite	8.5	57	25	24[b]	
Pd/GNF	8.7	75	23	37[b]	
Pd_{10Med}/C_{PPh2}	1.7	5.7	--	1-2	[41]
Pd_{12Med}/C_{PPh2}	2.1	12.8	--	2	
Pd/C	5	8.5	6.7	5.9	[42]
CNF-Pt	2	4	v.s.[c]	--	[43]
CNF-Pd	2	18	13.6[d]	--	
CNF-Ru	2	20	v.s.[c]	--	
Pt/VC	19.2	12	2.7	2.2	[44]
Pt/VM	20	24	5.4	5.3	

[a] Notation preserved from reference
[b] Surface average size
[c] Diffraction peaks too broad or undetectable, very small particles
[d] Estimated from diffraction profile

3.3 Experimental

3.3.1 Catalyst Preparation

The Pd/C catalysts were prepared by strong electrostatic adsorption [68]. The carbon support was obtained from BASF (identified as CP-97) with surface area 615 m^2/g and point of zero charge (PZC) 8.5. Sodium tetrachloropalladate (98%), purchased from Aldrich, was employed as the precursor salt, dissolved in deionized water at a nominal concentration of 150 ppm. Adsorption experiments were done by contact of the support with the precursor solution at a surface loading of $500 m^2/L$. The initial pH of the precursor solution was varied to give different final, equilibrium pH after an hour of contact with vigorous shaking. An aliquot was then filtered by syringe and the Pd uptake was determined by measuring the change in concentration in the solution using inductively coupled plasma optical emission spectroscopy (ICP). The optimal pH for the adsorption of the $[PdCl_4]^{2-}$ ion to the support surface was determined from this uptake survey. Larger final batches of impregnated catalyst were prepared at this pH and were subsequently filtered and dried. Metal loading was obtained from ICP analysis of Pd in the precursor solution used for the final batch. Prior to reduction at 350°C for 2 h, the dried catalysts were first subjected to three different pretreatments: direct reduction at 150 °C for an hour, labeled as Pd/CP97; a second batch was annealed in helium at 300 °C for an hour, labeled as Pd/CP97-A; and another was calcined in air at 300 °C for an hour, labeled as Pd/CP97-C. The surface area of the Pd/CP97 catalyst decreased from 617 to 580 m^2/g, which is a smaller decrease (6 %) than expected with the addition of 10 wt% Pd but is within experimental error.

3.3.2 Catalyst Characterization

The series of carbon supported Pd catalysts were then characterized by XRD and pulse chemisorption to obtain average particle size estimates. A Rigaku Miniflex II X-Ray Diffractometer was used in obtaining the XRD profiles of the catalysts. Background stripping and deconvolution of peaks contributed by Pd and carbon support were done in PDXL 2.0 provided by Rigaku, using Split Pseudo-Voigt function for the peaks. The protocol used for chemisorption involved hydrogen titration of oxygen pre-covered Pd surfaces. A pretreatment step was included with reduction at 350°C for 2 h. The catalyst was then contacted with 10% oxygen in helium at 40 °C for 30 min to oxidize the surface Pd to PdO. Still at 40 °C, it was titrated with pulsed 10% hydrogen in argon to form water and surface Pd with chemisorbed hydrogen. In between reduction, oxygen pre-covering, and titration, flowing inert gas (argon or helium) purged the sample cell. The assumed overall stoichiometry is 0.667 Pd:1 H_2. Particle sizes were estimated from chemisorption assuming hemispherical geometry, while XRD based particle size was calculated using the Scherrer formula for line broadening.

3.3.3 Electron microscopy

Further particle size determination for the Pd/CP97-C catalyst was made with an aberration-corrected JEOL 2100F scanning transmission electron microscopy (STEM) using Z-contrast imaging.

3.3.4 Temperature Programmed Oxidation

The catalyst samples were loaded in a custom TPX System fitted with an Inficon Transpector 2 Mass Spectrometer. Moisture was removed by heating at 200 °C and flowing He, until the water signal is diminished. TPO was done immediately afterwards, with a ramp of 5 °C/min, flowing 10% oxygen in helium at 20 sccm. The oxygen and carbon dioxide signals were primarily monitored during the experiment. The spectrum from 1 to 50 amu was recorded. A control TPO experiment using only the support was also carried out for comparison with the catalyst samples.

3.3.5 Catalyst Surface Recovery

After TPO experiments, upon determining the burn-off temperature of decorating carbon, a method of recovering the catalyst surface was developed. For the Pd/CP97-C sample, TPO was carried out ramping up to the burn-off temperature and holding the temperature for half an hour. The system was purged with helium and cooled to room temperature and subjected to TPO again. Additional cycled TPO experiments featured in situ reduction in between the two TPO runs. The reduction was done in flowing hydrogen, ramping at 5 °C/min to temperatures of 50 °C, 200 °C, or 350 °C for an hour and subsequent purging and cool down in helium. Chemisorption with the same protocol as the cycled TPO experiments were performed to confirm recovery of Pd surface. In the chemisorption analysis, the second TPO is replaced with the oxygen pre-covering and pulsed hydrogen titration.

3.4 Results

The uptake survey for the SEA experiment using tetrachloropalladate precursor with the CP-97 powder is shown in Figure 3.1. Maximum uptake was observed at an equilibrium pH around 2.5. The loadings and size estimates of the final batches of catalysts prepared for this study are shown in Table 3.2. On average, a loading of 10% Pd was obtained using this method. It should be noted that deviations in the metal loading observed for this series of catalysts can happen when using SEA with a slight change in the equilibrium pH [64].

XRD profiles of the three samples are shown in Figure 3.2. The sizes were straightforwardly obtained for the directly reduced and annealed samples, giving particles sizes of 12 nm and 10.4 nm respectively. For the calcined sample, a bimodal size distribution was observed. By isolating the signal contribution from the Pd reflections using Fityk 0.9.8 [69], the peak contributions of the small (broad peak) and large size (sharp peak) fractions were deconvoluted as shown in Figure 3.3. Size estimates for each of the fractions were then calculated from peak broadening, with the data from the Pd reflections in agreement with each other giving 16 nm for the sharp peaks and 2 nm for the small peaks. From the relative areas of the deconvoluted peaks seen in Figure 3.3b and c, about 20% of the Pd was present as the large particles and 80% was present as the small particles. Using these mass fractions [70], the mean size was calculated to be 4.6 nm.

A STEM image of the Pd/CP97-C sample shown in Figure 3.4, representative of about 22 such images, reveals a majority of relatively well dispersed particles in addition to what appears to be some agglomerated Pd. The size distribution reported in the inset

chart in Figrue 3.4 was made from 740 of the well dispersed particles (the larger agglomerates were not quantified as they were too few in number to obtain sufficient counting statistics) and number, surface, and volume averages are provided in Table 3.3. The volume average is used for comparison with XRD and the surface average with chemisorption [71].

Size estimates for chemisorption are summarized in Table 3.2 and are compared to XRD estimated sizes. For the Pd/CP97-C, the EM volume average value of 5.6 nm is 22% above the XRD size estimate of 4.6 nm; this is relatively reasonable agreement. The higher value of the EM estimate suggests that some of the Pd particles are twinned, which XRD inherently detects but which is harder to observe in the relatively low magnification STEM images used for the particle size analysis. In any case, the chemisorption estimate of particle size of 17.2 nm, is three to four times higher than the XRD and EM estimates. For the other samples the chemisorption size is about 150% of the XRD estimate for the Pd/CP97-A sample, and 175% that of the Pd/CP97 sample. We attribute this discrepancy to the formation of a carbon overlayer during preparation. This resulted in lower hydrogen titrations due to substantially blocked Pd surfaces.

Assuming the presence of this decorating layer, TPO was conducted to see whether burn-off would occur in a manner distinguishable from bulk support combustion. The TPO profile of the pure carbon support is shown in Figure 3.5(a) and serves as a control experiment. The bulk carbon burn-off temperature is estimated at about 400 °C, where the CO_2 signal starts to take off and the O_2 signal drops until the system is oxygen limited at around 575 °C.

In comparison, for the directly reduced Pd/CP97 sample in Figure 3.5(b), the bulk carbon starts to burn off about 100 °C lower, at about 300°C. This is not unexpected as Pd will catalyze the oxidation of carbon. A notable feature of the TPO profile of the Pd/CP97 sample is the presence of two additional low temperature burn-off peaks, around 260 °C and 320 °C. The presence of these low temperature peaks suggests carbon with enhanced interaction with Pd. This would be expected for thin moieties of carbon decorating the Pd surface, compared to bulk support carbon.

The TPO profiles of the annealed and calcined samples, Pd/CP97-A and Pd/CP97-C, shown in Figure 3.5(c) and (d) respectively, also show Pd assisted oxidation of bulk carbon and the two low temperature oxidation peaks. The bulk burn-off of the Pd/CP97-C sample in Figure 3.5(d) begins at about 200-250 °C which is consistent with the presence of smaller particles with greater perimeter area. By calibration of the TPX system for CO_2, the amount of carbon burned off in the low temperature peaks were calculated from the deconvolution data. Using the XRD size as a basis for the amount of Pd on the surface of the particles, the equivalent amount of carbon decoration for each catalyst was determined and is summarized in Table 3.4. The Pd/CP97 and Pd/CP97-A samples, which showed prominent peaks in their TPO profiles have around six monolayers of carbon decoration. For the Pd/CP97-C sample, perhaps three monolayers of carbon was burned off. As chemisorption indicates at least some accessibility to the Pd surface, the decorating carbon likely exists as discrete islands or clusters dispersed on the surface of the Pd nanoparticle.

Based on the TPO results of Figrue 3.5, a low temperature oxidation procedure was developed to burn off the (presumed) decorating forms of carbon. The profiles for a

cycled TPO experiment using the Pd/CP97-C sample are presented in Figure 3.6. During the initial oxidation ramp and dwell period in Figure 3.6(a), the subtle low temperature oxidation peaks were present. After cooling and repeating the TPO, the low temperature peaks were no longer observed. For the repeated TPO, the bulk burn-off temperature is still lower than that of carbon support alone. Notably, the bulk burn-off at about 250 °C is approximately the same as the deconvoluted signal for catalyzed oxidation of bulk carbon presented earlier. The surface area after the burn-off increased from 580 to 640 m^2/g which is consistent with a roughening of the carbon surface consumed in the proximity of Pd nanoparticles.

In situ reduction at varying temperatures was incorporated in the cycled TPO experiments to determine whether reduction causes decoration. The profiles for these are presented in Figure 3.6(b)-(d). Repeat TPO after the in situ reduction step showed no low temperature carbon burn off peaks and the TPO profiles match that of Pd catalyzed oxidation of bulk carbon support. We conclude that carbon decoration does not occur during these reduction steps to a significant degree, and if so, the Pd surface should be wholly accessible to chemisorption.

Thus a pretreatment protocol for Pd/CP97-C based on the cycled TPO experiments with in situ reduction was implemented in the chemisorption apparatus. After oxidation up to the second burn off peak and reduction of the Pd at the various reduction temperatures, chemisorption resulted in the smaller particle size estimates shown in Table 3.5. Recall, for comparison, that the initial chemisorption without oxidation pretreatment was 17.2 nm (Table 3.3). In situ reduction at 50 °C and 200 °C yielded chemisorption sizes (6.2 and 5.6 nm) closer to the XRD size of 4.6 nm and the

STEM surface average size of 5.2 nm. The sample subjected to a higher reduction temperature of 350 °C however still gave a chemisorption size about twice of the XRD value, likely due to sintering at the higher re-reduction temperature [72].

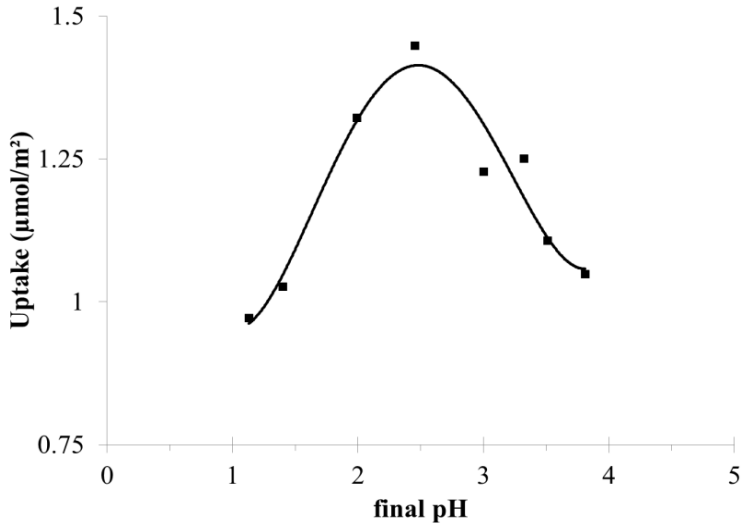

Figure 3.1 Uptake of $[PdCl_4]^{2-}$ on CP-97 carbon support as a function of equilibrium pH.

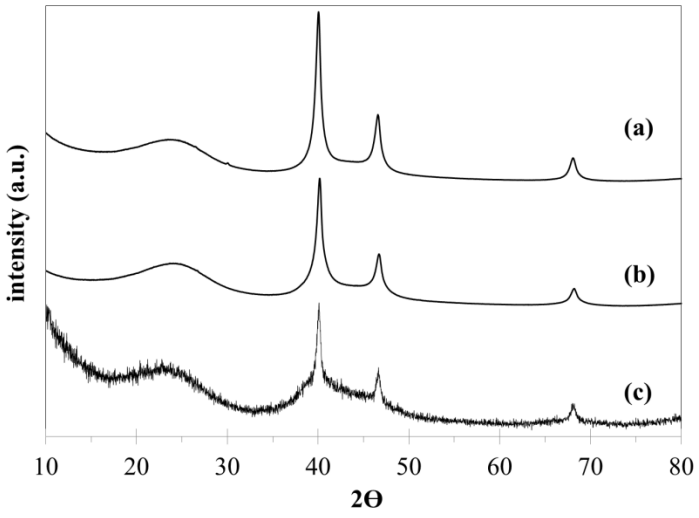

Figure 3.2 XRD profiles of the catalyst series (a) directly reduced - Pd/CP97, (b) annealed - Pd/CP97-A, (c) calcined - Pd/CP97-C.

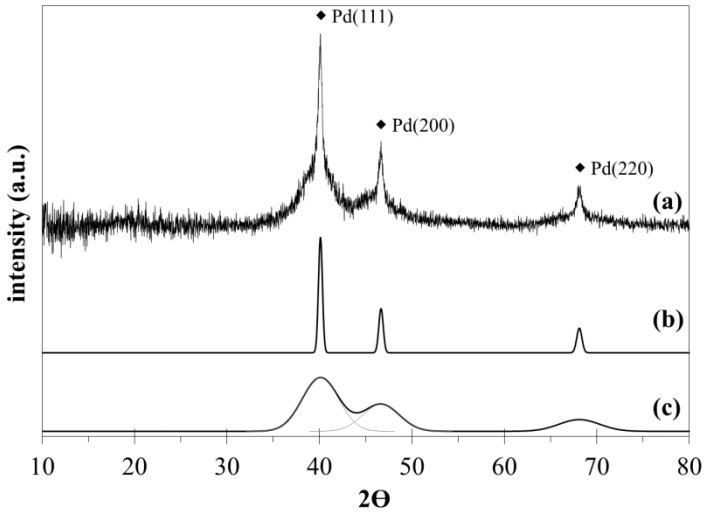

Figure 3.3 Deconvolution of bimodal size distribution XRD peaks for the Pd/CP97-C catalyst: (a) Isolated XRD signal contribution of Pd, (b) peak signal contribution from large particles, (c) peak signal contribution from small particles.

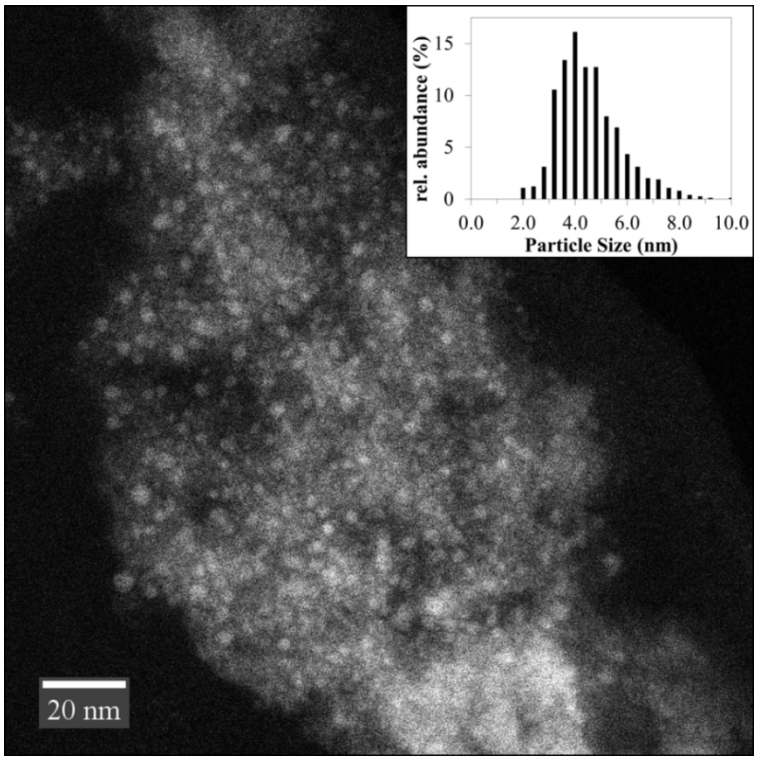

Figure 3.4 Representative STEM image showing presence of agglomerated Pd domains and size distribution (inset) of well dispersed Pd particles.

Table 3.2 Metal loadings of carbon supported Pd catalysts and estimated average particle sizes from XRD and chemisorption.

Catalyst	Pd Loading (%)	XRD Size (nm)	Chemisorption Size (nm)
Pd/CP97	9.8	12	21
Pd/CP97-A	8.2	10.4	14.7
Pd/CP97-C	12.2	4.6	17.2

Table 3.3 Average size of particles based on STEM images.

Type of Average	Formula[b]	Average Size (nm)
Number	$d_n = \frac{\sum_{i=1}^{j} n_i d_i}{\sum_{i=1}^{j} n_i}$	4.5
Surface	$d_s = \frac{\sum_{i=1}^{j} n_i d_i^3}{\sum_{i=1}^{j} n_i\, d_i^2}$	5.2
Volume	$d_v = \frac{\sum_{i=1}^{j} n_i d_i^4}{\sum_{i=1}^{j} n_i\, d_i^3}$	5.6

[b]Analysis class size = 1Å

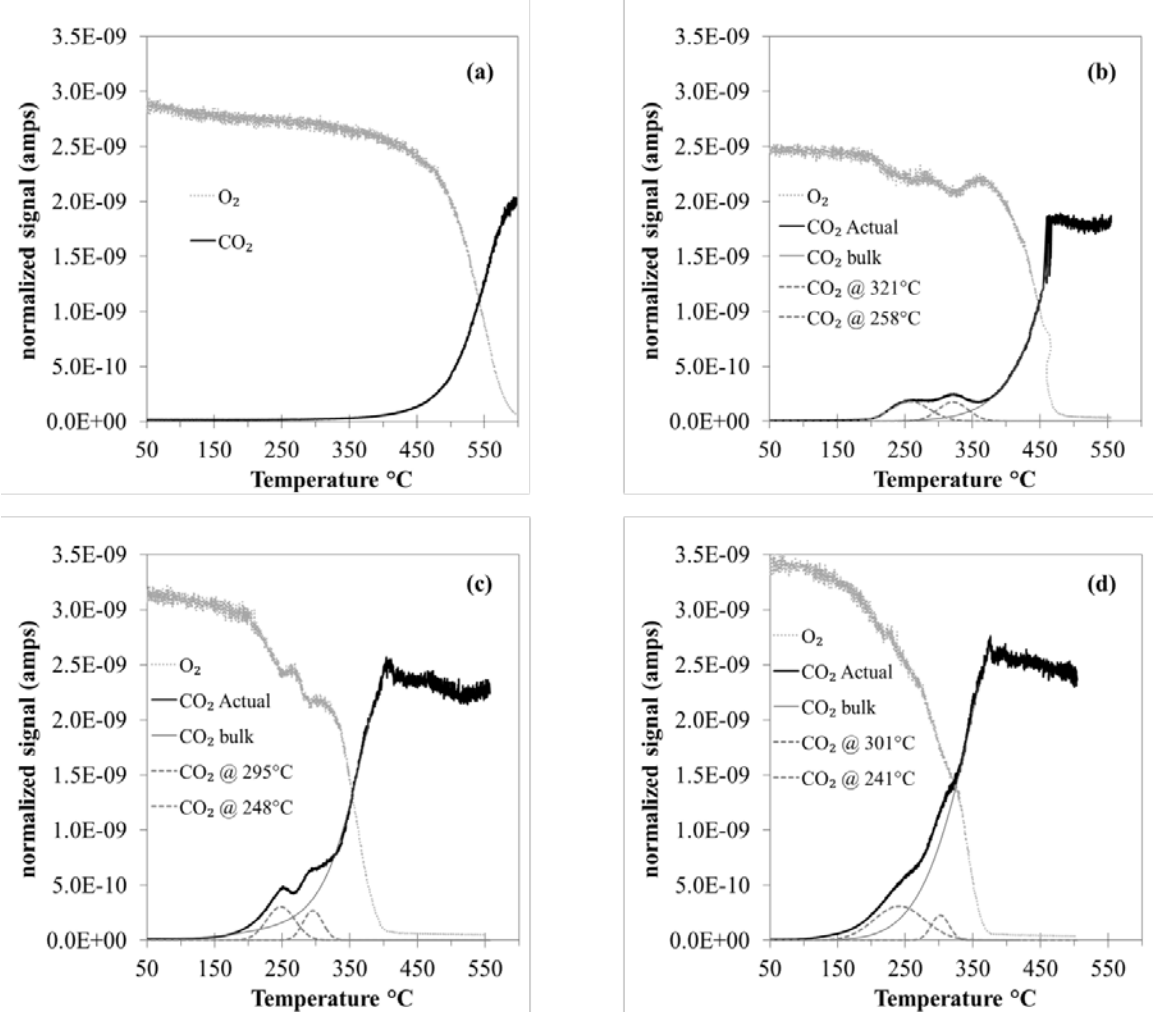

Figure 3.5 TPO profiles: (a) CP-97 carbon support control experiment, (b) Pd/CP97, (c) Pd/CP97-A, (d) Pd/CP97-C.

Table 3.4 Data for deconvoluted low temperature carbon burn-off peaks.

Catalyst	Peak Center (°C)	Total Area (amp·°C)	Equivalent Coverage (ML)[a]
Pd/CP97	258	1.33×10^{-8}	5.7
	321	1.00×10^{-8}	
Pd/CP97-A	248	1.61×10^{-8}	6.3
	295	9.80×10^{-9}	
Pd/CP97-C	241	2.90×10^{-8}	3.0
	301	7.50×10^{-9}	

[a] Based on surface Pd atoms estimated from XRD particle size

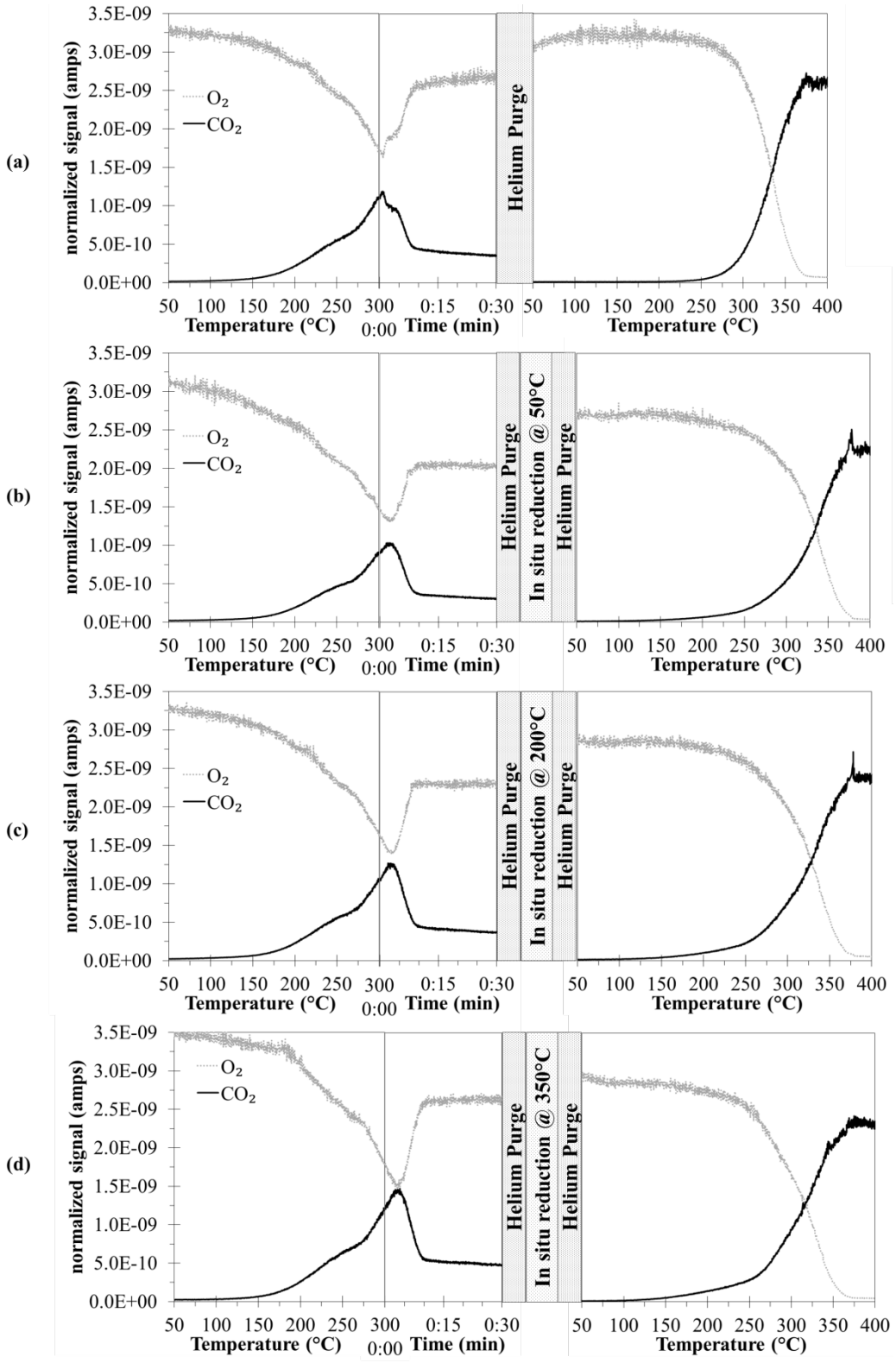

Figure 3.6 Cycled TPO profiles for Pd/CP97-C catalyst: (a) no reduction, (b) in situ reduction at 50°C, (c) reduction at 200°C, (d) reduction at 350°C.

Table 3.5 Chemisorption results for Pd/CP97-C catalyst using protocol with in situ TPO (burn off) and reduction at different holding temperatures.

In situ reduction temperature (°C)	Chemisorption size (nm)
50	6.2
200	5.6
350	8.6

3.5 Discussion

It would appear that the 40 °C temperature of the oxygen pre-covering step in the chemisorption protocol is too low to remove the surface carbon. The TPO experiments reveal that higher temperatures are required, with one burn off peak around 250-260 °C and another around 300-320°C. The presence of two burn off peaks suggests two types of carbon on palladium, having different interactions with the metal. A simulation study has shown that carbon dissolution is possible for the Pd/C system [50]. It was found that formation of carbon nucleation sites can vary depending on the exposed Pd surface. It was postulated that carbon coverage on Pd(1 0 0) will be most stable on the surface, while on Pd(1 1 1) carbon is most stable in the subsurface position. At higher coverages, carbon will likely dissolve into the Pd. This may also explain why Pd has at least some chemisorption capacity even with the relatively high amounts (3–6 ML) of decorating carbon. In the deconvolution of the TPO spectra for CO_2, the two lower temperature burn-off peaks are assigned to the carbon on Pd particles. While speculative, the peak at the slightly higher temperature may be attributed to the subsurface carbon as higher energy is needed to overcome diffusion limitations. In the absence of decorating carbon,

the presence of Pd can cause spillover oxidation, catalyzing burn-off of carbon support in close contact. The contributions of the oxidation of decorating carbon and support to the TPO spectra are illustrated in Figure 3.7.

The mechanism of decoration is still unkown. Decoration did not occur during reduction in the TPO cycles. Perhaps the oxidation removed not only the decorating carbon layer, but also a remnant from synthesis such as residual chloride [13], which had catalyzed carbon decoration of the metal surface. Alternately, chloride might be lost at the initial high temperature reduction [73] but only after decoration had been induced. The presence of residual chloride on carbon after low temperature reduction of chloride Pt precursors is common [74]; this may actually explain the frequency of the observed discrepancy. Unfortunately we could not detect molecular chlorine or chlorine dioxide due to the limited scan range (up to 50 amu) used in the experiments. On the other hand, only three of the five references listed in Table 3.1, [42],[43], and [44] employed chloride-based precursors, one used Pd nitrate [40] and another used carbonyl-phosphine palladium clusters. The role of the metal salt counterion in the mechanism for decoration is being explored further.

The cycled TPO experiments demonstrate a method to remove carbon decoration from nanoparticles, which recovers metal active surface area and enhances reactivity. The temperature of burn-off appears to be far enough below that of bulk support combustion such that the integrity of the support is retained. These results also suggest that mild oxidation should be incorporated into chemisorption protocols to properly characterize carbon supported metal nanoparticles. An appropriate in situ reduction temperature needs to be carefully determined as our results suggest that sintering occurs if the re-reduction

temperature is too high. This can be determined by a simple temperature programmed reduction experiment.

The literature survey summarized in Table 3.1 reveals that large size discrepancies occur for other carbon supported metals. Carbon decoration may well be widespread, as formation of stable metal carbides and carbon dissolution is not uncommon [75, 76]. We suspect this phenomenon is prevalent and are studying other types of carbon and other metals to confirm this, as well as to determine the mechanism of decoration.

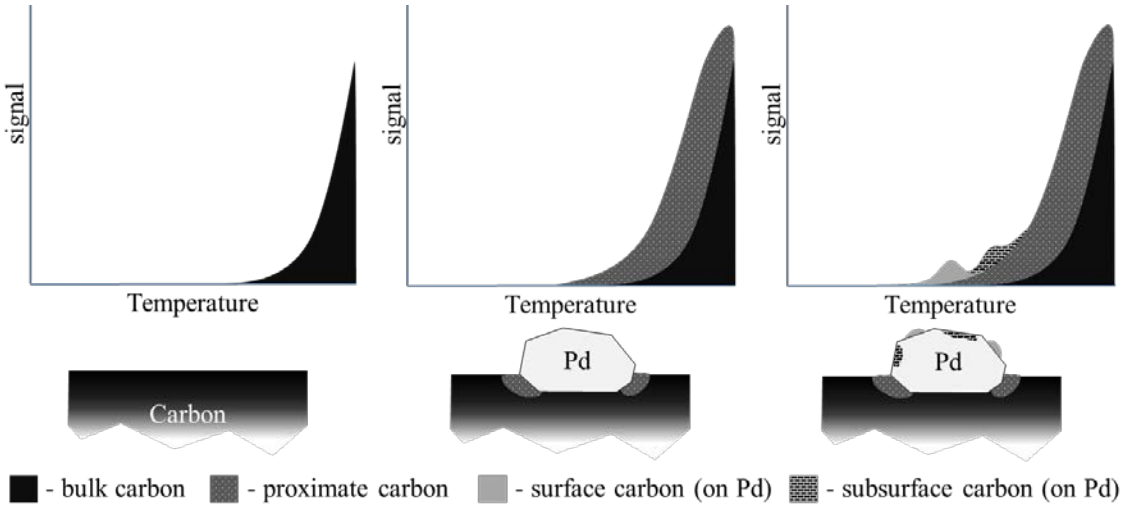

Figure 3.7 Illustration of mass spectroscopy CO_2 signal contribution from burn-off of different regions of carbon in Pd/C catalyst.

3.6 Conclusions

Particle size estimates from chemisorption are often seen to be much larger than estimates from XRD and/or EM. The current results suggest that this discrepancy is caused by a decorating layer of carbon, the genesis of which is still not understood, but the presence of which is clearly indicated by temperature programmed oxidation. The

decorating layer appears to burn off at a temperature sufficiently lower than bulk support oxidation, such that mild oxidation can be used to recover the entirety of the metal surface without destroying the pore volume of the support. TPO can be used to diagnose decoration when the discrepancy is observed, and the oxidation step and a mild re-reduction step should be accordingly incorporated into chemisorption protocols.

3.7 Acknowledgements

The authors would like to acknowledge Ritubarna Banerjee and Yunya Zhang for special assistance in this work, as well as the support of the center of Catalysis for Renewable Fuels (CReF) at USC.

CHAPTER 4

SYNTHESIS AND ELECTROCHEMICAL EVALUATION OF CARBON SUPPORTED PT-CO BIMETALLIC CATALYSTS PREPARED BY ELECTROLESS DEPOSITION AND MODIFIED CHARGE ENHANCED DRY IMPREGNATION[2]

[2] Tengco, J.M.M., Tavakoli Mehrabadi, B.A., Zhang, Y., Wongkaew, A., Regalbuto, J.R., Weidner, J.W., and Monnier, J.R. 2016
Submitted to *Catalysts (MDPI)*, 03/31/2016

4.1 Abstract

Carbon-supported bimetallic Pt-Co cathode catalysts have been previously identified as higher activity alternatives to conventional Pt/C catalysts for fuel cells. In this work, a series of Pt-Co/C catalysts were synthesized using electroless deposition (ED) of Pt on a Co/C catalyst prepared by modified charge enhanced dry impregnation. XRD and STEM characterization of the base catalyst showed highly dispersed particles. A basic ED bath containing $PtCl_6^{2-}$ as the Pt precursor, dimethylamine borane as reducing agent, and ethylenediamine as stabilizing agent successfully targeted deposition of Pt on Co particles. Simultaneous action of galvanic displacement and ED resulted in Pt-Co alloy formation observed in XRD and XEDS mapping. In addition, fast deposition kinetics resulted in hollow shell Pt-Co alloy particles while particles with Pt-rich shell and Co-rich cores formed with controlled Pt deposition. Electrochemical evaluation of the Pt-Co/C catalysts showed lower active surface but much higher mass and surface activities for oxygen reduction reaction compared to a commercial Pt/C fuel cell catalyst.

4.2 Introduction

Successful commercial adaptation of fuel cells is very much reliant on the economic viability of this technology. Proton exchange fuel cells (PEMFCs) are highly considered for wide scale use in small form factor applications such as vehicles and mobile technology owing to their high performance and compact design. Improving the cost competitiveness of PEMFCs can be done by enhancing the activity and durability of the catalyst employed [77, 78]. One of the most widely used catalysts for electrochemical (i.e. oxygen reduction reaction, ORR) applications is a carbon-supported platinum

catalyst (Pt/C) which has well-recognized issues with activity degradation from particle instability and corrosion of the metal and support. Increasing catalyst activity can be done by synthesizing smaller particle sizes to achieve greater metal dispersion, where dispersion is defined as the fraction of the metal atoms exposed on the surface. Various methods have been developed to increase metal dispersion specially for Pt/C catalysts, however there are also arguments against smaller Pt particles in ORR catalysts as some studies have pointed to lower specific activity for highly dispersed (50-100%) platinum for ORR applications [79-81]. Catalyst durability on the other hand largely depends on the stability of the metal-support system, mainly to the resistance of the metal towards sintering and corrosion in the electrochemical system. While smaller Pt particles may have higher active site concentrations for a given weight loading, they tend to sinter more easily giving larger particles with lower active site concentrations. One way to improve durability of Pt fuel cell catalysts is by anchoring particles on the support with a different metal that is more resistant to sintering, such as Pd or Co, or by forming Pt alloys with the second metals that have higher corrosion resistance [52, 82, 83]. The formation of alloyed Pt-M bimetallic catalysts, where M is another transition metal, can also increase catalyst activity, particularly with the Pt-Co system [82-84].

The conventional choice of method for commercial preparation of metallic catalysts is simple impregnation of an aqueous solution of a metal precursor salt into the pores of the support. This straightforward method often results in poor dispersion of the final metal particles and a wide distribution of particle sizes. Extending this method to bimetallic catalysts also results in poor distribution of the component metals and forms fractions of both monometallic components as well as bimetallic particles with a wide

range of compositions. The bimetallic particles can also be considered as bulk compositions, with little knowledge of the actual surface components. The methods of strong electrostatic adsorption (SEA) and its incipient wetness analog, charge enhanced dry impregnation (CEDI) have been used for the preparation of well dispersed catalysts with narrow size distributions [7, 85]. The manipulation of impregnation pH during SEA induces a charge on the surface of the support by protonation or deprotonation of surface functional groups depending on the point of zero charge of the support [64]. In effect, the charged surface electrostatically adsorbs an oppositely charged precursor complex wherein the strong complex-support interaction decreases mobility during thermal treatment to facilitate small particle formation. For the formation of bimetallic catalysts, the method of electroless deposition (ED) has been shown to form true bimetallic catalysts with no particles of each of the monometallic components [66, 86-88]. Further, because the first step in ED is the activation of a solution phase reducing agent on the surface of the base catalyst particles, there is targeted reduction of the secondary metal salt in solution (catalytic or auto-catalytic deposition) to form surfaces with known compositions of each metal.

The use of SEA and ED methods have been previously demonstrated for preparation of bimetallic fuel cell catalysts [22, 23, 31, 66, 85, 89, 90]. Specifically, ED has been previously used for preparation of a family of Pt-Co bimetallic PEMFC catalysts, where different amounts of Pt were deposited on the surface of cobalt particles [17]. The Co catalyst was prepared by impregnation of $CoCl_2$ on the carbon support to give Co particles varied in size from 3 – 15 nm in diameter. This work extends those previous studies by reformulation of the electroless developer bath and using Pt loadings

lower than those commonly used in commercial samples. Charge enhanced dry impregnation (CEDI) was used to prepare the Co core component to give well-dispersed and uniform sized particles as the base catalyst for ED of Pt. The catalysts have been well-characterized and evaluated for oxygen reduction reaction (ORR) performance. Results are compared with a commercially-available, high Pt loading catalyst.

4.3 Experimental

4.3.1 Carbon supported cobalt (Co/C) base catalyst

A modified CEDI method [7, 85] was employed in the preparation of the base Co/C catalyst for Pt deposition; nominal loadings of 2.5 wt% and 5.0 wt% Co were targeted. Appropriate amounts of cobalt(II) nitrate hexahydrate ($Co(NO_3)_2 \cdot 6H_2O$) and an equimolar amount of citric acid were dissolved in a volume of DI water required for pore filling of the carbon support to be impregnated. The pore volume of 3.5 mL/g for the carbon support (Acetylene Black, Toyota, specific surface area: 320 m^2/g, PZC = 3.4) was determined by saturation with deionized water to the state of moistness of the support. The cobalt nitrate-citric acid solution was added dropwise to the carbon with vigorous mixing during addition to give efficient distribution of the precursor liquid in the carbon. The resulting paste was then dried at 25°C before being crushed into powder.

Temperature programmed decomposition (TPD) of the precursor in flowing He was conducted on a small portion of the dried powder using a Micromeritics Autochem II 2920 Analyzer. Formation of decomposition products was monitored with a thermal conductivity detector (TCD). The peak decomposition temperature was then used for the annealing treatment in flowing He (4 h) for the remainder of the powder. A fraction of

the annealed powder was then used for temperature programmed reduction (TPR) analysis in the Autochem II analyzer with using 10% H_2/balance Ar. Hydrogen consumption was monitored using the TCD. The peak temperature for H_2 consumption was set as the reduction temperature (1 h) for the balance of the annealed powder. All annealing and reduction treatments were done in a horizontal tubular furnace and temperature ramp rates for all thermal treatments were set at 5 °C/min. The base Co/C catalyst was then characterized by powder X-ray diffraction (XRD) and high angle annular dark field - scanning transmission electron microscopy (HAADF-STEM) for determination of Co nanoparticle sizes and subsequent calculation of the concentration of cobalt surface sites, assuming spherical Co particles. Details of these characterization techniques are included in the latter part of this section.

4.3.2 Electroless deposition of Pt

The electroless developer bath used for the deposition of platinum was based on previous work by Beard et al. [22, 23, 31], with the modification of substituting citrate for ethylenediamine (EN) as a stabilizing and chelating agent for Pt^{4+} [89]. For the ED experiments, the aqueous bath was maintained at pH 10 and chloroplatinic acid (H_2PtCl_6) used as the Pt source (existing as $[PtCl_6]^{2-}$ complex in basic solution) and dimethylamine borane ($(CH_3)_2NH{\cdot}BH_3$, DMAB) as the reducing agent. Preliminary thermal stability experiments for the bath were conducted to determine a stable formulation of the Pt precursor, reducing agent, and stabilizer, ensuring that $PtCl_6^{2-}$ did not reduce or precipitate in solution. From the stability experiments, a formulation of Pt : DMAB : EN

= 1 : 5 : 4 molar ratio, which was stable at 50°C up to a maximum concentration of $PtCl_6^{2-}$ = 120 ppm, was used.

After addition of the Co/C base catalyst to the bath, Pt and Co concentrations were determined by Atomic Absorption Spectrometry (AAS, Perkin Elmer AAnalyst 400). Small aliquots of the bath were withdrawn and syringe-filtered at predetermined time intervals and then analyzed. Electroless deposition experiments were conducted for 60 minutes; a second aliquot of DMAB was added after 30 minutes. Particulars for the ED experiments are listed in Table 4.1. The amounts of $PtCl_6^{2-}$ initially present in the ED bath that correspond to the target coverage based on the calculation of available Co surface sites (from prior XRD characterization). One monolayer (ML) of monodisperse coverage of Pt corresponds to one atom of Pt per one Co surface site.

After each ED experiment, the slurry was filtered and the catalyst powder was washed thoroughly (~2 L) with DI water. Samples were then dried at room temperature before reduction at 200°C (5°C/min ramp rate) for 1h in flowing 25% H_2/balance He at 200 SCCM total flow.

Table 4.1 Electroless deposition experiment parameters.

Catalyst	Target Pt Coverage (ML)	Total Co/C amount used (g)	Total Bath Volume (mL)
2.5% Co/CB1	1.5	1.0	600
	3.0	0.5	600
5.0 % Co/CB1	1.5	1.0	1200
	3.0	0.5	1200

4.3.3 Catalyst Characterization

XRD characterization of the catalysts was done using a Rigaku Miniflex II benchtop diffractometer. The diffractometer is equipped with a Cu Kα X-ray source and fitted with a silicon slit detector that is capable of detecting particles in the sub-nanometer size range [67].

Micrographs from HAADF-STEM of the samples were acquired with the cold field emission JEOL JEM-ARM200CF STEM. The JEOL JEM-ARM200CF is probe aberration corrected with a 200kV beam and the particular microscope used is fitted with JEOL and Gatan detectors for HAADF imaging. Additional imaging of the Pt-Co/C ED particles were carried out using X-ray energy dispersive spectroscopy (XEDS) for elemental mapping of Pt and Co. These maps were generated using an Oxford Instruments X-Max100TLE SDD detector, also fitted to the JEM-ARM200CF.

4.3.4 Electrochemical evaluation

The electrochemical characteristics of the prepared catalysts were tested in a conventional three-electrode cell system. Cyclic voltammetry (CV) and rotating disk electrode (RDE) tests were performed in 0.1 M $HClO_4$ solution as electrolyte at room temperature. A glassy carbon electrode (GCE) of 5 mm diameter coated with catalyst, a Pt wire, and Ag/AgCl electrode served as working, counter, and reference electrodes, respectively, comprised the electrochemical cell. To form the catalyst ink, 10 mg catalyst was sonicated in a solution of 5.0 mL of DI water and 5.0 mL of isopropyl alcohol. The catalyst/GCE was prepared by casting 18.5 μL of catalyst ink on the glassy carbon surface, and after drying the sample was bound to the working electrode using a solution

of 5.0 wt% Nafion : IPA (1 : 20 ratio) [91]. All potentials throughout this paper were referenced to standard hydrogen electrode (SHE). The catalysts were conditioned at 50 mV/s between 0.0 to 1.2 V versus SHE for 50 cycles and then the CV measurements for determination of the catalyst electrochemical surface area were carried out using three cycles at 5 mV/s between 0.0 to 1.2 V versus SHE. The CV tests were performed in N_2-purged 0.1 M $HClO_4$. Upon completion of the CV measurements, the gas was switched to oxygen to saturate the electrolyte for at least 20 min before ORR activity was subsequently measured. All ORR measurements were performed at a scan rate of 5 mV/s, and the ORR voltammogram was recorded with a rotating disk electrode configuration with rotation speeds varied from 350 to 1600 RPM.

4.4 Results and Discussion

4.4.1. Thermal treatment and dispersion of Co/C base catalyst

Temperature programmed analyses of the cobalt-impregnated carbon were done on the sample with 5.0 wt% Co/C loading to increase the concentration of products to be detected by the TCD. During the TPD in flowing He of the impregnated carbon support, expectations were that exposure to elevated temperatures in flowing inert gas should cause decomposition of the $Co(NO_3)_2$ component to form Co_3O_4 and N_2, while the citric acid additive should decompose to form CO_2 and H_2O. The inverse peaks of the TPD profile in Figure 4.1 show thermal conductivity changes of the flowing He where the primary and most intense peak at approximately 60°C is attributed to water evolution while the second peak is associated with evolution of CO_2 and N_2 as decomposition products. The second and third peaks at 220 - 250°C and 420 – 440°C, respectively, may

be due to decomposition products such as N_2, CO_2, and H_2O; the actual compositions could not be identified because of the non-selective nature of the thermal conductivity detector. The highest temperature peak at 420 – 440C may also include CO_2 formed from oxidation of the carbon support from reaction with Co oxide(s) particles. Because of the possibility of support oxidation and the observation that major decomposition events occurred below 250°C, the annealing temperature was set at 250C for all compositions.

The TPR profile of the annealed sample is shown in Figure 4.2. The strong inverse peak centered at 400°C is associated with the reduction of unspecified cobalt oxide particles to form H_2O and Co^0. These reduction temperatures agree well with Co oxide reduction observed by others for carbon-supported cobalt [92, 93] and was chosen as the temperature for bulk reduction of Co oxide. The small, broad shoulder between 500 - 600°C can be associated with Co^0-assisted hydrogenation of the carbon support to methane [94, 95]. This temperature region should be avoided to minimize alteration of the support surface; thus, reduction temperatures for all compositions were limited to 400°C.

Determination of Co particle sizes for the reduced catalysts was necessary for ED experiments to approximate the coverages of Pt on the Co surface. However, H_2 chemisorption for Co is very unreliable due to the reversibility of adsorbed H [96]. Thus, Co particle sizes were determined using XRD. The XRD profiles of the freshly-reduced 2.5 wt% Co/C and 5.0 wt% Co/C samples are shown in Figure 4.3; the profiles for both loadings are virtually identical. By careful deconvolution of the Co^0 peak ($2\theta = 44.2°$) from the most prominent peak of Co_3O_4 ($2\theta = 36.9°$) and subsequent use of the Scherrer equation, an average Co particle diameter of 1.6 nm was calculated for both Co loadings.

For corroboration, HAADF-STEM micrographs of the 5.0 wt% Co/C sample were acquired and a representative image is shown in Figure 4.4. Contrast of Co particles to that of the support is weak; however, the outlines of the particles can still be made and, using visual estimation, correspond to about 2 nm particles, in good agreement with XRD determination. The 1.6 nm particle size was then used to calculate Co dispersion assuming hemispherical particles to yield a surface Co site concentration of 1.5×10^{20} atoms per gram of catalyst.

The Co particle size of 1.6 nm is very appropriate for ED since a thin shell of Pt should give a high concentration of Pt surface sites. The small particle size is attributed to the wetting effect of the citric acid on the carbon support which has two modes to aid the mechanism of small particle generation. Firstly, the interaction of citric acid with the support protonates the surface of the carbon [7, 85], and secondly, the resulting citrate anion complexes Co^{2+} to form an anionic species [97, 98] to induce the strong electrostatic interaction between the anionic cobalt citrate complex and the positively-charged carbon surface. Since SEA is limited to a sterically-limited, close packed monolayer of the ionic complex (including the hydration sheath) [64], the loading of Co is limited by the surface area of the support and the size of the hydrated ionic complex. For this study, the cobalt loadings for 5.0 wt% Co and 2.5 wt% Co correspond to 2.8 μmol/m² of surface and 1.4 μmol/m² of surface, respectively, which are higher than normally used for transition metal uptakes and may account for the resulting particle sizes that are larger than those usually observed for SEA (< 1 nm particles). Still, the particles are small and as the STEM images in Figure 4.4 indicate the distribution of sizes is quite narrow.

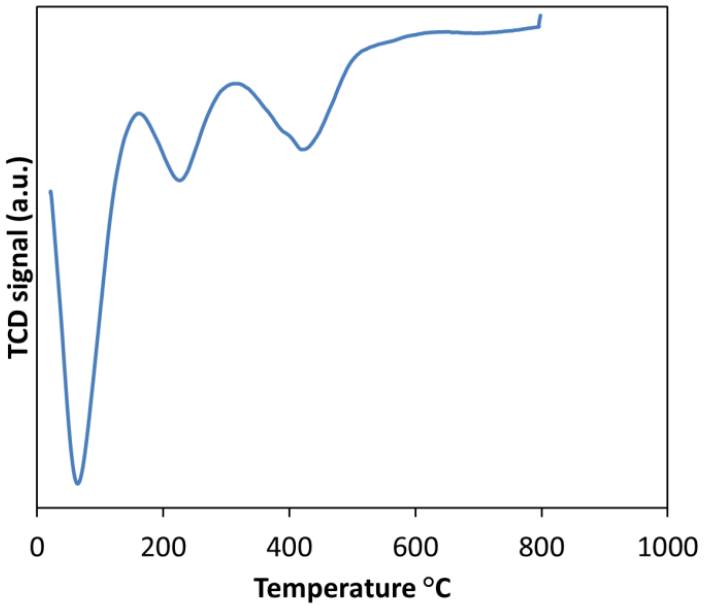

Figure 4.1 Temperature programmed decomposition of carbon impregnated with $Co(NO_3)_2$ and citric acid.

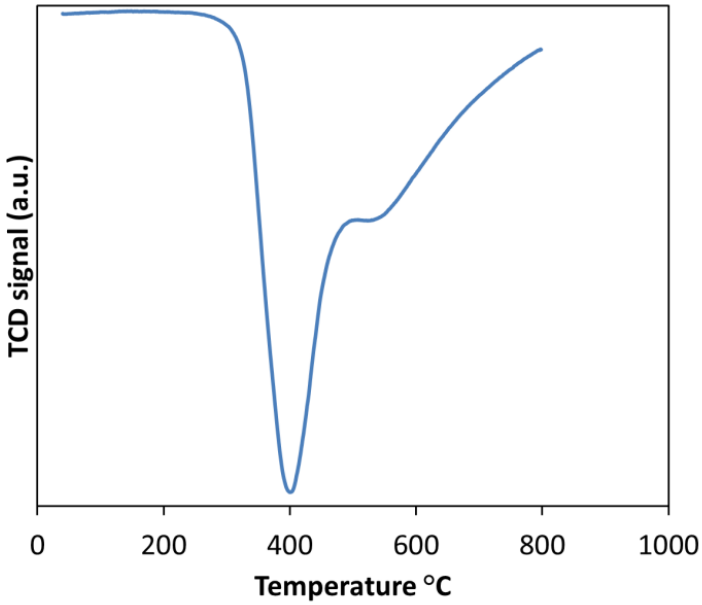

Figure 4.2 Temperature programmed reduction profile in 10% H_2/Ar of annealed Co/C sample.

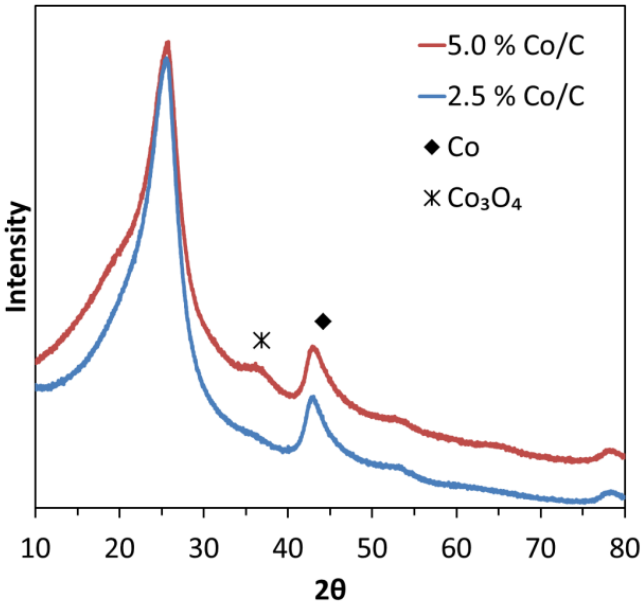

Figure 4.3 Powder X-ray diffraction profiles of the reduced 5.0 wt% and 2.5 wt% Co/C samples showing the positions of the most prominent cobalt and cobalt oxide peaks.

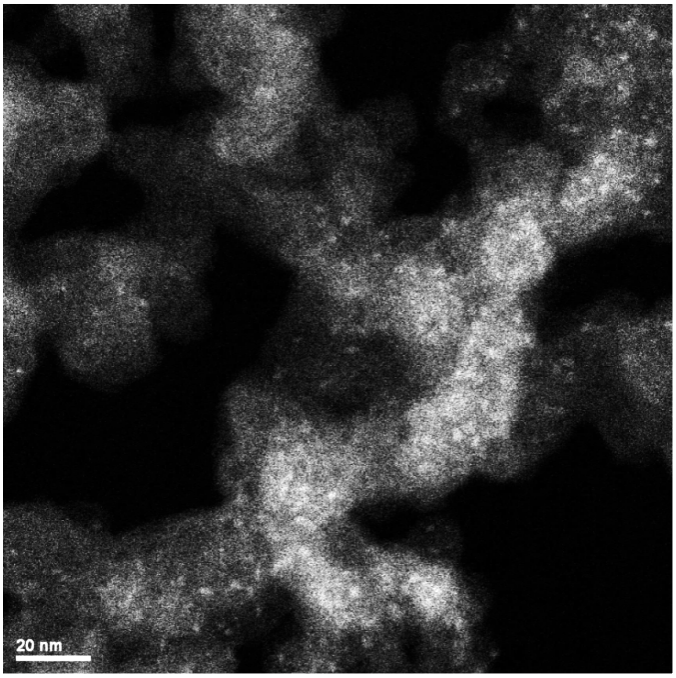

Figure 4.4 Representative micrograph from HAADF-STEM of the 5.0 wt% Co/C sample with the cobalt particles appearing as brighter spots compared to the carbon support that appears as a gray background.

4.4.2 Bimetallic Pt-Co/C catalysts from Electroless Deposition experiments

Preliminary bath stability experiments showed that the ED bath at 50°C containing the $[PtCl_6]^{2-}$ platinum precursor, DMAB reducing agent, and the EN stabilizer at a molar ratio of 1 : 5 : 4 was unstable above 120 ppm Pt. The instability was marked by a change from a clear pale yellow solution to dark brown coloration of the solution within five minutes of the experiment. This is due to the reduction of $PtCl_6^{2-}$ to Pt^0 in solution which was confirmed by AAS analysis of the filtered solution that showed loss of water-soluble $PtCl_6^{2-}$ after reduction to Pt^0 occurred. However, similar experiments showed that $PtCl_6^{2-}$ concentrations < 120 ppm (based on Pt) were stable in solution for at least 30 min.

Addition of Co/C to the bath resulted in catalytic reduction of $PtCl_6^{2-}$ that was completed in less than 15 min of exposure. A representative profile of $PtCl_6^{2-}$ concentration in solution during stability testing and electroless deposition of sufficient Pt to deposit 1ML of monodisperse coverage of Pt on Co is shown in Figure 4.5. The decrease in $PtCl_6^{2-}$ in solution was due to ED of Pt on the cobalt surface, and not electrostatic adsorption of $PtCl_6^{2-}$ on the carbon support. The bath pH (pH 10) was well above the point of zero charge (PZC) of the carbon support, meaning the carbon surface was deprotonated to give a net negative charge; previous work had shown the PZC was pH 3.4. The net negative charge on the surface repels the anionic $PtCl_6^{2-}$ complex [64]. Thus, as shown in previous studies the choice of precursor ion and pH of the solution appropriate for the PZC of the support effectively targets the deposition of the secondary metal only on the surface of the surface of the base catalyst [66, 89] and not on the support.

Analysis of the bath after ED experiments showed that there was also loss of cobalt into the solution. The cobalt leaching was observed as a pink coloration of the filtered solution, indicative of a Co^{2+} species, possibly as a cobalt-ethylenediamine complex [99]. Cobalt leaching was also observed in other ED experiments where pink coloration of the filtrate was observed approximately 15 min after addition of the Co/C catalyst, corresponding with complete $PtCl_6^{2-}$ deposition. It is likely that in addition to ED of Pt, galvanic displacement (GD) of Co^0 by Pt also occurred. For GD to occur, there must be a favorable redox potential for the oxidation of the primary metal from the base catalyst (Co^0, in this case) and the reduction of the secondary metal ion from the precursor (Pt^{4+}) [18-21]. Calculation of the cell potential for the oxidation of Co^0 to form Co^{2+} and the reduction of $PtCl_6^{2-}$ to form $Pt^0 + 6Cl^-$, shown in Equation 4-1, gives a net potential of 2.038V [100]. This positive cell potential indicates a spontaneous redox reaction can occur and that the moles of Co oxidized will be twice the moles of Pt reduced. Thus, both ED and GD of the platinum on the base catalyst can and likely does occur. This GD resulted in substantially lowered cobalt content in the final catalyst as shown in the calculated metal loadings after the ED experiments in Table 4.2.

$$\begin{array}{ll} Co^0 \leftrightarrow Co^{2+} + 2e^- & +0.277V \\ PtCl_6^{2-} + 4e^- \leftrightarrow Pt^0 + 6Cl^- & +1.484V \\ \hline 2Co^0 + PtCl_6^{2-} \leftrightarrow 2Co^{2+} + Pt^0 + 6Cl^- & +2.038V \end{array} \qquad (4\text{-}1)$$

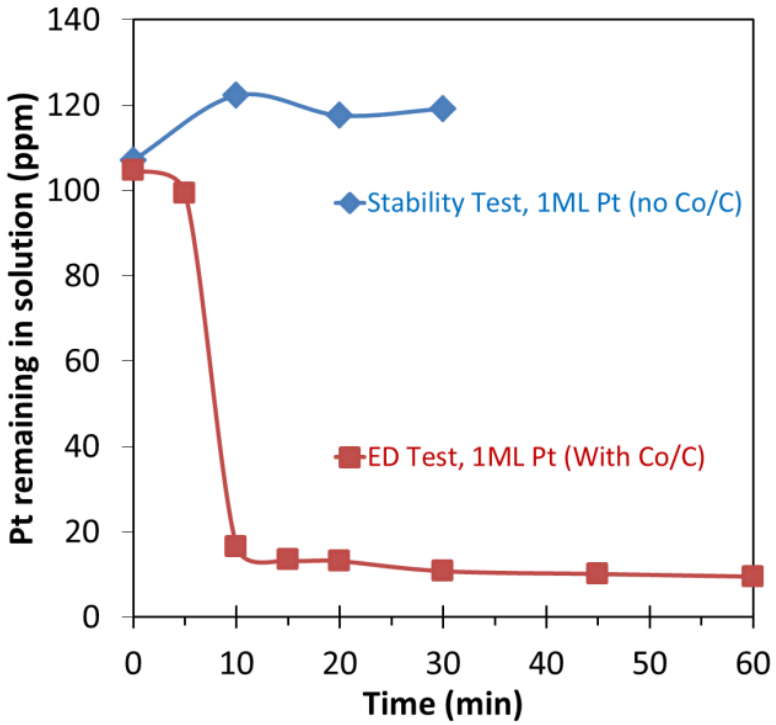

Figure 4.5 Stability test and ED profiles for electroless developer bath platinum concentration. ED bath maintained at pH 10 during the 60 min deposition period.

Table 4.2 Compositions of the ED prepared Pt-Co/C sample series.

Catalyst	Pt Coverage θ_{Pt} (theoretical)	Co loading before ED wt% (nominal)	Final Pt Loading		Final Co loading	
			wt%	atomic % (metal basis)	wt%	atomic % (metal basis)
A	1.5	2.5	6.7	70.1	0.9	29.9
B	3.0	2.5	12.2	75.6	1.2	24.4
C	1.5	5.0	12.6	61.5	2.4	38.5
D	3.0	5.0	22.2	71.9	2.6	28.1

4.4.3 XRD, HAADF-STEM and XEDS Characterization of Pt-Co/C catalysts

Powder X-ray diffraction profiles of the Pt-Co catalysts are shown in Figure 4.6. Prominent diffraction peaks corresponding to face centered cubic (fcc) reflections of Pt^0 are observed in the XRD patterns of all bimetallic samples. There are also significant shoulders to the right of the Pt peaks suggesting a different fcc phase with a lattice parameter slightly smaller than that of Pt. These shoulder peaks do not correspond to fcc Co^0 (PDF card # 01-077-7451). A representative deconvolution profile of one of the XRD patterns is shown in Figure 4.7. For all of the bimetallic samples the shoulder peaks are noticeably broad indicating that the phases of lower lattice parameter are small structures, about 2.5 nm in size. Using d-spacing calculation for the deconvoluted peaks, the lattice parameters for these shoulders averaged 3.86 Å. From previous studies, this lattice parameter is known to correspond to a Pt-Co alloy fcc phase [101]. The results of the lattice parameter calculations and line broadening size analyses using Scherrer formula are listed in Table 4.3.

A prior survey [101] of Pt-Co alloy lattice parameter dependence on metal composition is shown in Figure 4.8. Data from the current study are also included using the calculated lattice parameter of the Pt-Co alloy observed from XRD and the bulk atomic composition of the metal phases. The lattice parameters of the Pt-Co alloys in this study correspond to a metal composition ranging from 25 to 40 atomic percentage of cobalt by interpolation from the lattice parameter curve.

The formation of alloy phase in the Pt-Co/C samples is not an expected result of the electroless deposition process. Platinum was intended to deposit as a shell over the cobalt seed particles as prior studies have shown for transition metals [22, 23, 66, 89,

102], particularly on cobalt [31]. It is possible that the substitution of cobalt into the platinum lattice to form a Pt-Co alloy structure may be due to the simultaneous action of GD with ED, particularly the rapid ED kinetics resulting from the high initial concentration of $PtCl_6^{2-}$ and the DMAB reducing agent. Further, in addition to the deposition of Pt by ED and GD, the Co^{2+} in solution can be deposited by ED on the freshly-deposited Pt surface if sufficient DMAB remains in solution, since DMAB is also activated on platinum [103, 104]. Thus, we could have simultaneous co-deposition of Pt and Co by ED which might favor formation of Pt-Co alloy structures, since the metallic lattice would form in the presence of both Pt^0 and Co^0 atoms. Further, autocatalytic deposition of Pt on Pt likely occurs to form the large Pt phases calculated from the XRD patterns in Figure 4.6 and summarized in Table 4.3.

Representative HAADF-STEM images of the samples with the lowest (Sample A) and highest (Sample D) loadings of Pt are shown in Figure 4.9. Sample D exhibits particles that are mostly large and irregular which can be visually described as hollow shell-like structures having a thickness of about 2.5 nm. Sample A has particles with wide size distribution from 2 to 20 nm that have a more solid appearance. The structures of Samples B and C (not shown) are intermediate between the range of particle sizes and shapes of the nanoparticles found for Samples A and D, with a mix of both the small compact particles and the large hollow-like structures. The trend of the particle morphology for the Pt-Co/C samples is that higher Pt loadings (see Table 4.2) have more of the large hollow, shell-like particles. These structures are very likely due to the faster kinetics of electroless deposition, since the ED bath (constant volume bath) contains higher initial amounts of $PtCl_6^{2-}$ and, more importantly, DMAB, which undergoes rapid

catalytic decomposition to release H_2 [105, 106]. That DMAB is an inefficient reducing agent is well-known and is the reason why a 5-fold molar excess relative to $PtCl_6^{2-}$ is used during ED. This is also observed visually by the vigorous release of H_2 bubbles during the initial stages of deposition. The evolution of H_2 likely caused the expansion of the deposited metal shell until rupture occurred.

Energy dispersive x-ray spectroscopy (XEDS) was used to obtain elemental maps, providing information on where the Pt and Co resided in the particles. A representative XEDS micrograph of Sample D is shown in Figure 4.10, imaging both hollow shell and compact particles. Elemental distribution of the compact particles shows a Pt-rich shell phase and a small Co-rich core on the inside. The hollow shell structure on the other hand shows a more evenly distributed mix of Pt and Co, suggesting the shell is an alloyed Pt-Co phase. The elemental maps corroborate the results of the powder XRD where large domains of Pt-rich phases can be seen from the elemental maps and the exploded shells which are visibly alloyed as seen in XEDS, correspond to the thinner-dimensioned, Pt-Co alloy size estimate from XRD.

The formation of the alloyed hollow shell structures and the core-shell compact particles supports the hypothesis of GD as the mechanism for the loss of Co. The ruptured hollow shells permit access of Co for the GD process, whereas the shell of Pt on the compact particles prevented further Co loss by GD. The alloy formed in the particles with hollow shell morphology further supports the simultaneous GD-ED process for both platinum deposition and cobalt re-deposition and insertion into the alloy lattice.

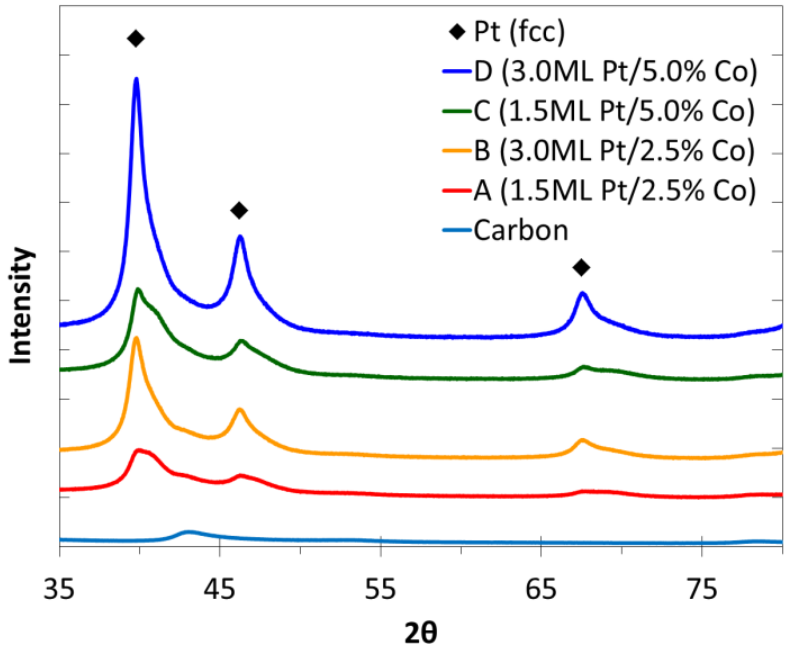

Figure 4.6 Powder X-ray diffraction profiles of Pt-Co/C series of samples. Peak positions of pure platinum phase are shown by black diamonds at the appropriate 2θ values.

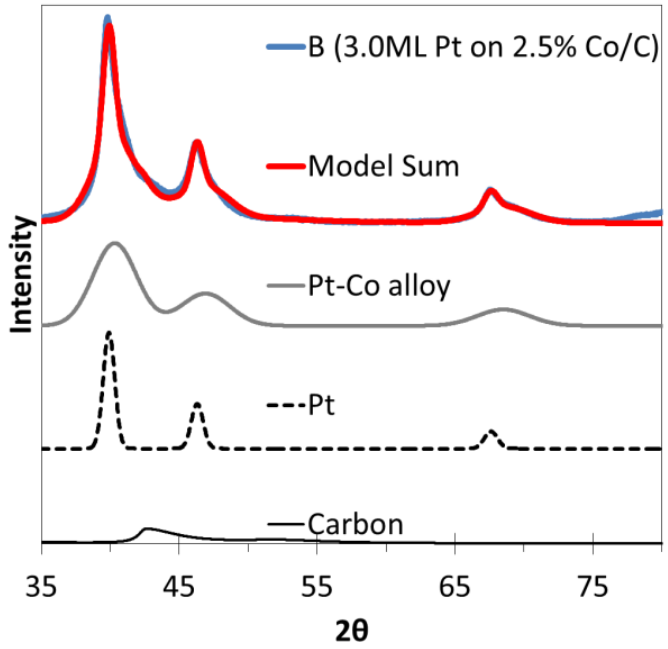

Figure 4.7 A representative illustration of the deconvoluted profiles of Pt and Pt-Co alloy phases in Sample B (3.0ML Pt on 2.5 wt% Co/C).

Table 4.3 Results of calculation of the Pt and Pt-Co phase sizes from deconvolution of X-ray line broadening profiles.

Catalyst	Theoretical Monodisperse Coverage of Pt (ML)	Initial Co loading (wt%)	XRD sizes		
			alloy (Pt-Co) phase		non-alloyed Pt size (nm)
			lattice parameter (Å)	size (nm)	
A	1.5	2.5	3.85	2.6	11.8
B	3.0	2.5	3.87	2.3	8.9
C	1.5	5.0	3.85	2.3	11.0
D	3.0	5.0	3.88	2.3	10.6

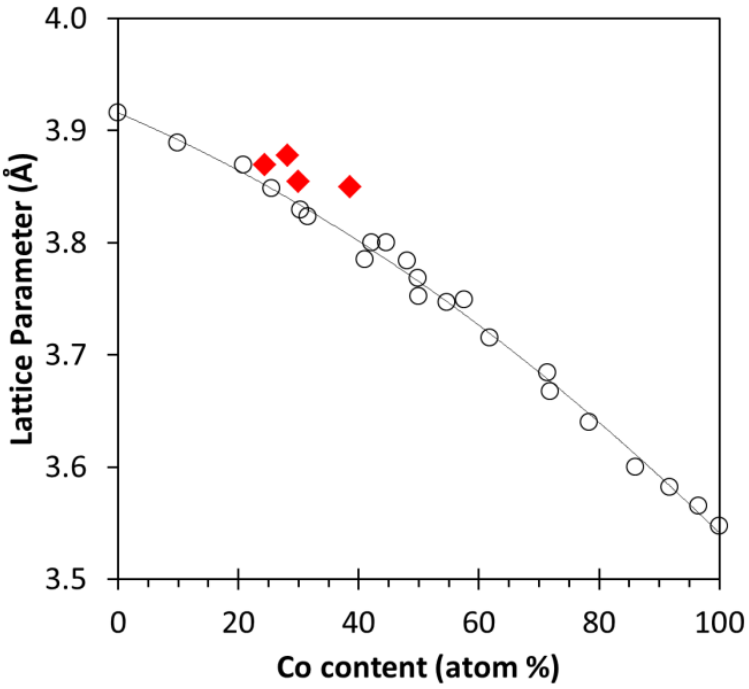

Figure 4.8 Lattice parameter curve for Pt-Co alloy phases indicating results from prior studies (circles) and current work (red diamonds).

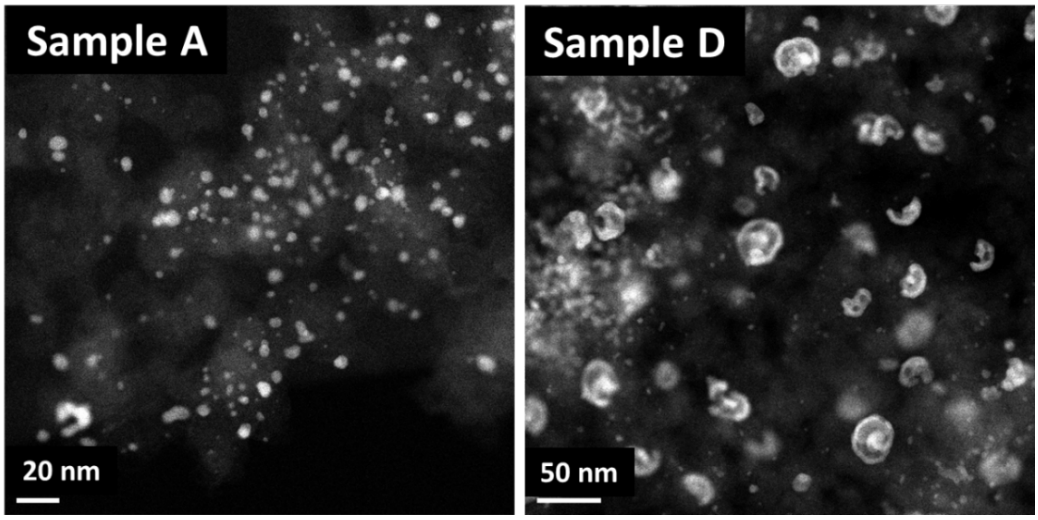

Figure 4.9 Representative micrographs from HAADF-STEM of ED Samples A (left) and D (right).

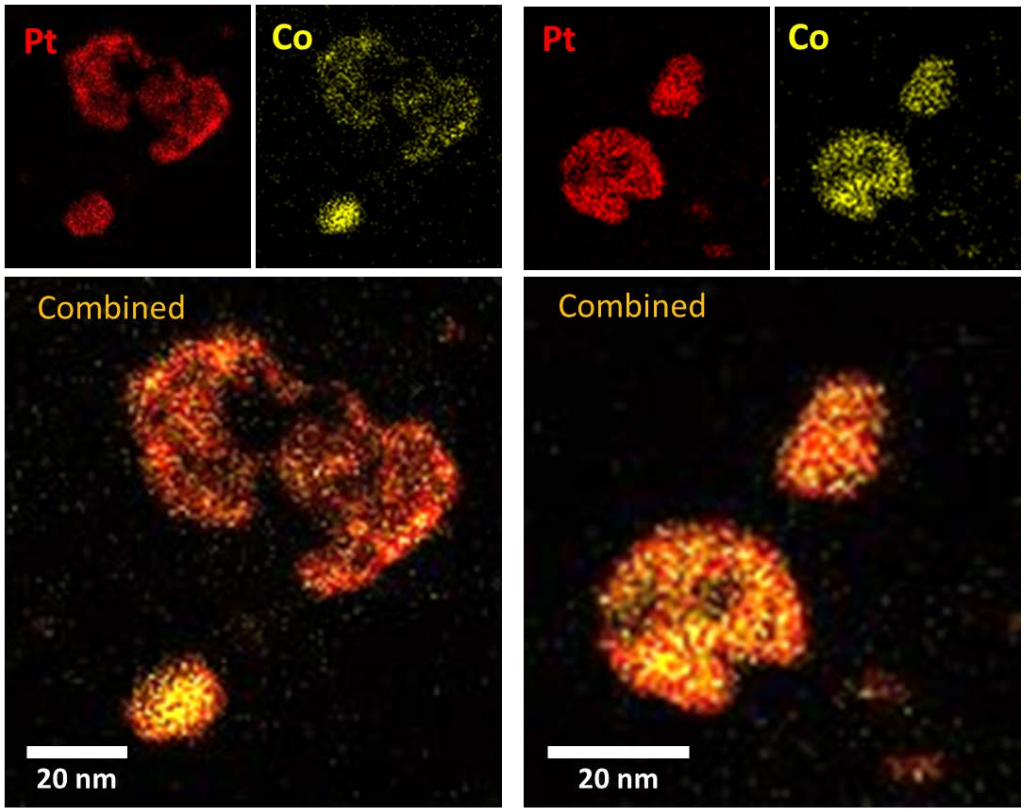

Figure 4.10 Representative X-ray energy dispersive spectroscopy elemental maps of Pt and Co for Sample D (22.2 wt% Pt with 2.6 wt% Co).

4.4.4 Catalyst electrochemical active surface area

Representative cyclic voltammograms of one of the samples (Sample B) and the commercial 20 wt% Pt/C under nitrogen purged electrolyte is shown in Figure 4.11. The electrochemical surface area (ECSA) was calculated in Equation 4-2 by measuring the charge density associated with the adsorption of hydrogen (q_{Pt}, in $\mu C/m^2$-electrode) between 0.05 and 0.40 V [107], the charge required to reduce a monolayer of protons on Pt (Γ) which is 210 $\mu C/cm^2_{Pt}$, and the Pt content or loading on the electrode (L), in g_{Pt}/m^2-electrode.

$$ECSA\left(\frac{m^2{}_{Pt}}{g_{Pt}}\right) = \frac{q_{Pt}}{\Gamma . L} \tag{4-2}$$

Comparison of ECSA values for the different catalysts is shown in Figure 4.12. The ECSA values ranged from 44 to 95 m^2_{Pt}/g_{Pt} for the different Pt-Co/C catalysts, depending on the catalyst composition and the morphology of the metal nanoparticles. The highest ECSA was recorded for the commercial 20 wt% Pt/C with 108.11 m^2_{Pt}/g_{Pt}. The ECSA of Sample A (6.7 wt% Pt with 0.9 wt% Co) was only slightly lower at 95.74 m^2_{Pt}/g_{Pt}. In contrast, Sample D (22.2 wt% Pt with 2.6 wt% Co) exhibited the smallest ECSA value which is attributed to the large Pt particles for this particular sample (Table 4.3) since large particle sizes have lower surface/volume ratios.

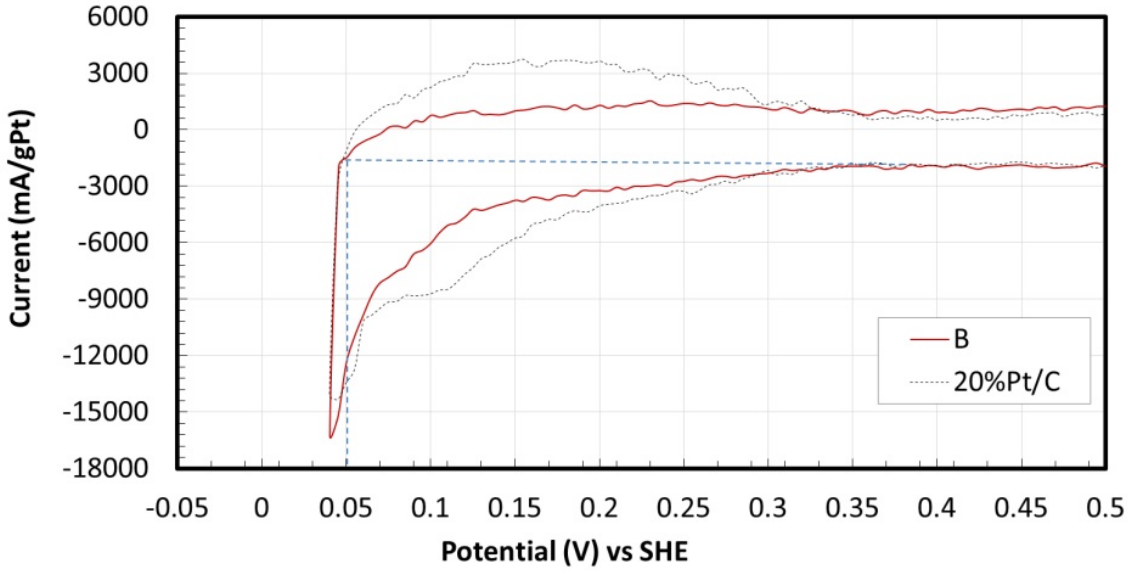

Figure 4.11 Comparison of CV at 5.0 mV/s in N_2 saturated 0.1 M $HClO_4$.

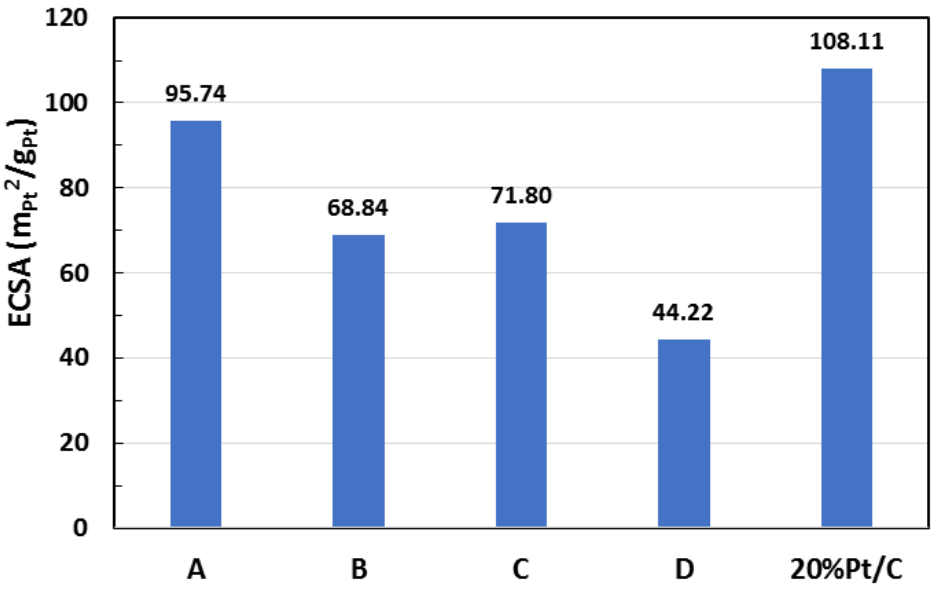

Figure 4.12 ECSA for 5.0 mV/s in N_2 saturated 0.1 M $HClO_4$.

4.4.5 Electrocatalytic activity toward ORR

The ORR polarization curves from RDE were obtained by linear potential sweep at a sweep rate of 5 mV/s and a rotation speed ranging from 350 to 1600 rpm. The responses are corrected by subtraction of background current measured at identical conditions in N_2-purged electrolyte without rotation. Figure 4.13 shows the RDE profiles for Sample B in O_2-saturated 0.1 M $HClO_4$. Note that the current was normalized by the geometric surface area of the RDE. All samples exhibited a plateau behavior at low potentials, indicating a diffusion-limited current regime. A mixed kinetic-diffusion region occurred at potentials greater than approximately 0.6 V vs. SHE. To remove the effect of diffusion and obtain the purely kinetic current density (i_k), the Koutecky-Levich relation was applied [83].

$$\frac{1}{i} = \frac{1}{i_k} + \frac{1}{i_D} \tag{4-3}$$

The analysis used the potential range between 0.75 and 1.0 V vs SHE as marked in Figure 4.13 to avoid significant mass-transfer corrections at high currents and excess noise relative to background at low currents. The diffusion limiting current density in Equation 3 (i_D) is equal to $R(w)^{0.5}$, with w as the rotation rate and R is a constant given by the Levich equation [108]. The value for R was obtained by averaging the slope of $1/i$ vs $1/w^{0.5}$ at all voltages in the potential window indicated above. The resulting R value was used to obtain the kinetic currents at all potentials and rotations rates, which are plotted in Figure 4.14, with the potential shown relative to the equilibrium potential for oxygen reduction, E^{eq} = 1.23 V vs. SHE. The overlap of the kinetic current at all rotation speeds indicate the mass transfer effects on the current were eliminated.

Assuming the kinetics can be represented by the Tafel equation given as:

$$E = E^{eq} + \beta \log(i_0) - \beta \log(i_k) \quad (4\text{-}4)$$

where i_0 is the exchange current density and β is the Tafel slope, these two kinetic parameters can be obtained from fitting Equation 4 to the kinetic-current data in Figure 4.14. The resulting estimate of i_0 is normalized by the geometric area, consistent with the current used in the fit. The Pt mass and Pt active surface area were then used to obtain the exchange current density normalized by either Pt mass ($i_{o,\,\mathrm{MA}}$) or Pt active area ($i_{o,\,\mathrm{ECSA}}$).

In order to compare mass activities of different catalysts, the exchange density was normalized to the mass of Pt used. All Pt-Co samples showed higher mass activity than the commercial Pt/C sample (Figure 4.15), with Sample B having a mass activity 4.8 times higher than the commercial sample.

Table 4.4 summarizes the ECSA and the SA values of all samples. Additionally, the comparison of SA values calculated from the exchange current density is shown in Figure 4.16. The results show all Pt-Co samples have much higher specific activities (i_0) than the commercial, Pt-only sample, demonstrating accelerated ORR kinetics on the surfaces of the Pt-Co catalysts. Sample B exhibited a specific activity of 0.0587 mA/m^2_{Pt}, 7.5 times greater than the Pt/C catalyst (0.0078 mA/m^2_{Pt}).

In summary, electroless deposition of controlled amounts of Pt on Co particles gives much more efficient use of Pt, since the bulk, or core, is composed of a different metal, Co in this study. In addition to ED of Pt on Co, galvanic displacement of Co^0 by $PtCl_6^{2-}$ forms additional Pt^0, releasing Co^{2+} into the ED bath. Once in the bath, co-deposition of both Pt and Co can occur which appears to facilitate the formation of true alloys of Pt and Co. XRD analysis suggests the preferred alloy composition is Pt_3Co which has been argued by others to be a superior ORR composition based on structural

and electronic factors [52, 82, 83, 109]. If the kinetics of ED are too rapid, particularly, the catalytic activation of the DMAB reducing agent, excessive H_2 evolution occurs which can rupture the Pt shell deposited by ED to form an “exploded” hollow shell structure. When activation of DMAB is less aggressive, typical Co core-Pt shell structures are formed.

Evaluation of the electrochemical active surface area (ECSA) of the ED-prepared Pt-Co/C catalysts using cyclic voltammetry indicated the concentration of active surface Pt sites was lower for the ED catalysts, compared to a commercially-available 20 wt% Pt/C catalyst. However, the ECSA for the bimetallic 6.7 wt% Pt - 0.9 wt% Co catalyst (Catalyst A) containing the lowest concentration of Pt deposited by ED was only slightly lower than that of the commercial Pt catalyst. The larger Pt particles for the catalysts with higher Pt loadings are likely the cause for the lower ECSA values. However, evaluation for the oxygen reduction reaction (ORR) showed considerably higher mass and surface activities for the ED catalysts compared to the commercial Pt/C sample. This appears to be due to formation of Pt-Co alloy structures for the ED catalysts, consistent with suggestions by others. What is encouraging from this initial study, however, is that much greater control of the ED process, and even carefully-designed co-deposition of both Pt and Co, can be easily implemented to greatly improve performance of the bimetallic Pt-Co system.

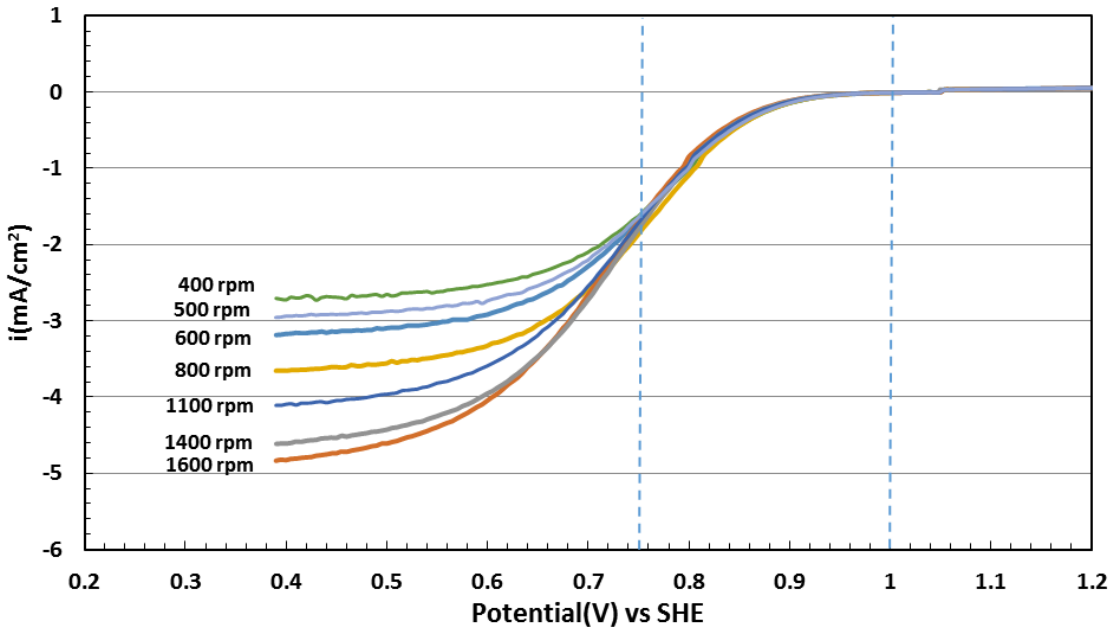

Figure 4.13 Current-potential curves at different electrode rotating rates, recorded on a glassy carbon electrode using a potential scan rate of 5.0 mV/s.

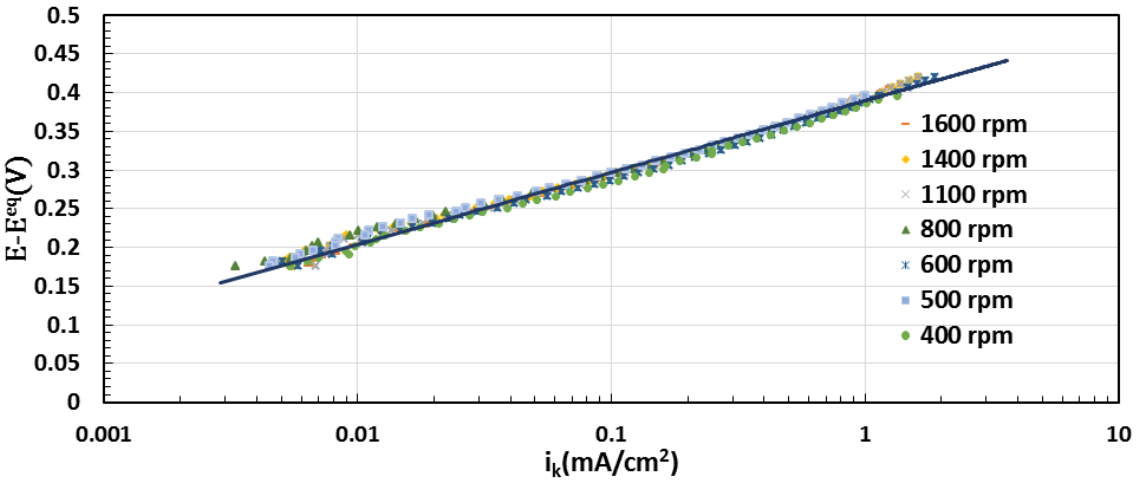

Figure 4.14 Examples of Tafel plots for oxygen reduction reaction on sample B at different rotation speeds. The line is showing the fit of Equation 4-4 to the data.

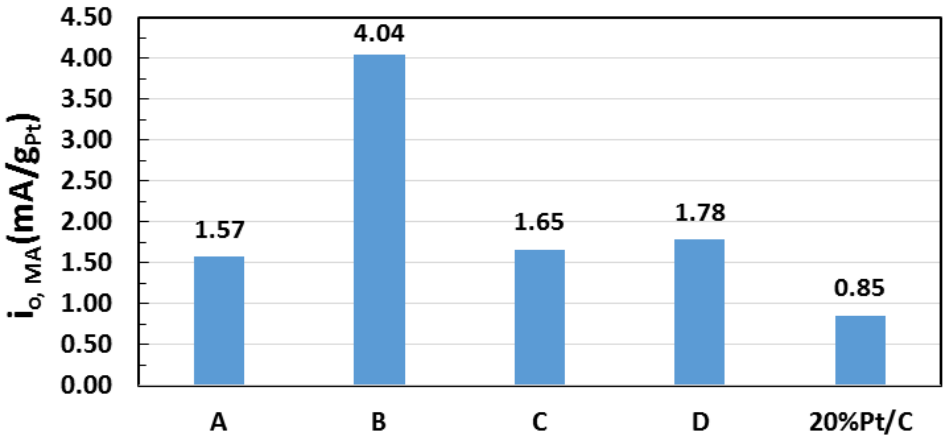

Figure 4.15 Mass activities (mA/g_{Pt}) of the different catalysts.

Table 4.4 Summary of the ECSA and the specific activity (SA) values of different catalysts.

Sample	Pt(%Loading)	ECSA(m^2/g_{Pt})	i_0(mA/m^2_{Pt})
A	6.71	95.7	0.016
B	12.2	68.8	0.059
C	12.6	71.8	0.023
D	22.2	44.2	0.040
20 wt%Pt/C*	20.0	108.1	0.008

*nominal

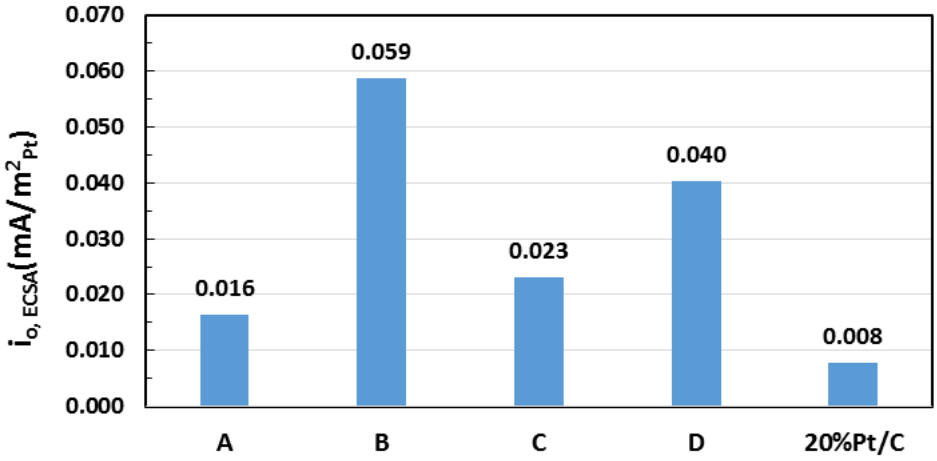

Figure 4.16 Specific activity (mA/m^2_{Pt}) of different catalysts.

4.5 Conclusions

A series of carbon-supported Pt-Co bimetallic catalysts have been prepared by electroless deposition (ED) of Pt on a Co base catalyst. The preparation of the Co/C catalyst, at loadings of 2.5 and 5.0 wt% Co, used a modified charge enhanced dry impregnation method (CEDI) with citric acid that acted as a chelating agent and support acidifier. This dual effect of the citric acid induced conditions that promoted strong interaction between the anionic cobalt-citrate complex and the positively-charged surface of the carbon. Thermal treatment experiments determined that the cobalt-impregnated carbon could be heated at 250°C in inert He flow and reduced at 400°C in dilute H_2 flow to yield small particles. X-ray diffraction (XRD) measurements of Co^0 and cobalt oxide peaks indicated approximately 1.6 nm particles were formed, which was confirmed by high-angle annular dark-field scanning transmission electron microscopy (HAADF-STEM). The Co particle size estimate from XRD was used as a basis for the coverage of Pt during ED experiments.

The electroless developer bath for Pt deposition contained 1:5:4 molar ratios of H_2PtCl_6, DMAB, and EN as Pt precursor, reducing agent, and stabilizer, respectively. The total amount of H_2PtCl_6 (actually $PtCl_6^{2-}$ at the basic, pH 10 conditions of the bath) was used to control the coverage at 1.5 ML and 3.0 ML Pt on both Co/C catalysts. Leaching of Co^{2+} into the ED bath from galvanic displacement of Co by $PtCl_6^{2-}$ was observed from ICP analysis. Once in the bath co-deposition of both Pt and Co likely occurred which facilitated the formation of true alloys of Pt and Co. Final loadings of Pt ranged from 6.7 to 22.2 wt% while Co was reduced by approximately 50% due to galvanic displacement. XRD analyses confirmed that in addition to Pt^0, a Pt-Co alloy

phase was indeed formed, and that based on the contracted lattice parameters calculated from the XRD profiles, Pt_3Co was the likely composition. Electron micrographs of the samples showed that for the samples with the highest Pt loadings, large particles with a thin hollow-shell morphology were formed. If the kinetics of ED were too rapid, especially the catalytic activation of the DMAB reducing agent, excessive H_2 evolution occurred which ruptured the Pt shell deposited by ED to form an "exploded" hollow shell structure. When activation of DMAB was less aggressive, typical Co core-Pt shell structures are formed. Finally, XEDS mapping determined that the thin hollow-shells were comprised of a Pt-Co alloy phase while the smaller compact particles consisted of Co-rich cores and thicker Pt-rich shells.

Evaluation of the electrochemical active surface area (ECSA) of the ED-prepared Pt-Co/C catalysts using cyclic voltammetry indicated the concentration of active surface Pt sites was lower for the ED catalysts, compared to a commercially-available 20 wt% Pt/C catalyst. However, the ECSA for the bimetallic 6.7 wt% Pt - 0.9 wt% Co catalyst (Catalyst A) containing the lowest concentration of Pt deposited by ED was only slightly lower than that of the commercial Pt catalyst. The larger Pt particles for the catalysts with higher Pt loadings are likely the cause for the lower ECSA values. However, evaluation for the oxygen reduction reaction (ORR) showed considerably higher mass and surface activities for the ED catalysts compared to the commercial Pt/C sample. This appears to be due to formation of Pt-Co alloy structures for the ED catalysts, consistent with suggestions by others.

This study has shown the viability of ED and CEDI methods for the production of carbon-supported bimetallic Pt-Co particles that have higher activity than current

commercially- available monometallic catalysts for ORR. Results from this initial study also suggest that with greater control of the ED process kinetics, and possibly co-deposition of both Pt and Co, greatly improve performance of the bimetallic Pt-Co system may be attained.

Further works on the fine tuning of bath conditions to achieve slower deposition rates and yielding better dispersed bimetallic particles are to be the subject of another study.

4.6 Acknowledgements

The authors would like to thank the Dr. Alan Nicholls and the Electron Microscopy Service of the University of Illinois at Chicago for the STEM and XEDS imaging. Appreciation is also extended to the Toyota Motor Company for supporting portions of this work.

CHAPTER 5

BIMETALLIC RU-PT/C CATALYSTS PREPARED BY STRONG ELECTROSTATIC ADSORPTION AND ELECTROLESS DEPOSITION FOR DIRECT METHANOL FUEL CELL APPLICATION

5.1 Abstract

The use of bimetallic catalysts is gaining popularity as these often have improved performance over their monometallic counterparts. In particular, for direct methanol fuel cells (DMFC) the Pt-Ru system was determined to have higher activity than Pt alone. Targeted deposition of Ru on the metal surface of Pt/C has been achieved using the method of electroless deposition (ED). However, the amount of active surface sites will depend on the base Pt/C catalyst used for ED. Strong electrostatic adsorption (SEA) can be used in preparing highly dispersed base catalysts for ED. In this study, ED of Ru on SEA prepared Pt/C was carried out at varying theoretical coverages of Ru, using established conditions for the electroless developer bath. The base catalyst had high dispersion, with average particle size of 1.4 nm from XRD. After ED the resulting catalyst has real Ru-Pt bimetallic surface as evidenced by XEDS mapping and is consistent with prior studies. The performance of the catalyst for DMFC application was evaluated and was found to follow the same trend as the catalysts series of Ru deposited by ED on commercial Pt/C. The ED-SEA catalysts also have higher activity compared to commercial Pt/C and Ru-Pt/C.

5.2 Introduction

The use of supported bimetallic nanoparticle catalysts can offer better performance than monometallic catalysts as fine tuning of the metal composition can result in enhanced activity, selectivity and stability. This improved performance can be due to bifunctional, electronic and/or ensemble bimetallic effects. While there is gaining popularity of using bimetallic catalysts in industry, conventional synthesis by simple

impregnation of precursors on powder supports does not ensure close interaction of the two metals. This can produce a mixture of monometallic particles of the component metals as well as some alloyed particles. Also, simple dry or wet impregnation can often result in poor dispersion and size distribution.

The method of Strong Electrostatic Adsorption (SEA) has been shown to provide greater control of supported catalyst particle size [110]. In SEA, by controlling the impregnation pH, the surface of the support can become charged due to protonation/deprotonation of functional groups, resulting in electrostatic interaction with an oppositely charged ionic precursor complex. Monometallic catalysts with high dispersion and narrow size distribution can be prepared using SEA. A secondary metal can then be deposited on the surface of the primary metal using the method of Electroless Depostion (ED) resulting in particles with a real bimetallic surface.

Ru-Pt bimetallic catalysts are of particular interest as higher activity catalysts in direct methanol fuel cells (DMFC) [111-114]. Prior work with the electroless deposition of Ru on commercially available Pt/C catalyst has shown that an increase in mass activity with DMFC evaluation was observed at 50% theoretical monodisperse coverage of Ru on the surface of the particles [90]. The particles of the Pt/C catalyst used in the said study are large, about 5 nm in average size, which corresponds to only 20% dispersion or the fraction of Pt metal on the surface. Smaller particles will have higher dispersion or more efficient utilization of the Pt available on the surface, giving larger count of active sites for the same amount of Pt. In the current work, SEA was used to prepare the base Pt/C catalyst for ED of Ru at varying coverages. The series of SEA-ED prepared Ru-Pt/C catalysts were evaluated for DMFC application and compared to the series synthesized by

ED of Ru on commercial Pt/C as well as commercially available 20% Ru-Pt/C (1:1 metal atomic ratio).

5.3. Experimental

5.3.1 Synthesis of Pt/C base catalyst by SEA

The preparation of Pt/C catalyst was done according to prior SEA studies on carbon supports [65]. Vulcan XC72-R carbon (250m^2/g, PZC = 8.5) was chosen as the support for the Pt/C base catalyst. As a high PZC material, the surface can be charged positively in low pH conditions and can electrostatically adsorb anionic precursor complexes. Chloroplatinic acid (CPA, H_2PtCl_6) was used as Pt precursor and was dissolved in de-ionized water to a Pt concentration of 200 ppm. The CPA solution pH was adjusted using NaOH to pH 3.0 and stored for 2 days for aging. After the aging period, the pH was adjusted back to pH 3.0 and aged for another 2 days. Once the pH of the solution did not significantly deviate from pH 3.0, a sample was taken for analysis of initial Pt concentration. The required amount of carbon support for a surface loading of 500 m^2/L was added. The slurry was mixed thoroughly using a shaker set at around 120 rpm speed for an hour. After shaking, the slurry pH was measured before being filtered to recover the solids using a vacuum filtration setup with ashless filter paper. The filtrate was sampled for analysis of remaining Pt in solution. Analysis of the initial and final Pt concentration was done using Inductively Coupled Plasma (ICP) - Optical Emission Spectroscopy (Perkin Elmer Optima 2000DV).

The recovered impregnated powder was dried at room temperature prior to drying in oven at 120 °C overnight. It was then subsequently reduced in a tubular furnace with

flowing 25% H2 balance He at 200 sccm flowrate and the temperature was ramped at 2.5 °C/min up to 200 °C with a dwell time of 1h. The reduced catalyst was cooled in inert He flow prior to removal from the furnace. The Pt/C catalyst was then characterized by powder X-ray diffraction (XRD), scanning transmission electron microscopy (STEM) imaging and chemisorption for determination of particle dispersion.

5.3.2 Electroless Deposition of Ru on Pt

A bath for the deposition of Ru on Pt has been developed from prior work using commercially available Pt/C [66]. In detail, Hexaammineruthenium(III) chloride (RuHA, $Ru(NH_3)_6Cl_3$) was used as the Ru precursor and formic acid (FA, HCOOH) as the reducing agent with the bath kept in an acidic (pH 3.0) condition using HCl or NaOH for pH adjustment. Temperature was kept at 90 °C by immersion of the stirred container (beaker) in a heated water bath with evaporation control. For Ru deposition at or above 0.8 ML, a higher temperature of 120 °C was used using an oil immersion bath while using a round bottom flask with a reflux condenser connected to running cooled tap water. For the bath formulation, an initial ratio of Ru : FA = 1 : 6 was used with FA, in the same amount as initially present, added every 30 min. The bath volume to base catalyst amount ratio used was 100 mL of bath to 0.5 g of Pt/C catalyst. The coverage of Ru or amount of Ru deposited on Pt surface was controlled by initial amount of Ru in the bath, determined by ICP. The ED experiment was run for 2 h to ensure deposition of the Ru in the bath, with the final concentration verified by ICP. Coverage of Ru on Pt was determined from the amount of Ru deposited and the amount of surface Pt sites determined from chemisorption dispersion measurement. A series of varying Ru

theoretical monodisperse coverage was synthesized using the described experimental conditions.

After the ED experiments, samples were recovered using vacuum filtration and then copiously washed with de-ionized water (~2 L) before being dried at room temperature. The Ru-Pt/C ED series were then characterized with XRD, while one sample with equimolar surface Ru-Pt was imaged with STEM and XEDS mapping.

5.3.3 Cyclic voltammetry evaluation

The method used for evaluation of the Ru-Pt bimetallic catalysts was based on work done by Garrick et.al. [90]. Inks from the catalyst powders were made by weighing 10 mg and were sonicated with 10 mL equal volumes de-ionized water and isopropyl alcohol. Of this ink, 18.5 µL was placed on the surface of a 5 mm diameter Pt disk using 5 µL of 5 wt% nafion in isopropyl alcohol [91] to secure the powder on the surface. Once dried, the catalyst coated Pt disk served as a working electrode for cyclic voltammetry experiments at 25 °C, with a luggin capillary $Hg/HgSO_4$ reference electrode and Pt wire counter electrode. The electrolyte was composed of 0.5 M H_2SO_4 with 1 M methanol. Scanning was done between -0.1 to 1.3 V vs SHE reference with conditioning scan rates of 50 mV/s for 35 cycles and 5 mV/s for 3 cycles where the peak current was recorded. The CV for each catalyst used was repeated 10 times to ensure reproducibly of results.

5.4 Results and Discussion

5.4.1 Uptake and dispersion of Pt/C catalyst

From the analysis of the difference in Pt concentration in solution after SEA experiment, the uptake of Pt was determined to be 1.4 μmol Pt/m^2. Given the surface area of the carbon support, this corresponds to 6.3 wt% Pt loading in the reduced catalyst. The XRD profile of the SEA prepared base Pt/C catalyst, hereby denoted as Pt_{SEA}, indicating peak positions for fcc phase Pt is shown in Figure 5.1. Broad peaks corresponding to metallic Pt phase were observed, indicating well dispersed Pt particles. Deconvolution of these Pt phase peaks from carbon support signal contribution and using Scherrer formula for XRD line broadening resulted in an average particle size of 1.4 nm. Likewise, STEM imaging of the Pt_{SEA} catalyst showed small Pt particles as seen in Figure 5.2a. In contrast, commercially available 20 wt%Pt/C catalyst (Premetek, Pt_{COMM}) imaged with STEM showed large particle sizes, shown in Figure 5.2b. Respective size distributions (Figure 5.2c and d) also indicate that the Pt_{SEA} sample has a narrower size distribution compared to Pt_{COMM}. Thus, the well dispersed particles in the Pt_{SEA} sample has higher amount of surface sites, $9.56x10^{19}$ surface Pt atoms per gram of catalyst.

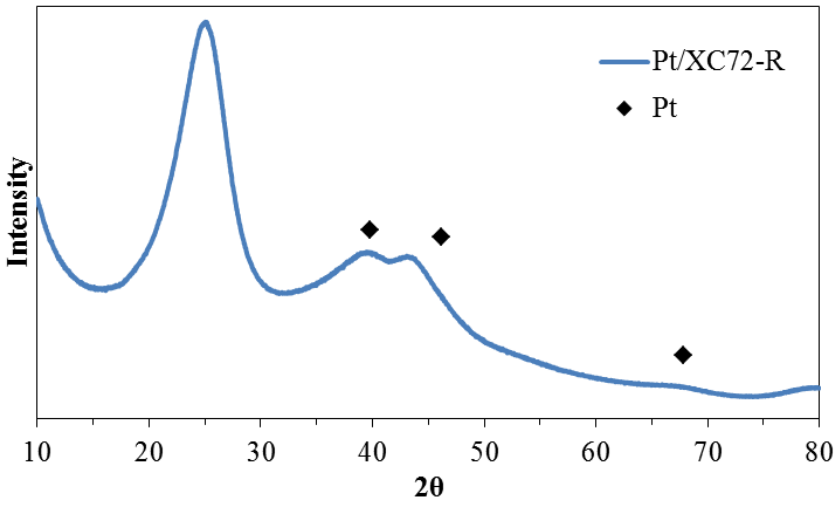

Figure 5.1 XRD profile of the Pt_{SEA} sample.

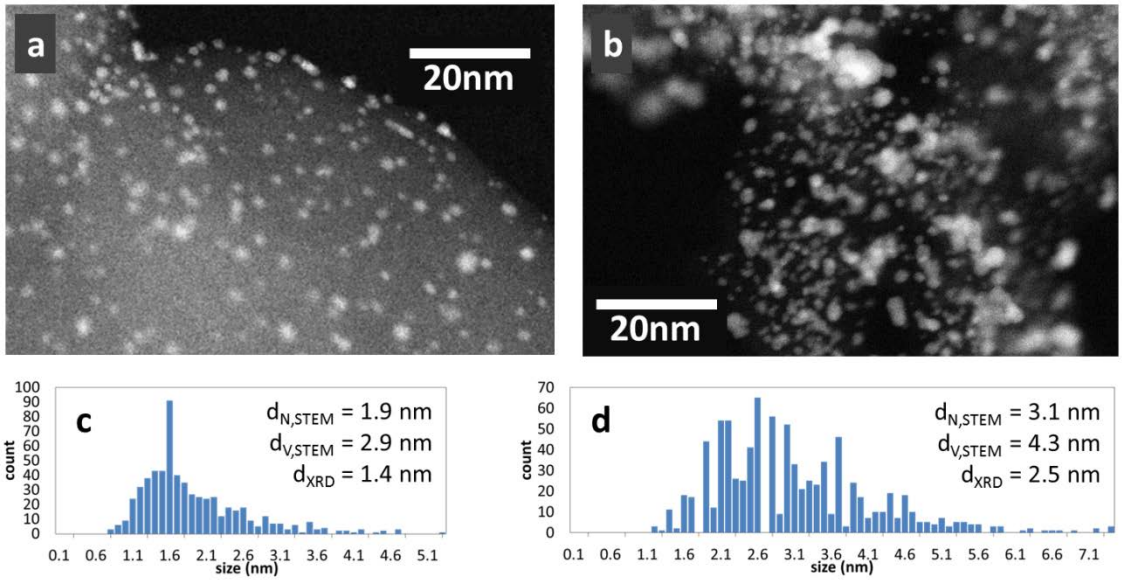

Figure 5.2 HAADF-STEM micrographs and corresponding size distributions of the (a and c) Pt_{SEA} and (b and d) Pt_{COMM} samples.

5.4.2 Electroless deposition of Ru on Pt_{SEA}

The series of Ru-Pt_{SEA} catalysts prepared by ED along with their respective loadings calculated from difference in Ru concentration in the ED bath are listed in Table 5.1. For the synthesis of this series, the bath pH was kept acidic at pH 3 for two reasons: (1) below the PZC of the support, it facilitates protonation of carbon support surface, preventing electrostatic adsorption of cationic hexaammineruthenium complex onto the support [64, 115] and (2) FA has been studied as an active reducing agent for ED of Ru in acidic conditions [24, 25]. XRD analyses of the series did not show formation of separate Ru phase indicating thin moieties of Ru, undetectable with XRD, have been deposited, consistent with prior results (Ru-Pt_{COMM}) [66].

Elemental maps of the 0.50 Ru-Pt_{SEA} were obtained by XEDS and are shown in Figure 5.3, in comparison to similar maps of a Ru-Pt_{COMM} sample (0.96 ML theoretical monodisperse Ru coverage) from a previous study [66, 90]. This analysis confirms the targeted deposition of Ru on the surface of the Pt particles.

Table 5.1 Catalysts prepared by electroless deposition of Ru on SEA prepared Pt/C.

Catalysts	**Pt loading wt%)**	**Ru loading (wt%)**	**Theoretical monodisperse coverage θ_{Ru} on Pt**
0.8 Ru-Pt_{SEA}	6.2	1.3	0.82
0.7 Ru-Pt_{SEA}	6.2	1.1	0.69
0.5 Ru-Pt_{SEA}	6.2	0.8	0.50
0.4 Ru-Pt_{SEA}	6.3	0.64	0.40
0.2 Ru-Pt_{SEA}	6.3	0.32	0.20
Pt_{SEA}	6.3	0	0

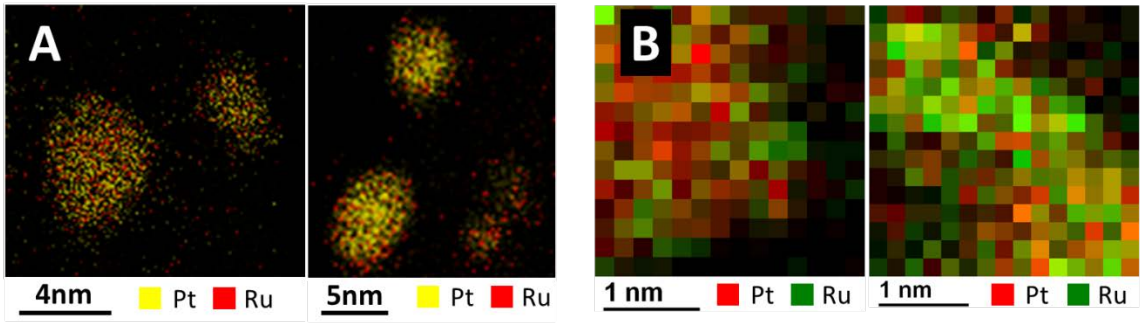

Figure 5.3 XEDS maps of the (A) 0.96 ML Ru on Commercial Pt/C (Ru-Pt_{COMM}) and (B) 0.5 Ru-Pt_{SEA}.

5.4.3 Methanol oxidation electrochemical evaluation

The peak currents normalized with respect to mass of Pt are shown in Figure 5.4 displaying results from using Ru-Pt_{SEA} catalysts (current study) comparing with the results of the study using commercial Pt/C as base catalysts for ED [66, 90]. CV evaluation of a commercially available 20 wt% Ru-Pt/C (bulk Ru : Pt = 1 : 1) catalyst was also done and included in the comparison. The peak current is indicative of the activity of the electrocatalysts for oxidation of methanol [111]. For the Ru-Pt_{SEA} series, the peak currents are higher compared to commercial Ru-Pt/C and Pt/C, and overall have better performance than most of the Ru-Pt_{COMM} series. Both series of catalysts were observed to have optimum composition giving highest activities at 0.50 ML theoretical monodisperse coverage of Ru. However, the peak current of the Ru-Pt_{SEA} sample at this composition is lower than that of Ru-Pt_{COMM} which may be attributed to less Pt loading in the catalyst resulting in lowered conductivity of the electrode.

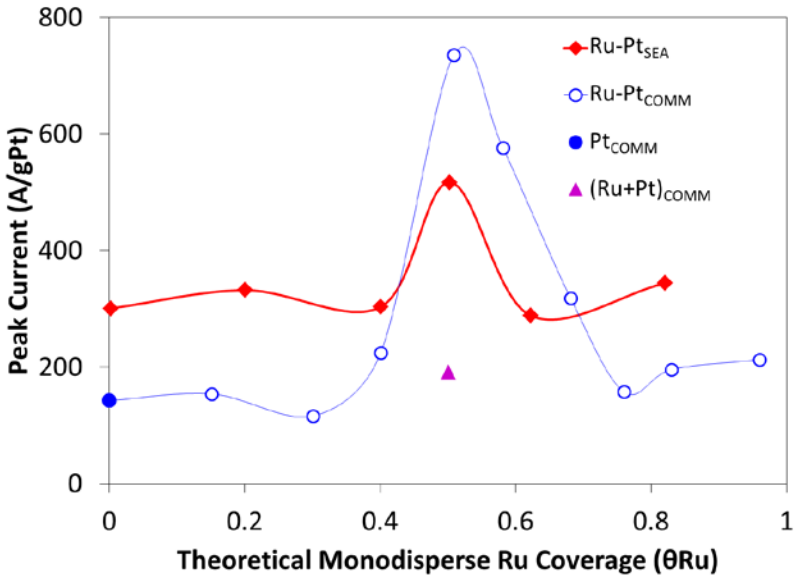

Figure 5.4 Methanol electrooxidation performance of the SEA-ED prepared catalysts ($Ru\text{-}Pt_{SEA}$) vs catalysts prepared by ED of Ru on commercial Pt ($Ru\text{-}Pt_{COMM}$ and Pt_{COMM}) as well as commercial 1 : 1 bulk molar Ru-Pt ratio catalyst ($(Ru+Pt)_{COMM}$).

5.5 Conclusions

With the increased interest in Ru-Pt bimetallic system for DMFC application, the use of ED for the preparation of such catalyst was extended to well dispersed Pt/C base catalyst prepared by SEA. The maximum loading of the base catalyst with single SEA cycle was only 6.3 wt%, compared to commercially available fuel cell catalyst at 20 wt% Pt. However, there was increased dispersion or higher availability of Pt surface sites for the SEA sample. A series of carbon supported Ru-Pt bimetallic catalysts were synthesized by ED of Ru on the SEA prepared Pt/C catalysts using an established acidic bath with Hexaammineruthenium chloride as Ru source and formic acid as reducing agent. Varying coverages of Ru deposition on Pt was achieved with the ED bath. The prepared Ru-Pt/C ED/SEA catalysts were evaluated for methanol electrooxidation and showed higher activity than commercial samples. A similar trend in activity with Ru

surface composition to prior studies was observed, with optimum Ru coverage corresponding to equimolar Ru and Pt on the surface. However, there is apparent effect of the Pt loading as the SEA samples deposited with Ru, having lower Pt content, did not reach the same maximum activity as commercial high metal loading Pt/C deposited with Ru. Further investigation is needed, where additional SEA cycles are done to increase loading of Pt in order to isolate this effect.

5.6 Acknowledgements

The efforts of Bahareh Tavakoli Mehrabadi, Weijian Diao, Taylor Garrick, the University of South Carolina Electron Microscopy Center with Dr. Doug Blom are appreciated for contributing to this study.

CHAPTER 6

SUMMARY AND CONCLUSIONS

In the studies presented in this work, preparation of well dispersed supported metal catalysts was demonstrated using the methods of strong electrostatic adsorption and electroless deposition. In the characterization of these catalysts that use carbon as the support, it was observed that there is a significant discrepancy between sizes obtained from bulk characterization techniques such as STEM and XRD, to size estimates from surface characterization, i.e. chemisorption. This discrepancy is pervasive in studies of transition metals on carbon which often cite the formation of carbon overlayer(s) on the particle surface but such hypothesis has not been directly observed.

In the elucidation of the cause for the discrepancy in size estimates, the use of temperature programmed oxidation was determined to be a useful tool to detect the presence of carbon on the surface of metal nanoparticles. This was done by preparing a series of carbon supported palladium catalysts subjected to different thermal treatments that exhibited the described discrepancy. The Pd/C catalysts were subjected to TPO treatment where low-temperature burn-off peaks for carbon was observed, distinct from catalytic oxidation of the support. These peaks were attributed to decorating carbon as the proximity to Pd surface sites give greater ease of catalyzed burn-off and the finite amount results in consumption peaks. The Pd/C catalyst was subjected to oxidative treatment at the temperature corresponding to decorating carbon burn-off and then reduced to recover metallic Pd surface. The reduced catalyst then had better agreement between XRD, STEM, and chemisorption particle size estimate, while further TPO did not show low temperature carbon oxidation peaks. Thus, the Pd/C catalysts can be cleaned of carbon overlayer and metal surface can be recovered where actual dispersion can be measured with surface characterization. The recovery of particle surface without support occlusion

is paramount in catalytic applications that require high availability of active sites, particularly in the case of ED.

In the preparation of platinum based bimetallic catalysts, electroless deposition has been shown from prior work to be effective in directed deposition of secondary metal on the surface of a primary metal. The Pt-Co bimetallic catalyst system is of particular interest for PEMFC application due to their higher activity and durability compared to just Pt. A series of Pt-Co/C catalyst were prepared by ED of Pt on Co cores synthesized by modified CEDI. The Co/C base catalysts used had small particles confirmed by XRD and STEM. A basic electroless developer bath modified from previous work was used. The bath contained $PtCl^{6-}$, EN, and DMAB as Pt-precursor, stabilizer, and reducing agent respectively. Pt was successfully deposited on the Co/C catalyst and resulted in formation of Pt-Co alloy particles as evidenced by alloy phase peaks in XRD and overlapping maps of Pt and Co from XEDS imaging. The simultaneous action of galvanic displacement and ED was the cause for the alloy formation. In addition, irregular "exploded" hollow shell particles observed from STEM resulted from fast deposition kinetics while core-shell type particles were preferred for controlled deposition. Electrochemical evaluation of the Pt-Co/C catalysts showed lower electrochemical surface area due to the formation of large particles from uncontrolled ED. However, much higher mass and surface activities were registered for the Pt-Co/C catalysts compared to commercially available high loading Pt/C catalysts. This is apparently due to the alloy formation and is in agreement with studies using Pt-Co alloys for oxygen reduction reactions. Further research on ED bath parameter modification for Pt deposition on Co will be necessary for better control of the morphology of the resulting bimetallic particles for ORR application.

Another Pt based bimetallic catalyst of interest in fuel cell application is the Pt-Ru system. Prior works have shown that the addition of Ru to Pt catalyst for DMFC application significantly increases activity. Often, the addition of Ru is done by simple impregnation resulting in irregular composition distribution. Recently, the ED of Ru on a commercial high metal loading Pt/C catalyst was demonstrated to yield true bimetallic Pt-Ru surfaces and resulted in significant increase in performance. The investigation of ED for Ru deposition on Pt is extended in the study presented in this work, where the same electroless developer bath is used with a highly dispersed Pt/C catalyst prepared using SEA. The resulting series of bimetallic Ru-Pt/C catalysts showed similar trends where optimum Ru at 50% coverage of the Pt surface gives the highest mass activity. While the activity may be lower than the Ru-Pt/C catalyst from ED of Ru on commercial Pt/C due to the lower Pt loading, the performance was still better than commercial Pt/C or commercially available Ru-Pt/C.

The effectiveness of using SEA/CEDI and ED in the preparation of catalysts with better performance than conventionally prepared commercial ones has been substantiated in the studies discussed herein. Furthermore, with the importance of availability of supported metal nanoparticle surface, the recovery of which from carbon overlayer obstruction has been demonstrated. Overall, results of research conducted here contribute valuable information for the rational design of catalysts that can be fine-tuned for specific applications.

REFERENCES

1. Zhong, C. J.; Regalbuto, J. R., 7.04 - Metal Nanoparticle Synthesis. In *Comprehensive Inorganic Chemistry II (Second Edition)*, Poeppelmeier, J. R., Ed. Elsevier: Amsterdam, 2013; pp 75-102.
2. Niemantsverdriet, J. W., *Spectroscopy in Catalysis*. Wiley: 2007.
3. Shiju, N. R.; Guliants, V. V., Recent developments in catalysis using nanostructured materials. *Applied Catalysis A: General* **2009,** *356*, 1-17.
4. Hostetler, M. J.; Zhong, C.-J.; Yen, B. K. H.; Anderegg, J.; Gross, S. M.; Evans, N. D.; Porter, M.; Murray, R. W., Stable, Monolayer-Protected Metal Alloy Clusters. *Journal of the American Chemical Society* **1998,** *120*, 9396-9397.
5. Park, J.; Regalbuto, J. R., A Simple, Accurate Determination of Oxide PZC and the Strong Buffering Effect of Oxide Surfaces at Incipient Wetness. *Journal of Colloid and Interface Science* **1995,** *175*, 239-252.
6. Hao, X.; Spieker, W. A.; Regalbuto, J. R., A further simplification of the revised physical adsorption (RPA) model. *Journal of Colloid and Interface Science* **2003,** *267*, 259-264.
7. Zhu, X.; Cho, H.-R.; Pasupong, M.; Regalbuto, J. R., Charge-Enhanced Dry Impregnation: A Simple Way to Improve the Preparation of Supported Metal Catalysts. *ACS Catalysis* **2013,** *3*, 625-630.

8. Shah, A. M.; Regalbuto, J. R., Retardation of platinum adsorption over oxide supports at pH extremes: oxide dissolution or high ionic strength? *Langmuir* **1994,** *10*, 500-504.

9. Park, C.; Fenter, P. A.; Sturchio, N. C.; Regalbuto, J. R., Probing outer-sphere adsorption of aqueous metal complexes at the oxide-water interface with resonant anomalous X-ray reflectivity. *Physical Review Letters* **2005,** *94*.

10. Cho, H.-R.; Regalbuto, J. R., The rational synthesis of Pt-Pd bimetallic catalysts by electrostatic adsorption. *Catalysis Today* **2015,** *246*, 143-153.

11. D'Souza, L.; Regalbuto, J. R., Strong electrostatic adsorption for the preparation of Pt/Co/C and Pd/Co/C bimetallic electrocatalysts. In *Studies in Surface Science and Catalysis*, E.M. Gaigneaux, M. D. S. H. P. A. J. J. A. M.; Ruiz, P., Eds. Elsevier: 2010; Vol. Volume 175, pp 715-718.

12. Burattin, P.; Che, M.; Louis, C., Characterization of the Ni(II) Phase Formed on Silica Upon Deposition−Precipitation. *The Journal of Physical Chemistry B* **1997,** *101*, 7060-7074.

13. Zanella, R.; Louis, C.; Giorgio, S.; Touroude, R., Crotonaldehyde hydrogenation by gold supported on TiO2: structure sensitivity and mechanism. *Journal of Catalysis* **2004,** *223*, 328-339.

14. Nguyen, D. L.; Umbarkar, S.; Dongare, M. K.; Lancelot, C.; Girardon, J. S.; Dujardin, C.; Granger, P., Deposition–precipitation versus anionic-exchange Au/Al2O3 catalysts: A comparative investigation towards the selective reduction of NOx. *Catalysis Communications* **2012,** *26*, 225-230.

15. Hermans, L. A. M.; Geus, J. W., Interaction Of Nickel Ions With Silica Supports During Deposition-Precipitation. In *Studies in Surface Science and Catalysis*, B. Delmon, P. G. P. J.; Poncelet, G., Eds. Elsevier: 1979; Vol. Volume 3, pp 113-130.

16. Rebelli, J.; Detwiler, M.; Ma, S.; Williams, C. T.; Monnier, J. R., Synthesis and characterization of Au–Pd/SiO2 bimetallic catalysts prepared by electroless deposition. *Journal of Catalysis* **2010,** *270*, 224-233.

17. Schaal, M. T.; Pickerell, A. C.; Williams, C. T.; Monnier, J. R., Characterization and evaluation of Ag–Pt/SiO2 catalysts prepared by electroless deposition. *Journal of Catalysis* **2008,** *254*, 131-143.

18. Micheaud, C.; Marécot, P.; Guérin, M.; Barbier, J., Preparation of alumina supported palladium–platinum catalysts by surface redox reactions. Activity for complete hydrocarbon oxidation. *Applied Catalysis A: General* **1998,** *171*, 229-239.

19. Podlovchenko, B. I.; Zhumaev, U. E.; Maksimov, Y. M., Galvanic displacement of copper adatoms on platinum in solutions. *Journal of Electroanalytical Chemistry* **2011,** *651*, 30-37.

20. Lee, C.-L.; Tseng, C.-M., Ag−Pt Nanoplates: Galvanic Displacement Preparation and Their Applications As Electrocatalysts. *The Journal of Physical Chemistry C* **2008,** *112*, 13342-13345.

21. Lee, C.-L.; Tseng, C.-M.; Wu, R.-B.; Wu, C.-C.; Syu, S.-C., Catalytic characterization of hollow silver/palladium nanoparticles synthesized by a displacement reaction. *Electrochimica Acta* **2009,** *54*, 5544-5547.

22. Beard, K. D.; Schaal, M. T.; Van Zee, J. W.; Monnier, J. R., Preparation of highly dispersed PEM fuel cell catalysts using electroless deposition methods. *Applied Catalysis B: Environmental* **2007,** *72*, 262-271.

23. Beard, K. D.; Van Zee, J. W.; Monnier, J. R., Preparation of carbon-supported Pt–Pd electrocatalysts with improved physical properties using electroless deposition methods. *Applied Catalysis B: Environmental* **2009,** *88*, 185-193.

24. Mustain, W. E.; Hyea, K.; Osborn, T.; Kohl, P. A., Deposition of PtxRu1-x Catalysts for Methanol Oxidation in Micro Direct Methanol Fuel Cells. *Israel Journal of Chemistry* **2008,** *48*, 251-257.

25. Mustain, W. E.; Kim, H.; Narayanan, V.; Osborn, T.; Kohl, P. A., Electroless Deposition and Characterization of Pt[sub x]Ru[sub 1 - x] Catalysts on Pt/C Nanoparticles for Methanol Oxidation. *Journal of Fuel Cell Science and Technology* **2010,** *7*, 041013-041017.

26. Ohno, I., Electroless Deposition of Palladium and Platinum. In *Modern Electroplating*, John Wiley & Sons, Inc.: 2010; pp 477-482.

27. Barbier, J.; Marécot, P.; Del Angel, G.; Bosch, P.; Boitiaux, J. P.; Didillon, B.; Dominguez, J. M.; Schiftef, I.; Espmosa, G., Preparation of platinum-gold bimetallic catalysts by redox reactions. *Applied Catalysis A: General* **1994,** *116*, 179-186.

28. Ménézo, J. C.; Hoang, L. C.; Montassier, C.; Barbier, J., Preparation and characterization of Ru−Pb supported catalysts. *Reaction Kinetics and Catalysis Letters* **1992,** *46*, 1-6.

29. Vasilic, R.; Viyannalage, L. T.; Dimitrov, N., Epitaxial Growth of Ag on Au (111) by Galvanic Displacement of Pb and Tl Monolayers. *Journal of The Electrochemical Society* **2006,** *153*, C648-C655.

30. Okinaka, Y.; Wolowodiuk, C., Electroless Plating of Platinum Group Metals. In *Electroless Plating: Fundamentals and Applications*, Noyes Publications/William Andrew Publishing, LLC: New York, 1990; pp 421-440.

31. Beard, K. D.; Borrelli, D.; Cramer, A. M.; Blom, D.; Van Zee, J. W.; Monnier, J. R., Preparation and Structural Analysis of Carbon-Supported Co Core/Pt Shell Electrocatalysts Using Electroless Deposition Methods. *ACS Nano* **2009,** *3*, 2841-2853.

32. Chien-Liang, L.; Chun-Ming, T.; Chen-Chung, W., Catalytic activity of Ag-Pd nanoparticles prepared by N2H4 reduction in electroless nickel deposition. *Journal of the Chinese Institute of Engineers* **2010,** *33*, 105-109.

33. Ohashi, M.; Beard, K. D.; Ma, S.; Blom, D. A.; St-Pierre, J.; Van Zee, J. W.; Monnier, J. R., Electrochemical and structural characterization of carbon-supported Pt-Pd bimetallic electrocatalysts prepared by electroless deposition. *Electrochimica Acta* **2010,** *55*, 7376-7384.

34. Ohashi, M.; Monnier, J. R.; Van Zee, J. W. In *Electrochemical characterization of various carbon-supported Pt-Pd bimetallic electrocatalysts prepared by electroless deposition*, 10th Polymer Electrolyte Fuel Cell Symposium, PEFC 10 - 218th ECS Meeting, October 10, 2010 - October 15, 2010, Las Vegas, NV, United states, 2010; Electrochemical Society Inc.: Las Vegas, NV, United states, 2010; pp 171-179.

35. Rebelli, J.; Rodriguez, A. A.; Ma, S.; Williams, C. T.; Monnier, J. R., Preparation and characterization of silica-supported, group IB-Pd bimetallic catalysts prepared by electroless deposition methods. *Catalysis Today* **2011,** *160*, 170-178.

36. Schaal, M.; Williams, C.; Monnier, J.; Pickerell, A.; Hoang, T. In *Characterization and kinetic evaluation of silver-containing bimetallic catalysts prepared via electroless deposition*, 05AIChE: 2005 AIChE Annual Meeting and Fall Showcase, October 30, 2005 - November 4, 2005, Cincinnati, OH, United states, 2005; American Institute of Chemical Engineers: Cincinnati, OH, United states, 2005; p 10326.

37. Schaal, M. T.; Metcalf, A. Y.; Montoya, J. H.; Wilkinson, J. P.; Stork, C. C.; Williams, C. T.; Monnier, J. R., Hydrogenation of 3,4-epoxy-1-butene over Cu-Pd/SiO2 catalysts prepared by electroless deposition. *Catalysis Today* **2007,** *123*, 142-150.

38. Okinaka, Y., Electroless Plating of Gold and Gold Alloys. In *Elecroless Plating: Fundamentals and Applications*, Mallory, G. O.; Hadju, J. B., Eds. Noyes Publications/William Andrew Publishing, LLC: New York, 1990; pp 401-420.

39. Valenzuela, K.; Raghavan, S.; Deymier, P. A.; Hoying, J., Formation of copper nanowires by electroless deposition using microtubules as templates. *J Nanosci Nanotechnol* **2008,** *8*, 3416-3421.

40. Amorim, C.; Keane, M. A., Palladium supported on structured and nonstructured carbon: A consideration of Pd particle size and the nature of reactive hydrogen. *Journal of Colloid and Interface Science* **2008,** *322*, 196-208.

41. Willocq, C.; Dubois, V.; Khimyak, Y. Z.; Devillers, M.; Hermans, S., Hydrogenation of nitrobenzene over Pd/C catalysts prepared from molecular carbonyl–phosphine palladium clusters. *Journal of Molecular Catalysis A: Chemical* **2012,** *365*, 172-180.

42. Li, J.; Ma, L.; Li, X.; Lu, C.; Liu, H., Effect of Nitric Acid Pretreatment on the Properties of Activated Carbon and Supported Palladium Catalysts. *Industrial & Engineering Chemistry Research* **2005,** *44*, 5478-5482.

43. Taboada, C. D.; Batista, J.; Pintar, A.; Levec, J., Preparation, characterization and catalytic properties of carbon nanofiber-supported Pt, Pd, Ru monometallic particles in aqueous-phase reactions. *Applied Catalysis B: Environmental* **2009,** *89*, 375-382.

44. Nores-Pondal, F. J.; Vilella, I. M. J.; Troiani, H.; Granada, M.; de Miguel, S. R.; Scelza, O. A.; Corti, H. R., Catalytic activity vs. size correlation in platinum catalysts of PEM fuel cells prepared on carbon black by different methods. *International Journal of Hydrogen Energy* **2009,** *34*, 8193-8203.

45. Bowker, M.; Stone, P.; Morrall, P.; Smith, R.; Bennett, R.; Perkins, N.; Kvon, R.; Pang, C.; Fourre, E.; Hall, M., Model catalyst studies of the strong metal–support interaction: Surface structure identified by STM on Pd nanoparticles on TiO2(110). *Journal of Catalysis* **2005,** *234*, 172-181.

46. Weerachawanasak, P.; Praserthdam, P.; Arai, M.; Panpranot, J., A comparative study of strong metal–support interaction and catalytic behavior of Pd catalysts supported on micron- and nano-sized TiO2 in liquid-phase selective

hydrogenation of phenylacetylene. *Journal of Molecular Catalysis A: Chemical* **2008,** *279,* 133-139.

47. Tengco, J. M. M.; Lugo-José, Y. K.; Monnier, J. R.; Regalbuto, J. R., Chemisorption–XRD particle size discrepancy of carbon supported palladium: Carbon decoration of Pd? *Catalysis Today* **2015,** *246,* 9-14.

48. Lesiak, B.; Stobinski, L.; Kövér, L.; Tóth, J.; Kurzydłowski, K. J., Ar ion bombardment modification of Pd–Au/MWCNTs catalyst surfaces studied by electron spectroscopy. *physica status solidi (a)* **2011,** *208,* 1791-1795.

49. Krishnankutty, N.; Vannice, M. A. In *Palladium carbide formation in Pd/C catalysts and its effect on adsorption, absorption and catalytic behavior*, Proceedings of the 1994 MRS Fall Meeting, November 28, 1994 - December 2, 1994, Boston, MA, USA, 1995; Materials Research Society: Boston, MA, USA, 1995; pp 81-86.

50. Seriani, N.; Mittendorfer, F.; Kresse, G., Carbon in palladium catalysts: A metastable carbide. *The Journal of Chemical Physics* **2010,** *132,* -.

51. Dubau, L.; Maillard, F.; Chatenet, M.; André, J.; Rossinot, E., Nanoscale compositional changes and modification of the surface reactivity of Pt3Co/C nanoparticles during proton-exchange membrane fuel cell operation. *Electrochimica Acta* **2010,** *56,* 776-783.

52. Xu, Q.; Kreidler, E.; He, T., Performance and durability of PtCo alloy catalysts for oxygen electroreduction in acidic environments. *Electrochimica Acta* **2010,** *55,* 7551-7557.

53. Stamenkovic, V. R.; Fowler, B.; Mun, B. S.; Wang, G.; Ross, P. N.; Lucas, C. A.; Marković, N. M., Improved Oxygen Reduction Activity on Pt3Ni(111) via Increased Surface Site Availability. *Science* **2007,** *315*, 493-497.

54. Xiong, L.; Kannan, A. M.; Manthiram, A., Pt–M (M=Fe, Co, Ni and Cu) electrocatalysts synthesized by an aqueous route for proton exchange membrane fuel cells. *Electrochemistry Communications* **2002,** *4*, 898-903.

55. Ding, E.; More, K. L.; He, T., Preparation and characterization of carbon-supported PtTi alloy electrocatalysts. *Journal of Power Sources* **2008,** *175*, 794-799.

56. Maillard, F.; Martin, M.; Gloaguen, F.; Léger, J. M., Oxygen electroreduction on carbon-supported platinum catalysts. Particle-size effect on the tolerance to methanol competition. *Electrochimica Acta* **2002,** *47*, 3431-3440.

57. Jalan, V.; Taylor, E. J., Importance of Interatomic Spacing in Catalytic Reduction of Oxygen in Phosphoric Acid. *Journal of The Electrochemical Society* **1983,** *130*, 2299-2302.

58. Jia, Q.; Segre, C. U.; Ramaker, D.; Caldwell, K.; Trahan, M.; Mukerjee, S., Structure–property–activity correlations of Pt-bimetallic nanoparticles: A theoretical study. *Electrochimica Acta* **2013,** *88*, 604-613.

59. Garrick, T.; Diao, W.; Tengco, J.; Monnier, J.; Weidner, J. W., The Effect of Bimetallic Surface Composition on the Activity Towards Ethanol Oxidation. *Meeting Abstracts* **2014,** *MA2014-01*, 922.

60. Diao, W.; Tengco, J. M. M.; Regalbuto, J. R.; Monnier, J. R., Preparation and characterization of Pt-Ru bimetallic catalysts synthesized by electroless deposition methods. *ACS Catalysis* **2015,** *5*, 5123-5134.

61. Hwang, B. J.; Kumar, S. M. S.; Chen, C.-H.; Monalisa; Cheng, M.-Y.; Liu, D.-G.; Lee, J.-F., An Investigation of Structure−Catalytic Activity Relationship for Pt−Co/C Bimetallic Nanoparticles toward the Oxygen Reduction Reaction. *The Journal of Physical Chemistry C* **2007,** *111*, 15267-15276.

62. Galhenage, R. P.; Xie, K.; Diao, W.; Tengco, J. M. M.; Seuser, G. S.; Monnier, J. R.; Chen, D. A., Platinum-ruthenium bimetallic clusters on graphite: a comparison of vapor deposition and electroless deposition methods. *Physical Chemistry Chemical Physics* **2015**.

63. Lai, F.-J.; Sarma, L. S.; Chou, H.-L.; Liu, D.-G.; Hsieh, C.-A.; Lee, J.-F.; Hwang, B.-J., Architecture of Bimetallic PtxCo1−x Electrocatalysts for Oxygen Reduction Reaction As Investigated by X-ray Absorption Spectroscopy. *The Journal of Physical Chemistry C* **2009,** *113*, 12674-12681.

64. Regalbuto, J. R., Strong Electrostatic Adsorption of Metals onto Catalyst Supports. In *Catalyst Preparation: Science and Engineering*, Regalbuto, J. R., Ed. Taylor and Francis/CRC Press: 2007; pp 297-318.

65. Hao, X.; Quach, L.; Korah, J.; Spieker, W. A.; Regalbuto, J. R., The control of platinum impregnation by PZC alteration of oxides and carbon. *Journal of Molecular Catalysis A: Chemical* **2004,** *219*, 97-107.

66. Diao, W.; Tengco, J. M. M.; Regalbuto, J. R.; Monnier, J. R., Preparation and Characterization of Pt–Ru Bimetallic Catalysts Synthesized by Electroless Deposition Methods. *ACS Catalysis* **2015,** *5*, 5123-5134.

67. O'Connell, K.; Regalbuto, J. R., High Sensitivity Silicon Slit Detectors for 1 nm Powder XRD Size Detection Limit. *Catalysis Letters* **2015,** *145*, 777-783.

68. Kratzer, E., *The Synthesis of Carbon Supported Palladium Catalysts by Strong Electrostatic Adsorption*. University of Illinois at Chicago: 2006.

69. Wojdyr, M., Fityk: a general-purpose peak fitting program. *Journal of Applied Crystallography* **2010,** *43*, 1126-1128.

70. Fisher, A. T.; Underwood, M. B., Calibration of an X-ray diffraction method to determine relative mineral abundances in bulk powders using matrix singular value decomposition; a test from the Barbados accretionary complex. *ODP Ocean Drilling Program* **1995,** *156*, 28-37.

71. Datye, A. K.; Xu, Q.; Kharas, K. C.; McCarty, J. M., Particle size distributions in heterogeneous catalysts: What do they tell us about the sintering mechanism? *Catalysis Today* **2006,** *111*, 59-67.

72. Mallát, T.; Szabó, S.; Petró, J.; Mendioroz, S.; Folgado, M. A., Real and apparent dispersion of carbon supported palladium—cobalt catalysts. *Applied Catalysis* **1989,** *53*, 29-40.

73. Cant, N. W.; Angove, D. E.; J. Patterson, M., The effects of residual chlorine on the behaviour of platinum group metals for oxidation of different hydrocarbons. *Catalysis Today* **1998,** *44*, 93-99.

74. Chou, P.; Vannice, M. A., Benzene hydrogenation over supported and unsupported palladium: I. Kinetic behavior. *Journal of Catalysis* **1987,** *107*, 129-139.

75. Moeller, K.; Holmlid, L., ELECTRON EMISSION STUDY OF A GRAPHITE COVERED PLATINUM EMITTER FOR THERMIONIC ENERGY CONVERSION: DISSOLUTION OF CARBON INTO THE BULK OF THE METAL. *Applied Surface Science* **1987,** *29*, 474-478.

76. Najbar, M.; Pietruszka, B.; Borzeckaprokop, B., *DEACTIVATION AND REACTIVATION OF RU/SIO2 CATALYST*. Elsevier Science Publ B V: Amsterdam, 1994; Vol. 88, p 513-518.

77. Redmond, E. L.; Setzler, B. P.; Juhas, P.; Billinge, S. J. L.; Fuller, T. F., In-Situ Monitoring of Particle Growth at PEMFC Cathode under Accelerated Cycling Conditions. *Electrochemical and Solid-State Letters* **2012,** *15*, B72-B74.

78. Takeuchi, N.; Fuller, T. F., Modeling and Investigation of Carbon Loss on the Cathode Electrode during PEMFC Operation. *Journal of The Electrochemical Society* **2010,** *157*, B135-B140.

79. Kinoshita, K., Particle Size Effects for Oxygen Reduction on Highly Dispersed Platinum in Acid Electrolytes. *Journal of The Electrochemical Society* **1990,** *137*, 845-848.

80. Kabbabi, A.; Gloaguen, F.; Andolfatto, F.; Durand, R., Particle size effect for oxygen reduction and methanol oxidation on Pt/C inside a proton exchange membrane. *Journal of Electroanalytical Chemistry* **1994,** *373*, 251-254.

81. Wikander, K.; Ekström, H.; Palmqvist, A. E. C.; Lindbergh, G., On the influence of Pt particle size on the PEMFC cathode performance. *Electrochimica Acta* **2007,** *52*, 6848-6855.

82. Nikkuni, F. R.; Dubau, L.; Ticianelli, E. A.; Chatenet, M., Accelerated degradation of Pt3Co/C and Pt/C electrocatalysts studied by identical-location transmission electron microscopy in polymer electrolyte environment. *Applied Catalysis B: Environmental* **2015,** *176–177*, 486-499.

83. Wang, D. L.; Xin, H. L. L.; Hovden, R.; Wang, H. S.; Yu, Y. C.; Muller, D. A.; DiSalvo, F. J.; Abruna, H. D., Structurally ordered intermetallic platinum-cobalt core-shell nanoparticles with enhanced activity and stability as oxygen reduction electrocatalysts. *Nature Materials* **2013,** *12*, 81-87.

84. Habibi, B.; Ghaderi, S., Synthesis, characterization and electrocatalytic activity of Co@Pt nanoparticles supported on carbon-ceramic substrate for fuel cell applications. *International Journal of Hydrogen Energy* **2015,** *40*, 5115-5125.

85. Cao, C.; Yang, G.; Dubau, L.; Maillard, F.; Lambert, S. D.; Pirard, J.-P.; Job, N., Highly dispersed Pt/C catalysts prepared by the Charge Enhanced Dry Impregnation method. *Applied Catalysis B: Environmental* **2014,** *150–151*, 101-106.

86. Rodriguez, A. A.; Williams, C. T.; Monnier, J. R., Selective liquid-phase oxidation of glycerol over Au-Pd/C bimetallic catalysts prepared by electroless deposition. *Applied Catalysis A: General* **2014,** *475*, 161-168.

87. Zhang, Y.; Diao, W.; Williams, C. T.; Monnier, J. R., Selective hydrogenation of acetylene in excess ethylene using Ag- and Au-Pd/SiO2 bimetallic catalysts

prepared by electroless deposition. *Applied Catalysis A: General* **2014,** *469*, 419-426.

88. Schaal, M. T.; Pickerell, A. C.; Williams, C. T.; Monnier, J. R., Characterization and evaluation of Ag-Pt/SiO2 catalysts prepared by electroless deposition. *Journal of Catalysis* **2008,** *254*, 131-143.

89. Wongkaew, A.; Zhang, Y.; Tengco, J. M. M.; Blom, D. A.; Sivasubramanian, P.; Fanson, P. T.; Regalbuto, J. R.; Monnier, J. R., Characterization and evaluation of Pt-Pd electrocatalysts prepared by electroless deposition. *Applied Catalysis B: Environmental* **2016,** *188*, 367-375.

90. Garrick, T. R.; Diao, W.; Tengco, J. M.; Stach, E. A.; Senanayake, S. D.; Chen, D. A.; Monnier, J. R.; Weidner, J. W., The Effect of the Surface Composition of Ru-Pt Bimetallic Catalysts for Methanol Oxidation. *Electrochimica Acta* **2016,** *195*, 106-111.

91. Fuentes, R. E.; García, B. L.; Weidner, J. W., Effect of Titanium Dioxide Supports on the Activity of Pt-Ru toward Electrochemical Oxidation of Methanol. *Journal of The Electrochemical Society* **2011,** *158*, B461-B466.

92. Bezemer, G. L.; Radstake, P. B.; Koot, V.; van Dillen, A. J.; Geus, J. W.; de Jong, K. P., Preparation of Fischer–Tropsch cobalt catalysts supported on carbon nanofibers and silica using homogeneous deposition-precipitation. *Journal of Catalysis* **2006,** *237*, 291-302.

93. Yang, Y.; Jia, L.; Meng, Y.; Hou, B.; Li, D.; Sun, Y., Fischer–Tropsch Synthesis over Ordered Mesoporous Carbon Supported Cobalt Catalysts: The Role of

Amount of Carbon Precursor in Catalytic Performance. *Catalysis Letters* **2011,** *142*, 195-204.

94. LÜ, J.; Huang, C.; Bai, S.; Jiang, Y.; Li, Z., Thermal decomposition and cobalt species transformation of carbon nanotubes supported cobalt catalyst for Fischer-Tropsch synthesis. *Journal of Natural Gas Chemistry* **2012,** *21*, 37-42.

95. Bychko, I.; Kalishyn, Y.; Strizhak, P., TPR Study of Core-Shell Fe@Fe3O4 Nanoparticles Supported on Activated Carbon and Carbon Nanotubes. *Advances in Materials Physics and Chemistry* **2012,** *2*, 17-22.

96. Reuel, R. C.; Bartholomew, C. H., The stoichiometries of H2 and CO adsorptions on cobalt: Effects of support and preparation. *Journal of Catalysis* **1984,** *85*, 63-77.

97. Bergwerff, J. A.; Lysova, A. A.; Espinosa-Alonso, L.; Koptyug, I. V.; Weckhuysen, B. M., Monitoring Transport Phenomena of Paramagnetic Metal-Ion Complexes Inside Catalyst Bodies with Magnetic Resonance Imaging. *Chemistry – A European Journal* **2008,** *14*, 2363-2374.

98. Mochizuki, T.; Hara, T.; Koizumi, N.; Yamada, M., Novel preparation method of highly active Co/SiO2 catalyst for Fischer-Tropsch synthesis with chelating agents. *Catalysis Letters* **2007,** *113*, 165-169.

99. Miulović Snežana, M.; Nikolić Vladimir, M.; Laušević Petar, Z.; Aćimović Danka, D.; Tasić Gvozden, S.; Marčeta-Kaninski Milica, P., Electrochemistry of cobalt ethylenediamine complexes at high pH. **2015,** *80*, 1515-1527.

100. Bard, A. J.; Faulkner, L. R., *Electrochemical Methods: Fundamentals and Applications*. Wiley: 2000.

101. Darling, A. S., Cobalt-platinum alloys. *Platinum Metals Review* **1963,** *7*, 96-104.

102. Ohashi, M.; Beard, K. D.; Ma, S.; Blom, D. A.; St-Pierre, J.; Van Zee, J. W.; Monnier, J. R., Electrochemical and structural characterization of carbon-supported Pt–Pd bimetallic electrocatalysts prepared by electroless deposition. *Electrochimica Acta* **2010,** *55*, 7376-7384.

103. Ohno, I., Electrochemistry of electroless plating. *Materials Science and Engineering: A* **1991,** *146*, 33-49.

104. Ohno, I.; Wakabayashi, O.; Haruyama, S., Anodic Oxidation of Reductants in Electroless Plating. *Journal of The Electrochemical Society* **1985,** *132*, 2323-2330.

105. Djokić, S. S., Electroless Deposition of Metals and Alloys. In *Modern Aspects of Electrochemistry*, Conway, B. E.; White, R. E., Eds. Springer US: Boston, MA, 2002; pp 51-133.

106. Haruyama, S.; Ohno, I. In *Catalytic aspects in electroless deposition*, 1988; Paunovic, M.; Ohno, I., Eds. Electrochemical Society: 1988; pp 20-36.

107. Cooper, K. R., In Situ PEM Fuel Cell Electrochemical Surface Area and Catalyst Utilization Measurement. *Fuel Cell Magazine* 2009.

108. Jiang, R.; Tran, D. T.; McClure, J. P.; Chu, D., Increasing the electrochemically available active sites for heat-treated hemin catalysts supported on carbon black. *Electrochimica Acta* **2012,** *75*, 185-190.

109. Ishiguro, N.; Saida, T.; Uruga, T.; Nagamatsu, S.-i.; Sekizawa, O.; Nitta, K.; Yamamoto, T.; Ohkoshi, S.-i.; Iwasawa, Y.; Yokoyama, T.; Tada, M., Operando Time-Resolved X-ray Absorption Fine Structure Study for Surface Events on a

Pt3Co/C Cathode Catalyst in a Polymer Electrolyte Fuel Cell during Voltage-Operating Processes. *ACS Catalysis* **2012,** *2,* 1319-1330.

110. Lambert, S.; Job, N.; D'Souza, L.; Pereira, M. F. R.; Pirard, R.; Heinrichs, B.; Figueiredo, J. L.; Pirard, J.-P.; Regalbuto, J. R., Synthesis of very highly dispersed platinum catalysts supported on carbon xerogels by the strong electrostatic adsorption method. *Journal of Catalysis* **2009,** *261,* 23-33.

111. Aricò, A. S.; Antonucci, P. L.; Modica, E.; Baglio, V.; Kim, H.; Antonucci, V., Effect of Pt□Ru alloy composition on high-temperature methanol electro-oxidation. *Electrochimica Acta* **2002,** *47,* 3723-3732.

112. Gasteiger, H. A.; Markovic, N.; Ross, P. N.; Cairns, E. J., Methanol electrooxidation on well-characterized platinum-ruthenium bulk alloys. *The Journal of Physical Chemistry* **1993,** *97,* 12020-12029.

113. Srinivasan, S.; Mosdale, R.; Stevens, P.; Yang, C., FUEL CELLS: Reaching the Era of Clean and Efficient Power Generation in the Twenty-First Century. *Annual Review of Energy and the Environment* **1999,** *24,* 281-328.

114. Scott, K.; Taama, W. M.; Argyropoulos, P.; Sundmacher, K., The impact of mass transport and methanol crossover on the direct methanol fuel cell. *Journal of Power Sources* **1999,** *83,* 204-216.

115. Regalbuto, J. R., Electrostatic Adsorption. In *Synthesis of Solid Catalysts*, Wiley-VCH Verlag GmbH & Co. KGaA: 2009; pp 33-58.

APPENDIX A

LIST OF PUBLICATIONS

1. Wongkaew, A., Zhang, Y., **Tengco, J.M.M.**, Blom, D.A., Sivasubramanian, P., Fanson, P., Regalbuto, J.R., Monnier, J.R., Characterization and Evaluation of Pt-Pd Electrocatalysts Prepared by Electroless Deposition. Appl. Catal., B., 188, 367-375.

2. Garrick, T.R., Diao, W., **Tengco, J.M.M.**, Stach, E.A., Senanayake, S.D., Chen, D.A., Monnier, J.R., Weidner, J.W., The Effect of the Surface Composition of Ru-Pt Bimetallic Catalysts for Methanol Oxidation. Electrochim. Acta., 195, 106-111.

3. Diao, W., **Tengco, J.M.M.**, Regalbuto, J.R., Monnier, J.R., Preparation and characterization of Pt-Ru bimetallic catalysts synthesized by electroless deposition methods. ACS Catalysis, 5 (9), 5123-5134.

4. Galhenage, R.P., Xie, K., Diao, W., **Tengco, J.M.M.**, Seuser, G.S., Monnier, J.R., Chen, D.A., Platinum-Ruthenium Bimetallic Clusters on Graphite: A Comparison of Vapor Deposition and Electroless Deposition Methods. Phys. Chem. Chem. Phys., 17 (42), 28354-28363.

5. **Tengco, J.M.M.**, Lugo-José, Y.K., Monnier, J.R., Regalbuto, J.R., Chemisorption–XRD particle size discrepancy of carbon supported palladium: Carbon decoration of Pd? Catal. Today, 246, 9-14.

6. **Tengco, J.M.M.**, Tavakoli Mehrabadi, B.A., Wongkaew, A., Zhang, Y., Weidner J.W., Regalbuto, J.R., Monnier, J.R., Synthesis and electrochemical evaluation of carbon supported Pt-Co bimetallic catalysts prepared by electroless deposition and modified charge enhanced dry impregnation. Submitted to Catalysts (MDPI), 2016.

7. Wongkaew, A., Zhang, Y., **Tengco, J.M.M.**, Regalbuto, J.R., Monnier, J.R., Preparation of electroless developer bath for the deposition of cobalt on carbon supported platinum. Article in Preparation.

8. **Tengco, J.M.M.**, Tavakoli Mehrabadi, B.A., Weidner J.W., Regalbuto, J.R., Monnier, J.R., Bimetallic Ru-Pt/C Catalysts Prepared by Strong Electrostatic Adsorption and Electroless Deposition for Direct Methanol Fuel Cell Application. Article in Preparation.

9. **Tengco, J.M.M.**, Liu, Q., Keels, J.M., Banerjee, R., Copple, J.E., Regalbuto, J.R., Supported Pt Particle Size Determination by Powder XRD with High Sensitivity Silicon Slit Detectors. Article in Preparation.

10. Banerjee, R., Liu, Q., Samad, J.E., **Tengco, J.M.M.**, Regalbuto, J.R., Support Microporosity Effects on the Stability of Platinum Nanoparticles. Article in Preparation.

APPENDIX B

PERMISSION TO REPRINT

ELSEVIER LICENSE
TERMS AND CONDITIONS

Mar 24, 2016

This is a License Agreement between John Meynard M Tengco ("You") and Elsevier ("Elsevier") provided by Copyright Clearance Center ("CCC"). The license consists of your order details, the terms and conditions provided by Elsevier, and the payment terms and conditions.

All payments must be made in full to CCC. For payment instructions, please see information listed at the bottom of this form.

Supplier	Elsevier Limited The Boulevard,Langford Lane Kidlington,Oxford,OX5 1GB,UK
Registered Company Number	1982084
Customer name	John Meynard M Tengco
Customer address	541 Main St COLUMBIA, SC 29208
License number	3835390600786
License date	Mar 24, 2016
Licensed content publisher	Elsevier
Licensed content publication	Catalysis Today
Licensed content title	Chemisorption–XRD particle size discrepancy of carbon supported palladium: Carbon decoration of Pd?
Licensed content author	John Meynard M. Tengco,Yuliana K. Lugo-José,John R. Monnier,John R. Regalbuto
Licensed content date	15 May 2015
Licensed content volume number	246
Licensed content issue number	n/a
Number of pages	6
Start Page	9
End Page	14
Type of Use	reuse in a thesis/dissertation
Portion	full article
Format	both print and electronic
Are you the author of this Elsevier article?	Yes
Will you be translating?	No
Title of your thesis/dissertation	Synthesis of Well Dispersed Supported Metal Catalysts by Strong Electrostatic Adsorption and Electroless Deposition

Expected completion date	Apr 2016
Estimated size (number of pages)	100
Elsevier VAT number	GB 494 6272 12
Permissions price	0.00 USD
VAT/Local Sales Tax	0.00 USD / 0.00 GBP
Total	0.00 USD
Terms and Conditions	

INTRODUCTION

1. The publisher for this copyrighted material is Elsevier. By clicking "accept" in connection with completing this licensing transaction, you agree that the following terms and conditions apply to this transaction (along with the Billing and Payment terms and conditions established by Copyright Clearance Center, Inc. ("CCC"), at the time that you opened your Rightslink account and that are available at any time at http://myaccount.copyright.com).

GENERAL TERMS

2. Elsevier hereby grants you permission to reproduce the aforementioned material subject to the terms and conditions indicated.

3. Acknowledgement: If any part of the material to be used (for example, figures) has appeared in our publication with credit or acknowledgement to another source, permission must also be sought from that source. If such permission is not obtained then that material may not be included in your publication/copies. Suitable acknowledgement to the source must be made, either as a footnote or in a reference list at the end of your publication, as follows:

"Reprinted from Publication title, Vol /edition number, Author(s), Title of article / title of chapter, Pages No., Copyright (Year), with permission from Elsevier [OR APPLICABLE SOCIETY COPYRIGHT OWNER]." Also Lancet special credit - "Reprinted from The Lancet, Vol. number, Author(s), Title of article, Pages No., Copyright (Year), with permission from Elsevier."

4. Reproduction of this material is confined to the purpose and/or media for which permission is hereby given.

5. Altering/Modifying Material: Not Permitted. However figures and illustrations may be altered/adapted minimally to serve your work. Any other abbreviations, additions, deletions and/or any other alterations shall be made only with prior written authorization of Elsevier Ltd. (Please contact Elsevier at permissions@elsevier.com)

6. If the permission fee for the requested use of our material is waived in this instance, please be advised that your future requests for Elsevier materials may attract a fee.

7. Reservation of Rights: Publisher reserves all rights not specifically granted in the combination of (i) the license details provided by you and accepted in the course of this licensing transaction, (ii) these terms and conditions and (iii) CCC's Billing and Payment terms and conditions.

8. License Contingent Upon Payment: While you may exercise the rights licensed immediately upon issuance of the license at the end of the licensing process for the transaction, provided that you have disclosed complete and accurate details of your proposed use, no license is finally effective unless and until full payment is received from you (either by publisher or by CCC) as provided in CCC's Billing and Payment terms and conditions. If full payment is not received on a timely basis, then any license preliminarily granted shall be

deemed automatically revoked and shall be void as if never granted. Further, in the event that you breach any of these terms and conditions or any of CCC's Billing and Payment terms and conditions, the license is automatically revoked and shall be void as if never granted. Use of materials as described in a revoked license, as well as any use of the materials beyond the scope of an unrevoked license, may constitute copyright infringement and publisher reserves the right to take any and all action to protect its copyright in the materials.

9. Warranties: Publisher makes no representations or warranties with respect to the licensed material.

10. Indemnity: You hereby indemnify and agree to hold harmless publisher and CCC, and their respective officers, directors, employees and agents, from and against any and all claims arising out of your use of the licensed material other than as specifically authorized pursuant to this license.

11. No Transfer of License: This license is personal to you and may not be sublicensed, assigned, or transferred by you to any other person without publisher's written permission.

12. No Amendment Except in Writing: This license may not be amended except in a writing signed by both parties (or, in the case of publisher, by CCC on publisher's behalf).

13. Objection to Contrary Terms: Publisher hereby objects to any terms contained in any purchase order, acknowledgment, check endorsement or other writing prepared by you, which terms are inconsistent with these terms and conditions or CCC's Billing and Payment terms and conditions. These terms and conditions, together with CCC's Billing and Payment terms and conditions (which are incorporated herein), comprise the entire agreement between you and publisher (and CCC) concerning this licensing transaction. In the event of any conflict between your obligations established by these terms and conditions and those established by CCC's Billing and Payment terms and conditions, these terms and conditions shall control.

14. Revocation: Elsevier or Copyright Clearance Center may deny the permissions described in this License at their sole discretion, for any reason or no reason, with a full refund payable to you. Notice of such denial will be made using the contact information provided by you. Failure to receive such notice will not alter or invalidate the denial. In no event will Elsevier or Copyright Clearance Center be responsible or liable for any costs, expenses or damage incurred by you as a result of a denial of your permission request, other than a refund of the amount(s) paid by you to Elsevier and/or Copyright Clearance Center for denied permissions.

LIMITED LICENSE

The following terms and conditions apply only to specific license types:

15. **Translation**: This permission is granted for non-exclusive world **English** rights only unless your license was granted for translation rights. If you licensed translation rights you may only translate this content into the languages you requested. A professional translator must perform all translations and reproduce the content word for word preserving the integrity of the article.

16. **Posting licensed content on any Website**: The following terms and conditions apply as follows: Licensing material from an Elsevier journal: All content posted to the web site must maintain the copyright information line on the bottom of each image; A hyper-text must be included to the Homepage of the journal from which you are licensing at http://www.sciencedirect.com/science/journal/xxxxx or the Elsevier homepage for books at http://www.elsevier.com; Central Storage: This license does not include permission for a scanned version of the material to be stored in a central repository such as that provided by Heron/XanEdu.

Licensing material from an Elsevier book: A hyper-text link must be included to the Elsevier homepage at http://www.elsevier.com . All content posted to the web site must maintain the copyright information line on the bottom of each image.

Posting licensed content on Electronic reserve: In addition to the above the following clauses are applicable: The web site must be password-protected and made available only to bona fide students registered on a relevant course. This permission is granted for 1 year only. You may obtain a new license for future website posting.

17. **For journal authors:** the following clauses are applicable in addition to the above:

Preprints:

A preprint is an author's own write-up of research results and analysis, it has not been peer-reviewed, nor has it had any other value added to it by a publisher (such as formatting, copyright, technical enhancement etc.).

Authors can share their preprints anywhere at any time. Preprints should not be added to or enhanced in any way in order to appear more like, or to substitute for, the final versions of articles however authors can update their preprints on arXiv or RePEc with their Accepted Author Manuscript (see below).

If accepted for publication, we encourage authors to link from the preprint to their formal publication via its DOI. Millions of researchers have access to the formal publications on ScienceDirect, and so links will help users to find, access, cite and use the best available version. Please note that Cell Press, The Lancet and some society-owned have different preprint policies. Information on these policies is available on the journal homepage.

Accepted Author Manuscripts: An accepted author manuscript is the manuscript of an article that has been accepted for publication and which typically includes author-incorporated changes suggested during submission, peer review and editor-author communications.

Authors can share their accepted author manuscript:

- immediately
  - via their non-commercial person homepage or blog
  - by updating a preprint in arXiv or RePEc with the accepted manuscript
  - via their research institute or institutional repository for internal institutional uses or as part of an invitation-only research collaboration work-group
  - directly by providing copies to their students or to research collaborators for their personal use
  - for private scholarly sharing as part of an invitation-only work group on commercial sites with which Elsevier has an agreement
- after the embargo period
  - via non-commercial hosting platforms such as their institutional repository
  - via commercial sites with which Elsevier has an agreement

In all cases accepted manuscripts should:

- link to the formal publication via its DOI
- bear a CC-BY-NC-ND license - this is easy to do
- if aggregated with other manuscripts, for example in a repository or other site, be shared in alignment with our hosting policy not be added to or enhanced in any way to appear more like, or to substitute for, the published journal article.

Published journal article (JPA): A published journal article (PJA) is the definitive final record of published research that appears or will appear in the journal and embodies all value-adding publishing activities including peer review co-ordination, copy-editing, formatting, (if relevant) pagination and online enrichment.
Policies for sharing publishing journal articles differ for subscription and gold open access articles:
Subscription Articles: If you are an author, please share a link to your article rather than the full-text. Millions of researchers have access to the formal publications on ScienceDirect, and so links will help your users to find, access, cite, and use the best available version.
Theses and dissertations which contain embedded PJAs as part of the formal submission can be posted publicly by the awarding institution with DOI links back to the formal publications on ScienceDirect.
If you are affiliated with a library that subscribes to ScienceDirect you have additional private sharing rights for others' research accessed under that agreement. This includes use for classroom teaching and internal training at the institution (including use in course packs and courseware programs), and inclusion of the article for grant funding purposes.
Gold Open Access Articles: May be shared according to the author-selected end-user license and should contain a CrossMark logo, the end user license, and a DOI link to the formal publication on ScienceDirect.
Please refer to Elsevier's posting policy for further information.
18. **For book authors** the following clauses are applicable in addition to the above:
Authors are permitted to place a brief summary of their work online only. You are not allowed to download and post the published electronic version of your chapter, nor may you scan the printed edition to create an electronic version. **Posting to a repository:** Authors are permitted to post a summary of their chapter only in their institution's repository.
19. **Thesis/Dissertation**: If your license is for use in a thesis/dissertation your thesis may be submitted to your institution in either print or electronic form. Should your thesis be published commercially, please reapply for permission. These requirements include permission for the Library and Archives of Canada to supply single copies, on demand, of the complete thesis and include permission for Proquest/UMI to supply single copies, on demand, of the complete thesis. Should your thesis be published commercially, please reapply for permission. Theses and dissertations which contain embedded PJAs as part of the formal submission can be posted publicly by the awarding institution with DOI links back to the formal publications on ScienceDirect.

Elsevier Open Access Terms and Conditions
You can publish open access with Elsevier in hundreds of open access journals or in nearly 2000 established subscription journals that support open access publishing. Permitted third party re-use of these open access articles is defined by the author's choice of Creative Commons user license. See our open access license policy for more information.
Terms & Conditions applicable to all Open Access articles published with Elsevier:
Any reuse of the article must not represent the author as endorsing the adaptation of the article nor should the article be modified in such a way as to damage the author's honour or reputation. If any changes have been made, such changes must be clearly indicated.
The author(s) must be appropriately credited and we ask that you include the end user license and a DOI link to the formal publication on ScienceDirect.
If any part of the material to be used (for example, figures) has appeared in our publication with credit or acknowledgement to another source it is the responsibility of the user to ensure their reuse complies with the terms and conditions determined by the rights holder.

Additional Terms & Conditions applicable to each Creative Commons user license:
CC BY: The CC-BY license allows users to copy, to create extracts, abstracts and new works from the Article, to alter and revise the Article and to make commercial use of the Article (including reuse and/or resale of the Article by commercial entities), provided the user gives appropriate credit (with a link to the formal publication through the relevant DOI), provides a link to the license, indicates if changes were made and the licensor is not represented as endorsing the use made of the work. The full details of the license are available at http://creativecommons.org/licenses/by/4.0.
CC BY NC SA: The CC BY-NC-SA license allows users to copy, to create extracts, abstracts and new works from the Article, to alter and revise the Article, provided this is not done for commercial purposes, and that the user gives appropriate credit (with a link to the formal publication through the relevant DOI), provides a link to the license, indicates if changes were made and the licensor is not represented as endorsing the use made of the work. Further, any new works must be made available on the same conditions. The full details of the license are available at http://creativecommons.org/licenses/by-nc-sa/4.0.
CC BY NC ND: The CC BY-NC-ND license allows users to copy and distribute the Article, provided this is not done for commercial purposes and further does not permit distribution of the Article if it is changed or edited in any way, and provided the user gives appropriate credit (with a link to the formal publication through the relevant DOI), provides a link to the license, and that the licensor is not represented as endorsing the use made of the work. The full details of the license are available at http://creativecommons.org/licenses/by-nc-nd/4.0.
Any commercial reuse of Open Access articles published with a CC BY NC SA or CC BY NC ND license requires permission from Elsevier and will be subject to a fee.
Commercial reuse includes:

- Associating advertising with the full text of the Article
- Charging fees for document delivery or access
- Article aggregation
- Systematic distribution via e-mail lists or share buttons

Posting or linking by commercial companies for use by customers of those companies.

20. **Other Conditions**:

v1.8

Questions? customercare@copyright.com or +1-855-239-3415 (toll free in the US) or +1-978-646-2777.